



3 1293 00898 7509

This is to certify that the

dissertation entitled

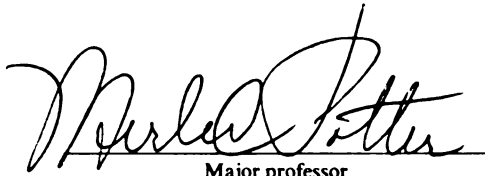
**Analysis of an Underground Electric Heating
System with Short Term Energy Storage**

presented by

Bassem Husni Ramadan

has been accepted towards fulfillment
of the requirements for

Ph.D. degree in Mechanical Engineering



Major professor

Date 12-20-91

**LIBRARY
Michigan State
University**

**PLACE IN RETURN BOX to remove this checkout from your record.
TO AVOID FINES return on or before date due.**

DATE DUE	DATE DUE	DATE DUE
SEP 25 1925	_____	_____
_____	_____	_____
_____	_____	_____
_____	_____	_____
_____	_____	_____
_____	_____	_____
_____	_____	_____

MSU is An Affirmative Action/Equal Opportunity Institution

**ANALYSIS OF AN UNDERGROUND ELECTRIC
HEATING SYSTEM WITH SHORT TERM
ENERGY STORAGE**

By

Bassem Husni Ramadan

A DISSERTATION

**Submitted to
Michigan State University
In partial fulfillment of the requirements
for the degree of**

DOCTOR OF PHILOSOPHY

Department of Mechanical Engineering

1991

ABSTRACT

ANALYSIS OF AN UNDERGROUND ELECTRIC HEATING SYSTEM WITH SHORT TERM ENERGY STORAGE

By

Bassem Husni Ramadan

The principal commercially active heat storage application where concrete is used as the storage media is in the use of subfloor electric heaters. The resistance heaters are energized when utility off-peak rates are in effect. The sand and concrete floor are then heated to some predetermined temperature. The floor then releases heat slowly and remains warm during the subsequent period of high demand.

Analysis of the slab-heating system for varying design parameters, such as the depth of placement of the heaters, the thickness and the placement of insulation beneath the heaters, soil properties, the thickness of the sand layer below the heaters, and heat input was considered.

The system was optimized, based on life-cycle costs, by varying the above system parameters, for a prototypical building in four representative U.S. cities.

A one-dimensional transient heat conduction computer program was used in the analysis of the below-grade region. For the above-grade region, energy consumption

of the building and peak load calculations were done using the ASEAM2.1 computer program. Load profiles were calculated using hourly weather data for January.

It was found that the response of the system was strongly affected by soil properties and the depth of placement of the heaters. Optimal insulation levels for the prototypical building in each of the representative cities were obtained. These optimal insulation levels were found to change when the soil thermal properties were varied. For no insulation, the heat lost to the ground below the mats was 30 percent of the heat input for sand with 20 percent moisture content, and about 48 percents for dry sand. The amount of heat lost to the ground was found to be also a function of mat depth when dry sand was used.

The study suggests that the heaters may need to be turned on during on-peak rates to prevent the slab surface from becoming cool during the afternoon hours. Because of the difficulty of controlling the space temperature, an expensive controller that implements load prediction algorithms is needed.

TO
MY WIFE MAY

ACKNOWLEDGEMENTS

Special thanks are due to Professor Merle C. Potter and the members of the Guidance Committee: Professors James V. Beck, Alejandro R. Diaz, Craig W. Somerton, and David Yen for their guidance and friendship. Thanks also to Dr. Joe Huang of Lawrence Berkeley Laboratory for supplying the weather data.

TABLE OF CONTENTS

LIST OF TABLES	viii
LIST OF FIGURES	xi
NOMENCLATURE	xv
CHAPTER I	1
INTRODUCTION	1
1.1 The Energy Crisis	1
1.2 How Utilities are Affected by the Energy Crisis	2
1.3 The Need for Energy Storage	3
1.4 The Deepheat Concept	4
CHAPTER II	7
METHODOLOGY	7
2.1 Description of the Solution Method	7
2.2 Above-grade Building Simulation	7
2.2.1 Description of the Building	8
2.2.2 Building Energy Analysis	9
2.3 Below-grade Analysis.	10
2.3.1 Governing Equations	10
2.3.2 Finite Difference Formulation	11
2.3.3 The Interface Conductivity	14
2.3.4 Solution of the System of Equations	17
CHAPTER III	21
OPTIMIZATION	21
3.1 Parametric Study	21
3.1.1 Determining the Optimum Mat Depth	22
3.1.2 Determining the Optimum Sand Bed Thickness	23
3.1.3 Determining the Optimum Insulation Level	24
3.1.3.1 Economic Analysis Approach	25
3.1.3.2 Method of Analysis	26
CHAPTER IV	32
CONTROLS	32

4.1	Introduction	32
4.2	Profile Prediction	36
4.2.1	Load Prediction	36
4.2.2	Temperature Prediction	37
4.3	Optimal Control	39
4.3.1	Design Sensitivity Analysis	40
CHAPTER V		48
RESULTS, DISCUSSION AND CONCLUSIONS		48
5.1	Results and Discussion	48
5.1.2	Effect of Moisture Content on Sand Thermal Properties ...	49
5.1.3	Effect of Sand Moisture Content on Heat Loss	53
5.1.4	Selection of Insulation Products	56
5.2	Conclusions	58
5.3	Recommendations for Future Work	61
TABLES		63
FIGURES		89
REFERENCES		135
General References		136
APPENDICES		140
Appendix A: Sample Output of ASEAM2.1		140
Appendix B: Computer Program Listing		147

LIST OF TABLES

<u>TABLE</u>		<u>PAGE</u>
1	List of climate cities	63
2	Description of prototype building in Washington DC	64
3	Description of prototype building in Chicago, IL	65
4	Description of prototype building in Minneapolis, MN	66
5	Description of prototype building in Las Vegas, NV	67
6	Characteristics of Eq. (2.8) for three values of the weighting factor γ	68
7	Properties of materials used	68
8	Peak load summary for prototype building in Washington, DC	69
9	Peak load summary for prototype building in Chicago, IL	70
10	Peak load summary for prototype building in Minneapolis, MN	71
11	Peak load summary for prototype building in Las Vegas, NV	72
12	Building energy consumption for various insulation levels	73
13	Fuel cost savings	73
14	Insulation costs	74
15	Economic parameters used in the analysis	74
16	Life-cycle Cost Analysis	75

17	Annual energy end use of prototype building in Washington, DC	76
18	Annual energy end use of prototype building in Chicago, IL	77
19	Annual energy end use of prototype building in Minneapolis, MN	78
20	Annual energy end use of prototype building in Las Vegas, NV	79
21	Monthly energy consumption for prototype building in Washington, DC	80
22	Monthly energy consumption for prototype building in Chicago, IL	80
23	Monthly energy consumption for prototype building in Minneapolis, MN	81
24	Monthly energy consumption for prototype building in Las Vegas, NV	81
25	Sensitivity of objective function to design variable ω for various values of ω and ϕ	82
26	Sensitivity of objective function to design variable ϕ for various values of ω and ϕ	82
27	Sensitivity of objective function to design variable ω	83
28	Sensitivity of objective function to design variable ϕ	83
29	Sensitivity of maximum slab-surface temperature to design variable ω for various values of ω and ϕ	84
30	Sensitivity of maximum heating-element temperature to design variable ω for various values of ω and ϕ	84
31	Sensitivity of maximum slab-surface temperature to ω	85
32	Sensitivity of maximum heating-element temperature to ω	85
33	Sensitivity of maximum slab-surface temperature to ϕ	86
34	Sensitivity of maximum heating-element temperature to ϕ	86
35	Life-cycle cost analysis for prototype building in Washington, DC	87

36	Life-cycle cost analysis for prototype building in Chicago, IL	87
37	Life-cycle cost analysis for prototype building in Minneapolis, MN	88
38	Life-cycle cost analysis for prototype building in Las Vegas, NV	88

LIST OF FIGURES

<u>FIGURE</u>		<u>PAGE</u>
1	Electrical energy production by fuel in the U.S.	89
2	Thermal energy storage	90
3	The deepheat concept	91
4	The one-dimensional grid	92
5	The interface conductivity	92
6	Variation of sand thermal properties with moisture content	93
7	Slab heat-flux as a function of mat depth	94
8	Slab heat-flux as a function of mat depth	94
9	Peak slab heat-flux versus mat depth for various energy inputs	95
10	Time of peak heat-flux as a function of mat depth	95
11	Slab heat-flux for various sand layer thicknesses	96
12	Slab heat-flux for various sand layer thicknesses	96
13	Slab heat-flux for various sand layer thicknesses	97
14	Slab heat-flux for various sand layer thicknesses	97
15	Slab heat-flux for various sand layer thicknesses	98
16	Slab heat-flux for various sand layer thicknesses	98
17	Variation of slab heat-flux for various insulation levels	99
18	Variation of slab heat-flux for various insulation levels	99

19	Variation of slab heat-flux for various insulation levels	100
20	Variation of slab heat-flux for various insulation levels	100
21	Variation of slab heat-flux for various insulation levels	101
22	Variation of slab heat-flux for various insulation levels	101
23	Variation of slab heat-flux for various insulation levels	102
24	Variation of slab heat-flux for various insulation levels	102
25	Variation of slab heat-flux for various insulation levels	103
26	Variation of slab heat-flux for various insulation levels	103
27	Variation of slab heat-flux for various insulation levels	104
28	Variation of slab heat-flux for various insulation levels	104
29	Life cycle cost of insulation options for Washington, DC	105
30	Life cycle cost of insulation options for Chicago, IL	105
31	Life cycle cost of insulation options for Minneapolis, MN	106
32	Life cycle cost of insulation options for Las Vegas, NV	106
33	Variation of slab heat-flux with mat depth	107
34	Slab heat-flux with intermittent heating	108
35	Slab heat-flux with intermittent heating	108
36	Slab heat-flux with intermittent heating	109
37	Slab heat-flux for various energy inputs	109
38	Block diagram of controller functions	110
39	Outside air temperature fluctuations in January for Minneapolis, MN	111
40	Outside air temperature fluctuations in January for Chicago, IL	111
41	Outside air temperature fluctuations in January for Washington, DC	112
42	Outside air temperature fluctuations in January for Las Vegas, NV	112

43	Load profile for day 3 in January, Chicago, IL	113
44	Load profile for day 9 in January, Chicago, IL	113
45	Load profile for day 19 in January, Chicago, IL	114
46	Load profile for day 29 in January, Chicago, IL	114
47	Load profile for day 3 in January, Las Vegas, NV	115
48	Load profile for day 10 in January, Las Vegas, NV	115
49	Load profile for day 19 in January, Las Vegas, NV	116
50	Load profile for day 29 in January, Las Vegas, NV	116
51	Load profile for day 3 in January, Minneapolis, MN	117
52	Load profile for day 10 in January, Minneapolis, MN	117
53	Load profile for day 17 in January, Minneapolis, MN	118
54	Load profile for day 24 in January, Minneapolis, MN	118
55	Load profile for day 3 in January, Washington, DC	119
56	Load profile for day 9 in January, Washington, DC	119
57	Load profile for day 19 in January, Washington, DC	120
58	Load profile for day 29 in January, Washington, DC	120
59	Variation of heating element temperature with mat depth	121
60	Maximum slab surface temperature as a function of mat depth and energy input	122
61	Maximum heating element temperature as a function of energy input	122
62	Variation of soil thermal resistivity with moisture content	123
63	Effect of soil moisture content on slab heat-flux	124
64	Effect of soil moisture content on slab heat-flux	124
65	Effect of soil moisture content on slab heat-flux	125

66	Effect of soil moisture content on slab heat-flux	125
67	Effect of soil moisture content on slab heat-flux	126
68	Effect of soil moisture content on slab heat-flux	126
69	Time of peak heat-flux as a function of mat depth and energy input for dry sand	127
70	Peak heat-flux as a function of mat depth and energy input for dry sand	127
71	Maximum slab surface temperature as a function of mat depth and energy input for dry sand	128
72	Variation of slab heat-flux with insulation R-value for dry sand	128
73	Variation of slab heat-flux with insulation R-value for dry sand	129
74	Variation of slab heat-flux with insulation R-value for dry sand	129
75	Maximum heating element temperature as a function of energy input for dry sand	130
76	Variation of slab heat-flux with mat depth for $\alpha_{\text{sand}} = 0.044 \text{ ft}^2/\text{hr}$	130
77	Variation of slab heat-flux with mat depth for $\alpha_{\text{sand}} = 0.044 \text{ ft}^2/\text{hr}$	131
78	Variation of slab heat-flux with mat depth for $\alpha_{\text{sand}} = 0.044 \text{ ft}^2/\text{hr}$	131
79	Variation of slab heat-flux for various sand layer thicknesses for $\alpha_{\text{sand}} = 0.044 \text{ ft}^2/\text{hr}$	132
80	Variation of slab heat-flux for various sand layer thicknesses for $\alpha_{\text{sand}} = 0.044 \text{ ft}^2/\text{hr}$	132
81	Variation of slab heat-flux for various sand layer thicknesses for $\alpha_{\text{sand}} = 0.044 \text{ ft}^2/\text{hr}$	133
82	Variation of slab heat-flux for various sand layer thicknesses for $\alpha_{\text{sand}} = 0.044 \text{ ft}^2/\text{hr}$	133
83	Variation of slab heat-flux for various sand layer thicknesses for $\alpha_{\text{sand}} = 0.044 \text{ ft}^2/\text{hr}$	134
84	Variation of slab heat-flux for various sand layer thicknesses for $\alpha_{\text{sand}} = 0.044 \text{ ft}^2/\text{hr}$	134

NOMENCLATURE

English Symbols

- A_B = area of inside surface of the building
- A_i = coefficient in Eq. (2.22)
- A_s = surface area of the slab
- a_i = coefficient in Eq. (2.19)
- $[B]$ = coefficient vector
- b_i = coefficient in Eq. (2.19)
- C = flag for income producing venture
- $[C]$ = coefficient matrix
- c = specific heat
- c_{conc} = specific heat of concrete
- c_i = coefficient in Eq. (2.19)
- D = domain length
- DP = down payment percentage
- d = discount rate
- d_i = sand bed thickness
- d_s = distance between heat mats and bottom of slab
- f = objective function
- g = heat source function

- g_i = constraint function
- h = combined radiative and convective heat transfer coefficient
- h_o = convective heat transfer coefficient
- i = general inflation rate
- i_F = fuel price inflation rate
- K = cost of electricity
- k = thermal conductivity
- k_{conc} = thermal conductivity of concrete
- L = mat depth below slab surface
- \mathcal{L} = Lagrangian
- M_s = ratio of first year miscellaneous costs to initial investment
- m = annual mortgage interest rate
- N_D = depreciation lifetime in years
- N_E = the analysis period
- N_L = term of loan
- N_{min} = years over which the mortgage payments contribute to the analysis
- N'_{min} = years over which depreciation contributes to the analysis
- P = time period
- PWF = present worth factor
- P_1 = ratio of present value of future fuel savings to the savings in the first year
- P_2 = ratio of life-cycle costs of conservation investment to the initial cost
- q = heat-flux
- q_l = heat-flux through building envelope

- q_p = peak heat-flux through building envelope
 q_s = heat-flux at slab surface
 R_i = coefficient in Eq. (2.22)
 r_i = coefficient in Eq. (2.19)
 R_v = ratio of resale value at the end of the period analysis to initial investment
 S = heat source strength
 T = temperature
 T_{int} = interior temperature of conditioned space
 T_{slab} = slab surface temperature
 T_{source} = heating element temperature
 \bar{T} = virtual temperature
 $[T]$ = temperature vector
 t = time
 t_i = insulation thickness
 t_r = property tax rate based on assessed value
 t_s = specified time in Eq. (3.16)
 \bar{t} = marginal tax bracket
 V = velocity
 V_r = ratio of assessed valuation of the foundation insulation in the first year
to the initial investment
 x = position variable

Greek Symbols:

- α = thermal diffusivity

- Δt = time step
- Δx = grid size
- $\hat{\delta}(x)$ = Dirac delta function
- ϵ_B = emissivity of building inner surface
- ϵ_s = emissivity of slab surface
- ϕ = mean of distribution
- Γ = domain boundary
- λ = adjoint variable
- $\bar{\lambda}$ = virtual adjoint variable
- μ_i = Lagrange multiplier
- Ω = problem domain
- ω = standard deviation
- ψ = function
- ρ = density
- τ = dummy time variable

Subscripts:

- $()_x$ = partial derivative with respect to x
- $()_t$ = partial derivative with respect to t

Superscripts:

- $()'$ = sensitivity with respect to design variable

CHAPTER I

INTRODUCTION

1.1 The Energy Crisis

The energy crisis that Americans experienced in the fall of 1973 and the winter of 1974 made everyone realize that a true energy crisis is building and cannot be avoided so long as the world continues to rely on fossil-fuel resources (or indeed on any finite terrestrial source) for its energy needs. Energy is no longer plentiful, and it must be used efficiently.

During the last two decades the percentage of total energy used in the United States in commercial and residential applications (excluding electricity) and for transportation purposes has remained nearly constant at twenty percent and twenty-five percent, respectively, of the total amount of energy used. The percentage used in industry (excluding electricity) has declined from thirty-six percent to twenty-five percent over the last twenty-five years, while the percentage utilized for electric generation has nearly doubled, from about fifteen percent in 1950 to twenty-nine percent in 1976. The actual quantity of U.S. electric generation from 1960 to 1976, increased from 0.75×10^{12} to 2.04×10^{12} KWH. This production was met primarily from fossil-fuel combustion: forty-six percent coal, sixteen percent oil, and fourteen percent natural gas. Hydroelectric power contributed another fourteen percent, nuclear fission nine percent, and less than one percent was obtained from all other

(mostly geothermal) sources (Green, 1981). Figure 1 shows the electrical energy production by fuel in the United States for 1989 and the projected production for 1998. In 1989, 54.2% of electricity produced in the U.S. was from coal, 20.8% from nuclear energy, 13.1% from oil and gas, and the rest from hydroelectric and non-utility (class notes, 1990).

1.2 How Utilities are Affected by the Energy Crisis

Since energy is becoming more and more expensive, power plant designers cannot deliberately oversize a plant's capacity to make sure the peak demand is met. The demand for electric energy in a utility is characterized by hourly, daily, and seasonal variations, whereas the supply from the generating system, in the majority of cases, has a fixed capacity. The capacity must be selected to correspond to the maximum demand plus a reasonable excess to take care of scheduled plant shutdowns for maintenance and unscheduled shutdowns due to abnormal occurrences. This results in large, expensive plants that operate much of the time below capacity, thus causing high operating and capital costs. Since more than 67% of electricity produced in the U.S. is from fossil fuels, the majority of power plants are steam power plants. Steam power plants are characterized by the fact that their thermal efficiency drops when operating at part-load. Lower efficiency leads to higher consumption of fuel. This also leads to an increase in the cost of fossil fuels because of increased demand. This increase in the cost of fuel has resulted in an increase in the production cost of electricity. As a result, the cost of electricity for the consumer has increased. Therefore, there is a need to improve power plants

i
i
l
c
e
p
1
fr
fr
st
Fi
Th
dar

efficiencies. One way of doing that is by having the plants operate at near full-load most of the time.

The decision by a utility company to construct additional power plants is based on the ability of the company to supply electricity at the time of peak demand. To avoid constructing additional power plants, many utilities use their pricing structure to encourage customers to use off-peak energy whenever possible. The cost of electricity is affected by generating facilities that must operate at part-load or remain idle during off-peak times. As mentioned above, the efficiency of a power plant drops when the plant is operating below capacity. Hence, the cost of electricity increases. As an incentive to delay some on-peak usage and thereby level their daily loads, some European and American utilities offer reduced rates for off-peak consumption, usually during the night. If large enough rate differentials are offered, electrical heating systems that incorporate thermal storage to utilize primarily off-peak power may operate more economically than conventional on-peak systems.

1.3 The Need for Energy Storage

The objective of energy storage is to counteract the disadvantages that result from the fluctuation in demand for electric energy by assuring a steady high output from existing power plants. When the demand is lower than capacity, energy is stored. When the demand is higher than capacity energy is released, as shown in Figure 2. The result is then a reliable, efficient and economical supply of electricity. The utilities will still be able to provide peak electrical demands on short notice during certain times of the day or week. Energy storage would allow the generating

plants to be designed for nearly constant load operation below peak demand, a process called peak shaving, which would thus reduce the demand for the construction of new plants to meet peak load. Energy storage becomes attractive only when the capital and operating costs of the storage system are more than offset by the reduction in the corresponding costs of the original system. Three options for incorporating storage into an electric heating system are hot water storage, block heaters, and slab warming. This study focuses on the performance of slab-type systems.

1.4 The Deepheat Concept

To provide the thermal storage required for use of off-peak power, the heating elements can be embedded in the concrete slab. With a conventional slab-on-grade construction, however, a midday boost of energy may be required to keep the slab from becoming too cool in the late afternoon (Harrison, 1959). The effective storage capacity is increased without resorting to a thicker slab by locating the heating elements in a sand layer beneath the slab. This configuration was used in this study.

The principal commercially active heat storage application where concrete is used as the storage media is in the use of subfloor heaters. A schematic of this concept is shown in Figure 3. The resistance heaters are energized when off-peak rates are in effect. The sand and concrete floor are then heated to some predetermined temperature. The floor then releases heat slowly over a time period dependent on the heaters placement depth and remains warm during the subsequent period of peak rates or high demand. Without a lower insulation layer, some heat

is lost to the earth; the manufacturer (Smith-Gates, 1990) claims that this is a small amount. A horizontal insulation layer placed beneath the mats may prevent this downward energy migration.

Because of the uncontrolled nature of energy release, precise temperature control of the heated space is extremely difficult. Thus the concept is not suitable for office buildings and living facilities, but is most suitable for storage facilities and maintenance facilities (Kedl, 1983). In addition, the concept is primarily of interest for new construction and not for retrofit applications.

A subfloor heating system of this type has certain characteristics that may be of special interest to the military because their requirements are quite often unique. For example, because of the massive energy storage system, a buildup with a subfloor heater may remain at a tolerable temperature for a much longer period of time than a conventionally heated building during a power outage. Secondly, since the electrical heating system can be installed totally external to the building envelope, it may be ideal for heating explosion prone spaces (Kedl, 1983).

Previously, the system has not been optimized for a particular configuration of underground insulation placement and heater location. In this study, the system was analyzed for various values of the following parameters:

- The location of the heaters.
- The thickness and depth of the horizontal insulation layer below the heating mats.
- Sand properties.
- The operation schedule of the heaters.

A warehouse with a slab-on-grade foundation type was considered. A wide range of insulation configurations and thicknesses were considered. The analysis was performed for four representative cities in the United States. Table 1 shows the four cities with their typical heating degree-day numbers. The time delays and amount of energy release from the concrete floor to the heated space as a function of depth of heater placement were also considered. The system was optimized (based on life cycle costs) by varying the system parameters. Because of the time lag, slab-heating requires sophisticated control systems in order to anticipate load many hours in advance of heater operation. The problem of control was also addressed in this study. The information detailing the energy and monetary savings provided by an optimized mat system could then be provided to perspective users of this system thus encouraging them to take advantage of the savings provided.

CHAPTER II

METHODOLOGY

2.1 Description of the Solution Method

To study the performance and the suitability of using the slab heating system to heat buildings in different cities in the U.S., knowledge of the energy consumption of the building was needed. In addition, hourly load profiles and peak loads were also required. For these reasons a prototypical building was selected. The building was a 250 x 400 ft warehouse with a slab-on-grade foundation. To complete the study, the performance of the heating system for various configurations of mat placement, insulation thicknesses, heat input, and sand layer thicknesses were also required. The study was divided into two parts; the building energy consumption and loads were determined in the first part, and the foundation heat loss and the heat flux delivered by the heating system at the slab surface were found in the second. The information from both parts were then combined and used to study the optimization and control of the system. The results of the optimization analysis are included in Chapter III, and the controls are discussed in Chapter IV.

2.2 Above-grade Building Simulation

To estimate the energy consumption of the building for various climate types, a prototypical building of average construction under typical conditions was simulated

using the ASEAM2.1 computer program. The annual energy consumption for heating the building was determined. The peak heating load was given by the computer program. The hourly load profiles were calculated using hourly temperature data for each of the representative cities.

2.2.1 Description of the Building

The prototypical building had a floor area of 100,000 ft² and a 1300 ft perimeter. The floor to ceiling height was 12 ft. The glass area was twenty percent of the total wall area. The U-values used for the simulation were derived from the ASHRAE90.1P Envelope Criteria. These U-values were modified according to the climate type of each of the four U.S. representative cities. The windows had double pane glass and the infiltration rate was 0.5 air-changes per hour; it corresponds to an air infiltration rate calculated using

$$\text{Air-changes} = 0.252 + 0.0251 V + 0.0184 \Delta T \quad (2.1)$$

where V is the average wind speed in Knots and ΔT is the inside-outside temperature differential in degrees Fahrenheit. The thermostat was set at 70°F during the heating season. The overall building mass was considered to be medium with 4" concrete exterior wall and 4" concrete floor slab. To determine the energy input required by the building baseboard heaters were selected to supply heating. Baseboard heaters were located along the walls within the building. They provide heating only and may be supplied by hot water or steam from the heating plant, or they may be electric resistance heaters. Tables 2-5 show the description of the building needed for the ASEAM2.1 energy analysis program for the four representative cities.

2.2.2 Building Energy Analysis

The ASEAM2.1 (A Simplified Energy Analysis Method, Version 2.1) which is a modified bin method computer program for calculating the energy consumption of residential and simple commercial buildings, was used to calculate the annual energy usage for the prototypical building. Wherever possible, ASEAM2.1 uses recognized algorithms from such sources as the American Society of Heating, Refrigerating, and Air-conditioning Engineers (ASHRAE, 1980), Illuminating Engineering Society (IES, 1984), the DOE-2 program (DOE, 1982), and the National Bureau of Standards (NBS). Like most building energy analysis programs, ASEAM2.1 performs calculations in four segments:

- **Loads:** Thermal heating and cooling loads (both peak and average) are calculated for each zone by month and outside bin temperature. Lighting and miscellaneous electrical consumption is calculated in the loads segment.
- **Systems:** The thermal loads calculated in the loads segment are then passed to the systems segment, which calculates "coil" loads for boilers and chillers. Note that the system coil loads are not equal to the zone loads calculated above owing to ventilation requirements, latent cooling, humidification requirements, economizer cycles, reheat, mixing, etc. Some building energy requirements are calculated in the systems segment (e.g., heat pump and fan electricity requirements).
- **Plant:** All of the systems coil loads on the central heating and cooling plant equipment are then combined, and calculations are performed for

each central plant type. Note that plant equipment can also impose loads on other plant equipment, such as cooling tower loads from chillers and boiler loads from absorption chillers or domestic hot water. The results of the plant calculations are monthly and annual energy consumption for each plant type.

- **Economic (optional):** Energy consumption from all the building end-use categories is then totaled and reported. If specified, the life-cycle costs of the total energy requirements, combined with other parameters, are calculated and reported. Comparisons of the base case with alternative cases may also be performed in the parametric and ECO (Energy Conservation Opportunities) calculation modes.

The hourly load profiles of the building for the four representative cities were calculated using hourly weather data for the month of January. The peak load and the time of the peak were determined also.

2.3 Below-grade Analysis

The heated slab was simulated in order to predict various aspects of the system performance under arbitrary weather and heat inputs, and for various configurations of the system parameters.

2.3.1 Governing Equations

The basic simulation was a one-dimensional transient heat transfer model in

the below-grade region shown in Figure 4. This region included the concrete slab, sand layer, heating mats, bottom insulation, and the earth below the building.

The region was modeled by application of the transient, one-dimensional heat conduction equation,

$$\frac{\partial}{\partial x} \left(k \frac{\partial T}{\partial x} \right) + g(x,t) - \rho c \frac{\partial T}{\partial t} \quad (2.2)$$

with appropriate initial and boundary conditions. The lower boundary of the region was held at a fixed temperature of 50°F at a distance of 21 ft, assumed to be outside the region of influence of the heating system. The slab surface was modeled as exchanging heat through convection with the inside air of the building that was held at a fixed temperature of 70°F, and through radiation with the inside surface of the building.

The calculation domain is a heterogeneous one due to the inclusion of the concrete slab, the heating mats, sand, insulation, and earth. As a result, a straight forward analytical solution of the governing equations was not attempted. A numerical solution using a finite difference scheme was implemented to solve for the temperature field. The computer program was used to calculate the heat flux at the slab surface, and the heat flux lost to the earth.

2.3.2 Finite Difference Formulation

The differential equation governing one-dimensional transient heat conduction with heat generation is

$$\frac{\partial}{\partial x} \left(k \frac{\partial T}{\partial x} \right) + g(x,t) - \rho c \frac{\partial T}{\partial t} \quad (2.3)$$

The control volume approach was used to approximate the partial differential equation Eq. (2.3). The control volume approach is based on the conservation of a specific physical quantity, such as mass, momentum, or thermal energy. It is also known as the finite volume approach. The approach employs numerical balances of a conserved variable over small control volumes.

The control volume approach starts from an integral conservation statement. Such a statement applies locally and globally. When applied to a specific control volume and approximated numerically in an appropriate fashion, the resulting numerical solution will satisfy the conservation principle for the control volume. It will also satisfy the governing differential equation in an average sense over the control volume. If appropriately formulated, the numerical solution will also satisfy the conservation principle globally.

The first step in the control volume approach is to state the governing conservation principle in integral form. For transient diffusion with a heat source, the appropriate integral form is given by

$$\frac{\partial}{\partial t} \int_{\Omega} \rho c T d\Omega - k \int_{\Gamma} \frac{\partial T}{\partial n} d\Gamma + \int_{\Omega} \dot{Q} d\Omega \quad (2.4)$$

where Ω is a planar region and Γ is the bounding curve. The integral equation applies to the whole region being considered and to any subvolume of the region.

The next step is to divide the physical region into a set of nonoverlapping control volumes, such as those shown by dashed lines in Figure 4. Then nodes were

located at the centers of the control volumes. This served to define the node locations on the variable grid.

After the control volumes were defined, the integral conservation statement was applied to a typical control volume. When Eq. (2.3) is applied to the i th control volume in Figure 4, the integral equation becomes, with no heat generation,

$$\int_t^{t+\Delta t} \int_{\Delta x} \rho c \frac{\partial T}{\partial t} dx dt - \int_t^{t+\Delta t} \left\{ \left[k \frac{\partial T}{\partial x} \right]_{i-1/2} + \left[k \frac{\partial T}{\partial x} \right]_{i+1/2} \right\} dt \quad (2.5)$$

For the representation of the term $\partial T / \partial t$, we shall assume that the grid-point value of T prevails throughout the control volume. Then,

$$\rho c \int_t^{t+\Delta t} \int_{\Delta x} \frac{\partial T}{\partial t} dx dt = (\rho c)_i \Delta x_i (T_i^{(n+1)} - T_i^{(n)}) \quad (2.6)$$

assuming $\rho c = \text{constant}$. And,

$$\left[k \frac{\partial T}{\partial x} \right]_{i-1/2} = \frac{k_{i-1/2} (T_{i-1} - T_i)}{(\Delta x_{i-1} + \Delta x_i)/2} \quad (2.7)$$

$$\left[k \frac{\partial T}{\partial x} \right]_{i+1/2} = \frac{k_{i+1/2} (T_i - T_{i+1})}{(\Delta x_{i+1} + \Delta x_i)/2}$$

$$\text{Let } \int_t^{t+\Delta t} T_i dt = [\gamma T_i^{(n+1)} + (1-\gamma) T_i^{(n)}] \Delta t \quad (2.8)$$

where γ is a weighting factor in the range $0 \leq \gamma \leq 1$ and is sometimes called the *degree of implicitness*. Using similar formulas for T_{i-1} and T_{i+1} , we get from Eq. (2.5)

$$\begin{aligned}
& (\rho c)_i \frac{\Delta x_i}{\Delta t} (T_i^{(n+1)} - T_i^{(n)}) - \gamma \left[k_{i-1/2} \frac{T_{i-1}^{(n+1)} - T_i^{(n+1)}}{(\Delta x_{i-1} + \Delta x_i)/2} + k_{i+1/2} \frac{T_{i+1}^{(n+1)} - T_i^{(n+1)}}{(\Delta x_{i+1} + \Delta x_i)/2} \right] \\
& + (1 - \gamma) \left[k_{i-1/2} \frac{T_{i-1}^{(n)} - T_i^{(n)}}{(\Delta x_{i-1} + \Delta x_i) / 2} + k_{i+1/2} \frac{T_{i+1}^{(n)} - T_i^{(n)}}{(\Delta x_{i+1} + \Delta x_i)/2} \right] + g \Delta x_i \quad (2.9)
\end{aligned}$$

This equation is then written for every node. A system of linear equations then results. The procedure used to solve the system depends on the value of the weighting factor, γ . The characteristics of Eq. (2.8) for three commonly employed values of γ are listed in Table 6. In particular, $\gamma = 0$ leads to the explicit scheme, $\gamma = 0.5$ to the Crank-Nicolson scheme, and $\gamma = 1$ to the fully implicit scheme. The Crank-Nicolson scheme was adopted for the solution of the system of equations in this study. The Thomas Algorithm (2.19) was used to solve the resulting system of equations. An implicit finite difference equation was developed for each node. Various values of insulation thickness, mat depth, and sand layer thickness were modeled by properly selecting the properties of the appropriate nodes. Property values used in the simulation are listed in Table 7.

2.3.3 The Interface Conductivity

In Eq. (2.9), the conductivity $k_{i-1/2}$ and $k_{i+1/2}$ has been used to represent the value of k pertaining to the control volume faces $i-1/2$ and $i+1/2$. When the conductivity k is a function of x , we often know the value of k only at the grid points (i) , $(i-1)$, $(i+1)$ and so on. We then need a prescription for evaluating the conductivity at the interface in terms of the grid point values.

The most straightforward procedure for obtaining the interface conductivity $k_{i-1/2}$ is to assume a linear variation of k between points $(i-1)$ and (i) . Hence, $k_{i-1/2} = \theta k_{i-1} + (1-\theta)k_i$ where θ , the interpolation factor, is a ratio defined in terms of the distances Δx_{i-1} and Δx_i as shown in Figure 5:

$$\theta = \frac{\Delta x_i}{\Delta x_{i-1} + \Delta x_i} . \quad (2.10)$$

If the interface were midway between the grid points, θ would be 0.5, and $k_{i-1/2}$ would be the arithmetic mean of k_{i-1} and k_i .

This simple approach leads to incorrect implications in some cases and cannot accurately handle the abrupt changes of conductivity that may occur in composite materials (Patankar, 1980). Fortunately, a much better alternative of comparable simplicity is available. In developing this alternative, we recognize that it is not the local value of conductivity at the interface that concerns us primarily. Our main objective is to obtain a good representation for the heat flux at the interface

$$q_{i-1/2} = k_{i-1/2} \frac{T_i - T_{i-1}}{(\Delta x_{i-1} + \Delta x_i)/2} \quad (2.11)$$

which has, in effect, been used in deriving the discretization equation (2.9).

The heat flux from node $(i-1)$ to the interface $(i-1/2)$, or from the interface $(i-1/2)$ to node (i) is the same as the heat flux from node (i) to $(i-1)$. Hence,

$$q_{i-1/2} = k_i \frac{T_i - T_{i-1/2}}{(\Delta x_i)/2} = k_{i-1} \frac{T_{i-1/2} - T_{i-1}}{(\Delta x_{i-1})/2} \quad (2.12)$$

Solving for $T_{i-1/2}$ we get,

$$T_{i-1/2} = \frac{k_i T_i / \Delta x_i + k_{i-1} T_{i-1} / \Delta x_{i-1}}{k_{i-1} / \Delta x_i + k_i / \Delta x_{i-1}} \quad (2.13)$$

Solving for $k_{i-1/2}$

$$k_{i-1/2} = \frac{k_{i-1} k_i (\Delta x_{i-1} + \Delta x_i)}{k_{i-1} \Delta x_i + k_i \Delta x_{i-1}} \quad (2.14)$$

When the interface is placed midway between the grid points then

$$k_{i-1/2} = 2 \frac{k_i k_{i-1}}{k_i + k_{i-1}} \quad (2.15)$$

The equation for an interior node (i) is then,

$$\begin{aligned} & \frac{1}{2} \left[\frac{k_{i+1} k_i (\Delta x_{i+1} + \Delta x_i)}{\Delta x_{i+1} k_i + \Delta x_i k_{i+1}} \right] \left[\frac{T_{i+1}^{(n+1)} - T_i^{(n+1)}}{(\Delta x_{i+1} + \Delta x_i)/2} + \frac{T_{i+1}^{(n)} - T_i^{(n)}}{(\Delta x_{i+1} + \Delta x_i)/2} \right] \\ & + \frac{1}{2} \left[\frac{k_{i-1} k_i (\Delta x_{i-1} + \Delta x_i)}{\Delta x_{i-1} k_i + \Delta x_i k_{i-1}} \right] \left[\frac{T_{i-1}^{(n+1)} - T_i^{(n+1)} + T_{i-1}^{(n)} - T_i^{(n)}}{(\Delta x_{i-1} + \Delta x_i)/2} \right] \\ & + g(\Delta x_i) - (\rho c)_i \Delta x_i \left[\frac{T_i^{(n+1)} - T_i^{(n)}}{\Delta t} \right] \end{aligned} \quad (2.16)$$

where $g = 0$ for a node without a heat source. The equation for the surface grid point shown in Figure 4 was obtained by writing the energy balance for the corresponding control volume. The equation is

$$\begin{aligned} & \frac{1}{2} (k)_{conc} \left[\frac{T_2^{(n+1)} - T_1^{(n+1)} + T_2^{(n)} - T_1^{(n)}}{(\Delta x_1 + \Delta x_2)/2} \right] + \frac{h_o}{2} [(T_{int} - T_1^{(n+1)}) + (T_{int} - T_1^{(n)})] \\ & - \frac{\sigma}{2} \left[\frac{T_1^{(n+1)^4} - T_{int}^4 + T_1^4 - T_{int}^4}{(1 - e_s)/e_s + 1 + (1 - e_B)A_s/e_B A_B} \right] - (\rho c)_{conc} \left(\frac{\Delta x_1}{2} \right) \left[\frac{T_1^{(n+1)} - T_1^{(n)}}{\Delta t} \right] \end{aligned} \quad (2.17)$$

The radiation term was simplified as:

$$(T_1^{(n+1)})^4 - T_{int}^4 = T_{int}^4 \left[4 \left(\frac{T_1^{(n+1)} - T_{int}}{T_{int}} \right) + 6 \left(\frac{T_1^{(n)} - T_{int}}{T_{int}} \right)^2 \right] \quad (2.18)$$

A finite difference equation was written for each node and the appropriate properties for each node were selected. A system of linear algebraic equations was then generated, the number of equations being equal to the number of unknowns. The unknowns are the temperature at each node. Hence, the number of equations is equal to the number of nodes.

2.3.4 Solution of the System of Equations

The solution of the system of finite difference equations for the one-dimensional case was obtained by the Gaussian-elimination method. Because of the particularly simple form of the equations, the elimination process turns into a rather convenient algorithm. This algorithm is often called the Thomas Algorithm or the Tri-diagonal Matrix Algorithm (TDMA). This designation refers to the fact that when the matrix of the coefficients of these equations is written, all the nonzero coefficients align themselves along three diagonals of the matrix.

For convenience in representing the algorithm, the discretization equations can be written as

$$a_i T_i - b_i T_{i+1} + c_i T_{i-1} + r_i \quad (2.19)$$

for $i = 1, 2, \dots, N$ with N being equal to the number of nodes. Thus, the temperature T_i is related to the neighboring temperatures T_{i+1} and T_{i-1} . For node 1, which is a boundary node, T_1 is given then the form of the equation for node 1 is trivial. If T_1

is unknown then T_0 is known. Hence, T_1 can be solved for in terms of T_2 . The equation for $i = 2$ is a relation between T_1 , T_2 , and T_3 . But, since T_1 can be written in terms of T_2 , then the equation for $i = 2$ reduces to a relation between T_2 and T_3 . This process of substitution is then continued until T_N is expressed in terms of T_{N+1} . But, because T_{N+1} has no meaningful existence, the numerical value of T_N is obtained. This then enables us to begin the "back-substitution" process in which T_{N-1} is obtained from T_N , T_{N-2} from T_{N-1} , ..., T_2 from T_3 and T_1 from T_2 (Patankar, 1980).

For node 1 Eq. (2.19) becomes

$$a_1 T_1 - b_1 T_2 + r_1 \quad (2.20)$$

or,

$$T_1 - A_1 T_2 + R_1 \quad (2.21)$$

for $i = 2$ we can write Eq. (2.21) as,

$$T_{i-1} - A_{i-1} T_i + R_{i-1} \quad (2.22)$$

substituting Eq. (2.22) into Eq. (2.19) gives

$$a_i T_i - b_i T_{i+1} + c_i (A_{i-1} T_i + R_{i-1}) + r_i \quad (2.23)$$

which can be written as

$$T_i - A_i T_{i+1} + R_i \quad (2.24)$$

where,

$$A_i = \frac{b_i}{a_i - c_i A_{i-1}} \quad (2.25)$$

and

$$R_i = \frac{r_i + c_i R_{i-1}}{a_i - c_i A_{i-1}} \quad (2.26)$$

These recurrence relations give A_i and R_i in terms of A_{i-1} and R_{i-1} . For $i = 1$ since $c_1 = 0$

$$A_1 = \frac{b_1}{a_1}, \quad R_1 = \frac{r_1}{a_1} \quad (2.27)$$

The recurrence process is then started. For $i = N$, $b_N = 0$ which leads to $A_N = 0$, and hence from Eq. (2.24) we get

$$T_N = R_N \quad (2.28)$$

The system of linear equations written in matrix form is:

$$[C][T] = [B] \quad (2.29)$$

An estimate of the temperature is then obtained at each time step.

The heat flux at the slab surface and the heat lost to the ground were calculated. This was repeated for various mat placements, insulation thicknesses and placements, and for various heating strategies (that is continuous versus intermittent operation of the mats). For proper operation of the system, the amount of heat entering the conditioned space at the slab surface must be approximately equal to the heat lost through the building envelope in order to maintain the conditioned space at a constant temperature of 70°F.

Several points should be noted about the assumptions made in the simulations. The thermal properties were assumed to remain constant. No soil moisture movement effects were modeled, and the seasonal variation in the soil thermal conductivity were ignored. Because the influence of soil moisture is still a research question and requires detailed knowledge of soil type, weather patterns, and site information, the assumption of a constant soil thermal conductivity can be considered valid given the extent and scope of this study. However, sand thermal properties for various moisture contents were used to investigate the effect of moisture content on the performance of the heating system. Figure 6 shows the variation of the sand thermal properties with moisture content (Salomone, 1988). The results of this investigation are discussed in detail in Chapter V.

CHAPTER III

OPTIMIZATION

3.1 Parametric Study

To investigate the short term response of the system and to determine which parameter(s) mostly influence the behavior of the heating system, the following parameters were considered:

- The depth of placement of the heaters.
- The thickness and placement of the horizontal insulation layer below the heaters.
- The thickness of the sand layer.
- The time-dependent heat input.
- The moisture content of the sand.

One parameter was varied at a time while the other parameters were kept constant. The finite difference computer program that was developed to solve for the temperature field in the below-grade region was used. The response of the system was then studied by calculating the heat flux at the slab surface. A database was generated by performing numerous computer simulations. The results from

these simulations were then plotted to show the response of the system for different conditions.

3.1.1 Determining the Optimum Mat Depth

The study was initiated by varying the mat depth. The results presented in Figures 7 and 8 show the history of the heat flux at the slab surface for mat depths of approximately 7 to 29 inches. The heating mats were considered to provide 200 Btu/hr-ft² of heat density from 2 to 4 a.m. A sand bed of approximately 2.5 inches provided a base for the mats. A 2 inch polystyrene board was considered to exist beneath the sand layer.

As expected the mat closest to the slab provided the highest value for the heat flux and the heat was released in the shortest period of time, as compared to other mat depths. With the heating mats at 24 inches below the slab lower values for the heat flux were provided for a longer period of time, as long as one week. A discussion of this observation is included in Chapter V.

In order to better study the effect of mat depth on the response of the system, the energy input to the mats was varied. The heating mats were energized two to five hours a day and the heat flux at the slab surface was calculated. The peak heat flux was recorded also. The values are presented in Figure 9. At a given mat depth and for a given period of energy input to the mats the peak value of the heat flux can be determined. For proper operation of the heating mats, the peak load on the building must be satisfied, otherwise the building will be either underheated or overheated.

In order to determine the optimal value for mat placement, knowledge of the peak load on the building for the four U.S. representative cities is needed. Simulations of the building were done using the ASEAM2.1 computer program. The results are listed in Tables 8-11. For example, the peak load for the building using weather data for Chicago is 10 Btu/hr-ft². This peak can be achieved with different mat placements and for various levels of energy input. However, a certain period of time delay between when the mats were energized and when the slab begins to feel warm may be desired. Numerous simulations were performed to determine the period of time lag as a function of mat depth and different levels of energy input. The results are shown in Figure 10. The time of peak represents the number of hours between when the peak heat flux occurred and when the heating mats were turned off. Hence, if 10 hours of delay are desired, the results in Figure 10 suggest that the heating mats should be placed about 8 inches below the concrete slab. Then, if a peak heat flux of 10 Btu/hr-ft² is required for proper operation of the system, the results in Figure 9 indicate that the mats must be energized for 3 hours.

Figures 9 and 10 provide a graphical tool for determining the optimal value of mat depth for any given heating requirements.

3.1.2 Determining the Optimum Sand Bed Thickness

The heating mats are usually installed on a surface free from any objects that can cut into them and cause them to fail. The manufacturer (Smith-Gates, 1990) of the heating mats recommends that a 2 inch sand bed for the mats be provided.

To study the effect of the thickness of the sand bed on the operation of the system, three sand bed thicknesses were simulated. These thicknesses were 0.5, 2.5, and 4.5 inches. The finite difference computer program was again used to predict the heat flux at the slab surface. The heating mats were simulated to operate at full power of 200 Btu/hr-ft² from 2 to 4 a.m. R-10 insulation was placed directly beneath the sand bed. Figures 11-16 show the results for various mat depths. The results indicate that a thicker sand bed leads to a lower peak heat- flux value, with less than 2% change in the total heat loss to the ground.

Since the purpose of having a sand bed beneath the mats is to provide a clean surface for the mats, a 2 inch sand bed was found to be sufficient. Hence, the effect of varying the sand bed thickness on the operation of the heating system was not pursued further.

3.1.3 Determining the Optimum Insulation Level

The response of the heating system to a number of insulation levels was studied. The optimum insulation R-value was determined based on life-cycle costs for the four U.S. representative cities.

Six insulation levels were considered: R-0, R-5, R-10, R-20, R-30 and R-40 ft² - °F-hr/Btu. The insulation thickness was varied in the computer program by selecting the properties for the appropriate nodes. The heat flux through the concrete slab was calculated. The heat lost to the ground was also calculated for every computer simulation. In all these simulations the sand bed thickness was held at 2.5 inches. Two sets of computer calculations were performed. The first set was

performed with the heating mats on at full power from 2 to 4 a.m. continuously. The second was performed with the heat source on from 2 to 6 a.m. Figures 17-22 show the results of the first set, while Figures 23-28 show the results of the second one. In both sets and for mat depths of 7 to 29 inches, the heat loss to the ground with no insulation was 28 to 35 percent, respectively. When an R-5 insulation was added the heat loss was on the average 40 percent less than for no insulation. A 58 percent decrease resulted when an R-10 insulation was added, and a 74 percent decrease occurred for R-20 insulation. An R-30 insulation caused the heat loss to decrease by 84 percent, and an R-40 insulation resulted in an 85 percent decrease. However, since about 30 percent of the heat input was lost to the ground for no insulation, increasing the insulation thickness may prove to be economically unfeasible for some situations, as will be shown later in this chapter.

3.1.3.1 Economic Analysis Approach

In Table 12 the results of the building energy use with various insulation levels are presented. Table 13 lists the fuel cost savings associated with the above building energy use. Detailed energy use information only is not sufficient to determine the cost-effectiveness of insulation. Calculating fuel cost savings provides a way to determine the simple payback, but this approach has its limitations. To determine the optimal insulation thickness accurately, an economic analysis is needed that takes into consideration a number of economic factors.

Energy conservation investments are typically characterized by high initial costs being slowly offset by reduced fuel expenditures. Hence, the basic economic problem

is comparing the cost of a known investment with estimated fuel expenses. In essence, improvements to the insulation levels are purchased today to reduce tomorrow's fuel bill (Labs et al., 1988).

"The tradeoff between investment and energy savings from foundation insulation is further complicated by the fact that the thermal returns from such improvements are characterized by strong diminishing returns. The first insulation increments typically yield large fuel savings; later ones produce only modest reductions. Other important economic factors to consider include the interest on borrowed money (or of foregone interest payments from a cash payment), applicable state, federal, and property taxes, and of course the future fuel prices. For foundation systems, the problem is to determine the level of insulation that will result in the lowest life-cycle cost for the building" (Labs et al., 1988).

3.1.3.2 Method of Analysis

The method used to optimize insulation levels was to evaluate the various insulation increments and then select the one with the lowest combined life-cycle cost for conservation of energy. The procedure to determine the optimum insulation thickness was as follows:

1. The practical levels of insulation were determined.
2. The energy consumption of the selected building for each case and for the four representative cities were estimated.
3. The installation cost for each case was determined.

4. The life-cycle cost of each case was then calculated.
5. The optimal level of insulation was determined.

The total cost of an energy-conserving investment is proportional to the sum of the investment and fuel-related costs for the project over its useful life.

The price of electricity was based on the fuel prices used to develop ASHRAE Standard 90.2P (Christian and Strzepek, 1987). The costs of insulation were taken from the ASHRAE Standard 90.2P. The costs are presented in Table 14. Note that the total cost includes all hard costs, including labor, as well as indirect costs such as builder overhead and profit and other fees. The data assumes all materials and labor costs are included as well as a 30 percent subcontractor markup and a 30 percent builder markup. This is generally a very conservative set of assumptions; the total costs are 169 percent of the hard costs, whereas more typical markups are on the order of 30 to 40 percent (Labs et al., 1988).

A comprehensive and quick economic evaluation procedure that is very useful to this analysis has been formulated by Brandemuehl and Beckman (1979). Parker and Carmody (1988) showed that two economic parameters P_1 and P_2 can be used to assess the life-cycle cost of any energy savings projects. The parameter P_1 is the ratio of the present value of the life-cycle fuel savings to the first year's fuel savings. It takes into account the inflation of fuel prices over time as well as the discounting of future fuel savings according to the opportunity cost of capital:

$$P_1 = (1 - \bar{C}_f) PWF(N_E, i_F, d) \quad (3.1)$$

$$PWF(N_E, i_F, d) = \sum_{j=1}^N \frac{(1+i_F)^{j-1}}{(1+d)^j} \begin{cases} \frac{1}{(d-i_F)} \left(1 - \left(\frac{1+i_F}{1+d}\right)^N\right) & \text{if } i_F \neq d \\ \frac{N_E}{(1+i_F)} & \text{if } i_F = d \end{cases} \quad (3.2)$$

where,

d = the discount rate

i_F = the fuel price inflation rate

N_E = the analysis period (years)

C = flag for income producing venture

\bar{t} = marginal tax bracket

PWF = present worth factor

The parameter P_2 is the ratio of the life-cycle cost incurred over the useful life of the project against the initial capital investment. It takes into account all of the parameters that affect the investment costs over time such as financing and tax effects:

$$\begin{aligned} P_2 = & DP + (1 - DP) \frac{PWF(N_{\min}, 0, d)}{PWF(N_L, 0, m)} (1 - DP) \bar{t} \\ & \times \left[PWF(N_{\min}, m, d) \left(m - \frac{1}{PWF(N_L, 0, m)} \right) + \frac{PWF(N_{\min}, 0, d)}{PWF(N_L, 0, m)} \right] \\ & + (1 - C \bar{t}) M_s \times PWF(N_E, i, d) + t_r (1 - \bar{t}) V_r \times PWF(N_E, i, d) \\ & + \left(1 - C \frac{\bar{t}}{N_D} PWF(N'_{\min}, 0, d) \right) - \frac{R_v}{(1+d)^{N_E}} \end{aligned} \quad (3.3)$$

where:

m = annual mortgage interest rate

i = general inflation rate

N_L = term of loan

N_{min} = years over which mortgage payments contribute to the analysis
(usually the minimum of N_E or N_D)

N_D = depreciation lifetime in years

N'_{min} = years over which depreciation contributes to the analysis (usually
the minimum of N_E or N_D)

t_r = property tax rate based on assessed value

DP = ratio of down payment to initial investment

M_S = ratio of first year miscellaneous costs (parasitic power, insurance
and maintenance) to initial investment

V_r = ratio of assessed valuation of the foundation insulation in first year
to the initial investment in the system

R_V = ratio of resale value at the end of the period analysis to initial
investment

All economic parameters are given in their nominal terms (including inflation). The assessment allows the financial structure of an individual, firm, or institution to be assessed in the economic evaluation. The base case financial parameters used for this analysis are based on the assumptions used in ASHRAE Standard 90.2P (Labs et al., 1988). The parameters are listed in Table 15.

Use of these parameters results in economic scalar values of 0.983 for P_2 (the ratio of life-cycle costs of the conservation investment to the initial cost) and 18.79 for P_1 (the ratio of the present value of future fuel savings to the savings in the first year). These values are very similar to the ones used in ASHRAE Standard 90.2P.

Generally, the optimization results are found to be moderately sensitive to the assumed discount rate and fuel price inflation rates, particularly for the locations with large heating budgets or when a high initial fuel price is assumed (Labs et al., 1988).

The total life-cycle cost for each level of insulation is the estimated annual fuel cost for that level multiplied by P_1 , plus the total investment cost for that level multiplied by P_2 .

The fuel for this study was electricity. The price of electricity used was about 28 percent higher than the medium fuel price used for 1985 in ASHRAE Standard 90.2P. The 28% increase represents that due to inflation in fuel prices from 1985 to 1990.

Using the economic assumptions and installation costs outlined above along with the energy use results from the computer simulations, the economic analysis was calculated. A life-cycle cost was computed for all competing insulation increments for the four representative cities. Then the insulation level with the lowest life-cycle cost was selected in each of the cities.

The results shown in Table 16 and in Figures 29-32, suggest that R-10 insulation is optimal for Las Vegas. R-20 insulation is optimal for Chicago and Minneapolis. And for Washington, D.C. either an R-10 or R-20 insulation is suggested. Tables 17-20 include the annual energy end-use of the prototype building in the four U.S.

representative cities. The monthly energy consumption for the building in the different cities are tabulated in Tables 21-24.

CHAPTER IV

CONTROLS

4.1 Introduction

Automatic controls for panel heating differ from those for convective heating because of the thermal inertia characteristics of the panel heating surface and the increase in the mean radiant temperature within the space under increasing loads for panel heating (ASHRAE, 1987).

Panels such as concrete slabs have large heat storage capacity and continue to emit heat long after the room thermostat has shut off the heating mats. In addition, there is a considerable time lag between thermostat demand and heat delivery to the space, since a large part of the heat must first be stored in the thermally heavy radiant surface. This inertia will cause uncomfortable variations in space conditions unless controls are provided to detect load changes early.

In panel heating systems, lowered night temperatures will produce unsatisfactory results with heavy panels such as concrete floors. These panels cannot respond to a quick increase or decrease in heating demand within the relatively short time required, resulting in a very slow reduction of the space temperature at night and a correspondingly slow pickup in the morning.

To determine the controls strategy or the heating cycle to be adopted for proper operation of the heating system, several computer simulations for various heating strategies were performed. First, to determine the effect of mat depth on the time lag between energy input to the heating mats and output at the slab surface, mat depths of 2 to 24 inches beneath the slab were used. Figure 33 indicates that the time delay increased with mat depth, and the peak heat-flux value at the slab surface decreased. Figure 10 shows that the period of time delay is independent of the energy input to the mats, but is only a function of mat depth. Figure 9 shows that the energy output represented by the heat-flux at the slab surface is dependent on both mat depth and the energy input. The peak heat-flux value decreased with mat depth, but increased with increased energy input. Hence, to better understand the response of the system to different heating strategies, more computer runs were performed.

Three different heating cycles were investigated; Figure 34 shows the response of the system. In all three cycles, the heating mats were turned on at midnight, and then turned off at 3 a.m. In the first cycle, the heating mats were then turned on at 10 a.m. for 15 minutes, and then every three hours for 15 minutes. In the second cycle, heating was restarted also at 10 a.m. for 15 minutes, and then every four hours. In the third cycle, the same was done as in the previous cycles but the 15 minute intervals were repeated every five hours. The results of turning the heating mats on from midnight until 2 a.m. and then back on at 10 a.m. for 15 minutes are shown in Figure 35. However, to maintain the same amount of energy input as in the previous case, the heating mats were energized for 15 minutes, every 5, 6, or 7 hours. Hence,

depending on the peak load to be met and the load profile of the building, the heating mats may have to be energized intermittently, or continuously for a number of hours during off-peak rates and then intermittently during on-peak periods. Figure 36 shows that the mat depth affects how the mats should be energized. In this case, the heating mats were energized at midnight for two hours, then turned back on for 15 minutes at 8 a.m., and then every three hours for fifteen minutes. The results show that this strategy may be suitable when the heating mats are installed at a depth of seven inches below the slab surface but not when installed at depths of 12 or 16 inches. Figure 37 clearly indicates that the result of higher energy input to the mats, by turning them on for a longer period of time, is higher slab surface temperatures, and thus larger heat-flux. For a given mat depth the heating elements were energized for 2, 3, and 4 hours. The curves show that the largest heat-flux values were obtained when the mats were energized for the longest period of time, and the lowest heat-flux values were obtained when the mats were energized the least. This indicates that the surface temperature of the floor slab is higher for higher energy input.

For comfort heating applications, the surface of the slab is held to a maximum of 80 to 85°F (Nevins et al., 1964). Therefore, when used as a primary heating system, thermostatic control devices sensing air temperature should not be used to control the slab temperature, but should be wired in series with a slab sensing thermostat. The remote sensing thermostat in the slab acts as a limit switch to control the maximum surface temperature allowed on the slab. Heated slabs with

the heating elements embedded in the concrete, use indoor-outdoor thermostats to vary the floor temperature inversely with the outdoor temperature (ASHRAE, 1987). If the heat loss of the building is calculated for 70 to 0°F and the floor temperature range is held from 70 to 85°F with a remote sensing thermostat, the ratio of outdoor temperature to slab temperature is 70:15, or approximately 5:1. This means that a 5°F drop in outdoor temperature requires a 1°F increase in the slab temperature. An ambient sensing thermostat is used to vary the ratio between outdoor and slab temperatures (ASHRAE, 1987). However, when the heating mats are installed some predetermined distance below the concrete slab, there is a considerable time lag between thermostat demand and heat delivery to the space; this will cause uncomfortable variations in space conditions. Hence, controls that can detect load changes early must be provided for this type of heating system.

Slab-heating systems of the type considered in this study are typically heat storage systems that are designed to reduce electric utility costs for a design-day profile. Many existing systems use the same operating strategy for all load conditions. For non-design days, which occur most of the time, an optimum operating strategy that uses the full potential of the storage system and rate structures is highly desirable.

An optimum strategy is one that seeks to minimize the utility bill with cost-effective heating of the building. This can be achieved by taking into account utility rate structures, building load profiles, peak load, time of peak load, and system constraints. The control actions to be taken by a supervisory controller are start-time

of energizing the mats, the period of charging, and whether a continuous or intermittent heating strategy should be deployed.

To determine these parameters properly, the optimal controller requires knowledge of the next day's building heating load profile, an adaptive update of the predicted profiles, a building nonheating electric use profile, a mechanism to use this updated load profile to determine the heat discharge profile, and the system constraints.

4.2 Profile Prediction

A load profile prediction algorithm that has been developed by MacArthur et al. (1989) for use in an optimal supervisory controller is discussed in this section. The load profile prediction algorithm is composed of two distinct functions. One is used to predict the load at each hour of the next day. The other is used to predict the temperature profile that the load prediction algorithm requires for inputs. The load algorithm itself performs two tasks - estimation and prediction. In the former, model coefficients are evaluated. In the latter, the model is used to predict the load profile. A description of both the load and temperature prediction algorithms is given in the following sections.

4.2.1 Load Prediction

The load prediction algorithm gives the predicted load at time k , using the loads at previous times and the input at time k , as well as inputs at previous times, the input being the ambient temperature.

An estimation technique was devised such that the difference between the predicted load and the actual load is as small as possible. This was accomplished by implementing a recursive least-squares (RLS) technique. The RLS algorithm used to estimate the parameters is given in terms of the estimation or prediction error, the parameter vector, and the covariance matrix updates. The details of the algorithm are given in MacArthur et al. (1989).

The form of the model is such that the results are fairly insensitive to the type of building or loads for which the predictions are desired. Only the load and ambient temperature need to be measured. Profiles are predicted one day in advance; that is, profiles or hourly loads for the i^{th} day are predicted at the end of the $(i-1)^{\text{th}}$ day. For example, to predict the heating load at noon tomorrow, the historical heating loads that occurred at noon on previous days are used in conjunction with tomorrow's predicted temperatures.

At the end of each day, the recursion algorithms are used to predict the 24 hourly loads for the next day. These predictions result in the load profile for the next day. The results presented by MacArthur et al. (1989) suggest that generally there is very good agreement between the actual and predicted loads.

4.2.2 Temperature Prediction

In Section 4.2.1 it was mentioned that the load profile prediction algorithm requires the temperature profile as its input. The ambient temperature prediction algorithms predict and update the ambient temperature profile for a 24-hour cycle

using the forecasted high and low temperatures and previously measured temperature histories. The forecasted high and low temperatures are input to the algorithms by the control operator or can be automatically input from a weather station. The historical profiles are used to determine a weighted average ratio between the high and low temperatures for a given clock hour. MacArthur et al. (1989) refer to this ratio as the shape factor for the hour. The predicted ambient temperature profile is determined using the computed shape factor profile and the high and low temperatures.

The temperature profile is continuously updated as actual measurements for the predicted period become available. The error between the predicted and measured temperatures is used to update the initial forecasted high and low temperature values and is also used to correct the shape factor profile for the remaining hours of the cycle.

A reasonableness check on the shape factor calculations is performed, and if any terms are too small or too large, or if the predicted shape factors are themselves unreasonable, the profile will not be modified. This precautionary measure will result in the use of old shape factor profiles and, hence, the following day's temperature profile will have a contour dictated by the last acceptable shape profile. The predicted high and low temperatures will be defined by the new forecasted high and low temperatures.

It is worthwhile mentioning that the efficiency of the load prediction algorithm is directly affected by the temperature prediction algorithm. The impact depends on

the correlation between load and temperature and on the accuracy of the forecasted high and low temperatures input to the algorithm. The developers of this prediction algorithm (MacArthur et al., 1989) indicated in their study that a forecast error of $\pm 5^{\circ}\text{F}$ resulted in load prediction errors that ranged from 5% to -15%.

The predictor has a built-in feature to treat special days such as weekends, holidays, or any day in which the building is not operated in a normal fashion. For these situations the prediction is generated in its usual recursive fashion. The parameter estimates, however, are not updated and the predicted loads are scaled based on past performance or on operator supplied building utilization.

The technique for predicting load profiles described in the previous sections was developed for use in conjunction with an optimal cold storage controller. Since it is a general technique it can be used in a variety of applications where knowledge of future loads is required. The next section includes a description on how the load prediction algorithm can be used for optimal control of the heating system.

4.3 Optimal Control

As mentioned earlier, concrete slabs have large heat storage capacity and continue to emit heat long after the room thermostat has shut off the heating mats. In addition, there is a considerable time lag between thermostat demand and heat delivery to the space, since a large part of the heat must first be stored in the thermally heavy radiant surface. This inertia will cause uncomfortable variations in space conditions unless controls are provided to detect load changes early.

In Section 4.1 it was shown that time lags of 10 to 14 hours can result at mat depths of approximately one foot below the slab surface. Hence, knowledge of the load 10 to 14 hours in advance is needed in order to determine when and for how long the heating mats must be turned on. The load prediction algorithm described previously can be used in this case.

To study the effect that small changes in the energy input have on the behavior of the system, design sensitivity analysis on the system was done.

4.3.1 Design Sensitivity Analysis

For optimal control of the system, the heating mats must supply the proper amount of heating at the right time to the conditioned space to meet the demand, or offset the heat loss through the building envelope at all times. Considering that the heating mats supply heat according to the following distribution function:

$$g(x,t) = S e^{-1/2\left(\frac{t-\phi}{\omega}\right)^2} \delta(x - L) \quad (4.1)$$

where, S is again the heat source strength, δ is the Dirac delta function, ω is the standard deviation of the distribution, and ϕ is the mean. The objective function or the criterion that will define optimality is

$$f = \frac{1}{2} \int_0^P [q_s - q_l]^2 dt \quad (4.2)$$

where, $q_s = h(T_{slab} - T_{int})$ and q_l is the predicted load.

The problem is then to find ω and ϕ that will minimize f subject to the following constraints:

$$g_1: (T_{slab})_{max} \leq 85^\circ F \quad (4.3)$$

$$g_2: (T_{source})_{max} \leq 130^\circ F \quad (4.4)$$

Additional constraints may be imposed on ω and ϕ explicitly that will limit energy use during off-peak hours only. However, the heating mats may require energy during on-peak hours to prevent the slab from becoming very cold. For this reason such constraints were not used.

In mathematical form the problem is then to find ω and ϕ that minimize

$$f = \frac{1}{2} \int_0^P [q_s - q_i]^2 dt \quad (4.5)$$

subject to

$$g_1: T_{slab}(t_1) \leq 85^\circ F \quad (4.6)$$

$$g_2: T_{source}(t_2) \leq 130^\circ F \quad (4.7)$$

where t_1 and t_2 are the time at which the maximum slab surface temperature and the maximum heating-element temperature occur.

In order to better understand the effect of ω and ϕ on the response of the system the sensitivity of the objective function f and the constraint functions g_1 and g_2 , can be determined using the adjoint variable formulation.

The sensitivity of the objective function and the constraints are obtained as follows:

$$\frac{df}{d\omega} = \frac{\partial f}{\partial \omega} + \frac{\partial f}{\partial T} \frac{dT}{d\omega} \quad (4.8)$$

where $\frac{\partial f}{\partial \omega}$ is always zero. Using the adjoint variable method Eq. (4.8) is written as

$$\frac{df}{d\omega} = \int_0^P \lambda(L,t) \left(\frac{\partial g}{\partial \omega} \right) dt \quad (4.9)$$

where

$$\frac{\partial g}{\partial \omega} = S e^{-\nu z \left(\frac{t-\phi}{\omega} \right)^2} \left(\frac{t-\phi}{\omega} \right)^2 \frac{\delta(x-L)}{\omega} \quad (4.10)$$

and λ is the adjoint variable given by the solution to the following system of differential equations:

$$- (\rho c)_i \lambda_t^{(i)} - k_i \lambda_{xx}^{(i)} - h[h(T_{slab} - T_{int}) - q_i] \delta(x) \quad (4.11)$$

with boundary conditions

$$\lambda_x(0,t) - \lambda_x(D,t) = 0 \quad (4.12a)$$

$$k_i \lambda_x^{(i)} \Big|_{x_i} - k_{i+1} \lambda_x^{(i+1)} \Big|_{x_i} \quad (4.12b)$$

$$\lambda^{(i)} \Big|_{x_i} - \lambda^{(i+1)} \Big|_{x_i} \quad i=1,2,3 \quad (4.12c)$$

and terminal condition

$$\lambda(x,P) = 0 \quad (4.13)$$

Similarly, $\frac{dg_1}{d\omega}$ is obtained as

$$\frac{dg_1}{d\omega} = \frac{\partial g_1}{\partial \omega} + \frac{\partial g_1}{\partial T} \frac{dT}{d\omega} + \frac{\partial g_1}{\partial t} \frac{dt_1}{d\omega} \quad (4.14)$$

The first and last terms on the right-hand side of Eq. (4.14) are zero. Using the adjoint variable method Eq. (4.14) becomes

$$\frac{dg_1}{d\omega} = \int_0^P \lambda(L,t) \frac{\partial g}{\partial \omega} dt \quad (4.15)$$

with λ being the solution to the following differential equation

$$-(\rho c)_t \lambda_t^{(0)} - k_t \lambda_{xx}^{(0)} = 0 \quad (4.16)$$

with the same boundary and initial conditions described in Eqs.(4.12a-c) and terminal condition

$$\lambda(x,t_1) = -\hat{\delta}(x) \quad (4.17)$$

Likewise, $\frac{dg_2}{d\omega}$ is obtained as

$$\frac{dg_2}{d\omega} = \frac{\partial g_2}{\partial \omega} + \frac{\partial g_2}{\partial T} \frac{dT}{d\omega} + \frac{\partial g_2}{\partial t} \frac{dt_2}{d\omega} \quad (4.18)$$

Again, the first and last terms on the right-hand side of Eq. (4.18) are zero. The adjoint variable method gives Eq. (4.18) as

$$\frac{dg_2}{d\omega} = \int_0^P \lambda(L,t) \frac{\partial g}{\partial \omega} dt \quad (4.19)$$

where λ is the solution to

$$- (\rho c)_i \lambda_t^{(0)} - k_i \lambda_{xx}^{(0)} = 0 \quad (4.20)$$

and boundary conditions as in Eqs. (4.12a-c) and terminal condition

$$\lambda(x, t_2) = -\hat{\delta}(x-L) \quad (4.21)$$

Similarly, we obtain

$$\frac{df}{d\phi} = \int_0^P \lambda(L, t) \frac{\partial g}{\partial \phi} dt \quad (4.22)$$

with

$$\frac{\partial g}{\partial \phi} = S e^{-1/2 \left(\frac{t-\phi}{\omega} \right)^2} \left(\frac{t-\phi}{\omega^2} \right) \hat{\delta}(x-L) \quad (4.23)$$

and λ is the solution to Eqs. (4.11), (4.12) and (4.13).

Next, $\frac{dg_1}{d\phi}$ is obtained in a similar manner. The result is

$$\frac{dg_1}{d\phi} = \int_0^P \lambda(L, t) \frac{\partial g}{\partial \phi} dt \quad (4.24)$$

λ being the solution to Eqs. (4.16), (4.17) and (4.12). Also, $\frac{dg_2}{d\phi}$ is obtained as

$$\frac{dg_2}{d\phi} = \int_0^P \lambda(L, t) \left(\frac{\partial g}{\partial \phi} \right) dt \quad (4.25)$$

with λ being the solution to the problem described in Eqs. (4.20), (4.21) and (4.12).

The sensitivity of f to ω for various values of ω and ϕ for a 1% perturbation in ω is listed in Table 25. Similarly, the sensitivity of f to ϕ for different values of ω and ϕ for a 1% perturbation in ϕ is listed in Table 26. Actual changes in f and the change predicted by the associated design sensitivity analysis method are also

tabulated. The relative error between the actual and approximate change is also tabulated in Tables 27 and 28.

The sensitivity of g_1 and g_2 to ω for various values of ω and ϕ for a 1% perturbation in ω are shown in Table 29 and Table 30. Table 33 and Table 34 show the sensitivity of g_1 and g_2 to ϕ for a 1% perturbation in ϕ . In this case the heaters were assumed to be on during the previous day. Tables 31-34 also show the % error in the computation of the sensitivities of g_1 and g_2 with respect to the variables ω and ϕ using the adjoint variable approach (Exact) and the finite difference approach (Approximate, based on a 1% step size). Tables 27 and 28 also list the % error in the computation of the sensitivities of f with respect to ω and ϕ .

The results for the sensitivity of g_2 obtained with the design sensitivity analysis are very accurate. However, the results of the sensitivity of f and g_1 are not as accurate due to the very small changes in f and g_1 , leading to inaccuracy in the difference between $f^{(1)}$ and $f^{(2)}$, $g_1^{(1)}$ and $g_1^{(2)}$ values in calculating the approximate change.

The design sensitivity analysis method will be used on a daily basis to determine the required sensitivities. For each new value of ω and ϕ the heat conduction equation is used to solve for the heat-flux at the slab surface, q_s , the maximum slab surface temperature, and the maximum heating element temperature. At the beginning of each day, the previous day's temperature distribution is used as the initial conditions for the current day. The sensitivities are then calculated and a new

value for ω and ϕ can be determined. The procedure is then repeated for the next day.

However, with this model there is no guarantee that f will approach zero at optimality. Moreover, the cost of electric usage is not minimized. A model that would insure minimum cost of electric usage, while meeting the required loads is now formulated. The problem is to find ω and ϕ that will minimize the cost of electric usage subject to the system constraints. In mathematical form the problem is to find ω and ϕ that minimize f the cost of electric usage, or

$$f = K \int_0^P g(x,t) dt \quad (4.26)$$

where

K = cost of electricity (\$/KWH)

g = heat source power (KW)

subject to

$$g_1: \frac{1}{2} \int_0^P [q_s - q_i]^2 dt \leq e \quad (4.27)$$

$$g_2: (T_{slab})_{max} \leq 85^\circ F \quad (4.28)$$

$$g_3: (T_{source})_{max} \leq 130^\circ F \quad (4.29)$$

In this case

$$f = K \int_0^P \int_0^D S e^{-1/2 \left(\frac{t-\phi}{\omega} \right)^2} \delta(x-L) dx dt \quad (4.30)$$

$$\frac{df}{d\omega} = K \int_0^P \int_0^D S e^{-1/2 \left(\frac{t-\phi}{\omega} \right)^2} \left(\frac{t-\phi}{\omega} \right)^2 \frac{\delta(x-L)}{\omega} dx dt \quad (4.31)$$

$$\frac{df}{d\phi} = K \int_0^P \int_0^D S e^{-1/2 \left(\frac{t-\phi}{\omega} \right)^2} \left(\frac{t-\phi}{\omega^2} \right) \delta(x-L) dx dt \quad (4.32)$$

A controller that utilizes the information from the load prediction algorithm and the results of the optimization algorithm can be used to operate the heating mats. Figure 38 is an illustration of the controller functions in block diagram form.

Hourly dry bulb temperatures for January for Chicago, Minnesota, Washington D.C., and Las Vegas are shown in Figures 39-42. Load profiles for different days in January were calculated for the four representative cities. The results are presented in Figures 43-58. These figures illustrate that some days are characterized by high load profile fluctuations, while others are characterized by nearly uniform load profiles. This suggests that no single strategy for operating the heating system over a period of one year will work. The load profiles change on an hourly, daily, and monthly basis. This fact makes it difficult to control the temperature of the air in the heated space. Hence, a controller such as the one described in this study is necessary to maintain a comfortable environment. For this reason such a heating system may not be suitable for heating residential or office buildings. However, it may be suitable for heating storage and maintenance facilities. An expensive control system may be economically unfeasible, however, if used in maintenance or storage facilities.

CHAPTER V

RESULTS, DISCUSSION AND CONCLUSIONS

5.1 Results and Discussion

In Section 3.2.1 the results of varying the heater placement were presented. The results indicate that higher slab surface temperatures were achieved when the heaters were installed closer to the concrete slab than when they were installed at a deeper location. There was a 50% decrease in the maximum heat-flux delivered by the slab when the mat depth was increased from 7 to 13 inches. However, the corresponding slab surface temperature decreased by only 5%. Installing the mats even deeper into the ground resulted in lower slab temperatures and thus lower heat-flux at the slab surface for the same energy input. The time lag between when the heater energy was input and when it was output at the slab surface was also affected by the depth of placement of the heaters. Even with the heaters installed at 2 inches beneath the slab, a 3 hour time lag was observed. However, time lags of up to 50 hours were recorded for mat depths of up to 2 feet. The reason for that is two-fold. First, with deeper mats, there is an increase in the storage capacity. Second, there is an increase in the thermal resistance between the heaters and the slab surface. This

results in the operation of the heaters at higher temperatures to meet the loads. Figure 59 shows that the deeper mats operated at higher temperatures. Hence, the slower diffusion of heat is a result of the combined effect of the larger storage volume being heated to a higher temperature.

The performance of the heating system is also affected by the amount of energy input to the mats. Figure 60 shows the maximum slab surface temperature as a function of mat depth for several energy inputs. The results indicate that the maximum allowable slab surface temperature was not exceeded at any mat depth even when the mats were operated at full power for 5 hours. Figure 61, however, shows that the maximum allowable temperature of the heating element was exceeded when the mats were energized for more than 3 hours. Determination of the optimum mat depth was discussed in Chapter III.

It was also found that the response of the system depends on the sand properties. The thermal properties of the sand vary with moisture content. Figure 5 shows the thermal properties of sand for different sand moisture contents. In the next section the response of the system for different sand properties is discussed.

5.1.2 Effect of Moisture Content on Sand Thermal Properties

In this section the importance of soil moisture content and its effect on the estimation of the heat loss through the building foundation is discussed. The information presented here is given in the Feasibility Study for Collecting Site Soil Characterization Thermal Property Data for Residential Construction (Salomone, 1988).

The impact of moisture in and around foundations on heat transfer is not completely understood. This has resulted in poor estimation of foundation heat loss. Computer models have generated results that differ by factors of two to three from measured data. The largest uncertainty in modeling heat and mass transfer around building foundations is the soil condition. To better estimate the seasonal energy loss through the foundation, some guidance in selecting the soil thermal properties must be provided to the building analyst. Information on where the moisture content is significant and should be included in the energy loss estimation, and where it can be ignored and its impact on heat transfer is also needed.

The thermal resistivity of soils is determined by the type and distribution of the soil components: minerals, organic matter, moisture and air. The thermal resistivity of soils usually depends on composition (percent sand, silt, clay and organic matter), moisture content and dry density.

Figure 62 shows the variation of sand thermal resistivity with moisture content. The figure shows that generally below the critical moisture content there is a large increase in the thermal resistivity for a small decrease in moisture content. In this region the thermal resistivity is considered to be unstable. Above the critical moisture content, the thermal resistivity is fairly constant and this region is called the "stable region". Hence, from this figure the thermal resistivity for a given moisture content can be determined.

For soils with a minimum moisture content greater than the critical moisture content, the soil can be considered stable, and a constant value of thermal resistivity can be used. However, if the minimum moisture content is less than the critical

moisture content, the appropriate value for thermal resistivity would fall between the value of thermal resistivity established for the stable region and the thermal resistivity of the soil in the dry state.

As moisture is added to the soil around the soil particles or wedges of water at the contacts, a path for the flow of heat bridges the air gap between the soil particles. By increasing the effective contact area between particles, the wedges of water greatly increase the thermal conductivity of the soil. As the moisture content increases further, the effective contact area no longer increases. Consequently, a significant increase in the thermal conductivity is not evident when more moisture is added to fill the pore space. The critical moisture content is then the moisture content at which no significant increase in thermal conductivity is observed. It has been shown by Salomone (1988) that the critical moisture content depends on density and soil type. The critical moisture content increases as density decreases and texture becomes finer. In addition to the importance of moisture contents in soils, the concept of moisture migration also plays a role in the estimation of foundation heat-flux.

The concept of moisture migration has been explained by Radhakrishna (1980) as follows: "Heat flow through a wet soil occurs mainly by conduction. At high moisture levels, liquid fills the gaps between soil particles and provides a continuous medium, making the soil-water mass an efficient thermal conductor. When a significant heat-flux is emitted from a source within a soil mass, liquids tend to vaporize near the heat source and to condense in cooler regions away from it. On the other hand, capillary suction causes a liquid return flow that tends to maintain

a constant moisture distribution throughout the soil (promoting thermal stability). Once the amount of liquid in the soil drops below the critical moisture content, the opposing heat flow causes the liquid thermal bridges between the soil particles to break down more rapidly than the capillary suction can replace them. This in turn increases the thermal gradients in the soil, causing more moisture migration and resulting in a significant increase in the thermal resistivity around the heat source. This condition is termed thermal instability or thermal runaway."

Therefore, in a purely diffusive field, the soil moisture content is usually lower in the higher temperature region and higher in the lower temperature region. Since the temperature distribution depends on the soil moisture flow and the thermal conductivity, which, in turn, is a function of the thermally driven moisture distribution, then the phenomenon of coupled heat and mass transfer exists in the ground. Results of computer simulations of a basement wall backfilled with a sandy soil have shown that the coupled effect increases the wall heat loss by 9% during the winter (Labs et al., 1988). Whereas for clay soil the coupled effect results in no appreciable differences (Shen, 1986). No coupled heat and mass transfer was included in this study.

Despite the influence of the above factor on thermal conductivity of soils, it has been reported by Salomone (1988) that a majority of existing computer models that are used to calculate foundation heat-fluxes do not account for variation in soil thermal conductivity. But rather, constant values of soil thermal properties are often used. Because of the uncertainty in modeling heat and mass transfer around

uninsulated building foundations, more representative values of soil thermal properties are required. The uninsulated case is needed in order to optimize the foundation insulation levels. Knowledge of the energy savings of going from no insulation to the first increment of insulation is needed to determine optimum insulation levels.

5.1.3 Effect of Sand Moisture Content on Heat Loss

To gain a better understanding of the influence of sand moisture content on the heat loss calculations, numerous computer simulations were performed for various sand properties with different moisture contents. Figures 63-68 show the heat-flux at the slab surface for various moisture contents. The results clearly indicate the dependency of heat-flux values on sand moisture content. Figure 63 indicates that when sand properties with zero percent moisture content were used, the slab heat-flux was lower than when sand properties with 10% or 20% moisture content were used. However, when sand with 40% moisture content was used the heat-flux was lower than that for dry sand. Figures 64 and 65 suggest that when the heating elements are installed deeper in the ground and hence a thicker sand layer is used, no definite relation can be made between percent moisture content and heat loss. However, the results in these figures show that moisture content also influences the heat diffusion rate. In all cases, when properties of dry sand were used in the computer simulations, the heat diffusion rate was the smallest. Figure 69 shows the time delay between when the energy was input to the heating elements, and when

it was output at the slab surface for various mat depths and heat inputs. As in the case of moist sand, the time delay was nearly independent of the energy input. However, it was found to be dependent on mat depth. When the heating mats were installed closest to the concrete slab the time delay was a minimum. When they were installed further away from the slab the time lag increased. With the heating mats installed about 6 inches from the slab surface the peak heat-flux occurred about 2 hours after the heating mats were turned off. However, for a mat depth of 21 inches about 56 hours elapsed between the time of the peak heat-flux and the time the energy input was terminated. Figure 70 shows the peak heat-flux versus mat depth for various energy inputs. The results shown in Figure 71 indicate that the maximum allowable slab temperature of 85° F was exceeded at mat depths less than 9 inches when the mats were energized for more than 3 hours. Whereas, when sand properties with 20% moisture content were used, the maximum allowable slab surface temperature was exceeded at a mat depth of 7 inches when the mats were energized for 5 hours, as shown in Figure 60. Because of the influence of sand moisture content on heat-flux calculations, computer simulations with thermal properties of dry sand were used to determine the optimal insulation levels for the four representative U.S. cities selected for these studies. The results are shown in Figures 72, 73 and 74.

In this case, when dry sand was used, the heat lost to the ground with no insulation was on the average 48% of the energy input. When an R-5 insulation layer was added the heat loss was 35%. When R-40 insulation was simulated the

heat lost to the ground was 12%, that is a 75% decrease from the case of no insulation.

Tables 33-36 list the results of the life-cycle cost analysis for each of the representative cities. For all four cities, R-20 insulation was the optimum insulation level, based on life-cycle costs, to be used. In Chapter III different insulation levels were selected as optimum for the different cities, when sand with a 20% moisture content was used. The results clearly indicate the effect of sand thermal properties on the optimum insulation levels to be selected for each city.

The effect of sand moisture content on the maximum allowable heating elements temperature was also investigated. Figure 75 shows the maximum allowable heating element temperature for various energy inputs, when dry sand was used. The results indicate that the maximum allowable temperature of 130°F was exceeded when the heaters were turned on for more than one hour. Whereas, Figure 61 shows that the heaters could be safely turned on as long as three hours. However, the maximum allowable temperature was exceeded when the heaters were energized for more than 3 hours.

The results presented in Figures 76-84 strongly emphasize the importance of using the appropriate soil thermal properties for foundation heat-flux calculations. Sand with a thermal diffusivity of 0.044 ft²/hr was used to generate these results. Figures 76-78 show the slab heat-flux history for various mat depths. Figures 79-81 represent the variation of the heat-flux for different sand bed thicknesses. The effect of varying insulation levels is presented in Figures 82-84. In this case, the results

suggest that some insulation must be added to reduce the heat loss to the ground. In addition, the results indicate that the first increment of insulation was sufficient. However, additional insulation was not economically feasible. Compared to the previous cases when dry sand and sand with 20% moisture content were used, the present case clearly demonstrates the effect of sand thermal properties on the heat-flux calculations, and hence on the performance of the heating system. The maximum heat-flux values were about 25% higher than for moist sand, and 1.6 times larger for dry sand. The heat diffusion rate was about 30% higher for moist sand, and 3.5 times that of dry sand.

5.1.4 Selection of Insulation Products

In general, insulation material can be placed on the outside or inside of the foundation walls or under the slab. In this study the insulation was placed horizontally below the heaters. In all cases the insulation is exposed to the soil or sand. Insulation materials, under these conditions, must not degrade or lose their thermal resistance when exposed to moisture. Acceptable materials are extruded polystyrene boards (XEPS) under any condition and molded expanded polystyrene boards (MEPS) for vertical applications when porous backfill and adequate drainage are provided (Labs et al., 1988).

Exterior insulation can be installed on the outside surface of basement, crawl space, and slab-on-grade foundation walls or extend horizontally away from them. Exterior placement is referred to whenever the insulation is in contact with the soil.

When insulation materials are placed outside the foundation structure, the following considerations are applicable:

1. When placed vertically on a foundation wall, the insulation must have sufficient compressive strength to withstand the lateral pressures generated by the backfill soil without excessively deforming the insulation layer (and, therefore, changing the insulation's thermal resistance). At a depth of 7 feet below ground, the lateral pressure is estimated to be between 200 psf and 450 psf. For a one-story basement depth or less, most rigid or semi-rigid insulations are strong enough to be serviceable (Labs et al., 1988).
2. When placed horizontally, the insulation must be strong enough to resist the vertical compressive stresses in the soil. These stresses increase at approximately 120 psf per foot depth below the ground surface (Labs et al., 1988). It must also resist the stresses and displacements imposed on it during backfilling and any subsequent settlement. The surface should be carefully prepared and compacted beneath the insulation to provide an even support to the insulation layer and backfilled above to prevent direct damage.
3. Labs et al. (1988) report that since waterproofing the foundation outside an external insulation is not recommended because of the problems of tracing a water leak, the insulation will usually be exposed to ground moisture conditions outside the waterproofing layer. The severity of this exposure can be mitigated by a good drainage

system around the foundation and by a polyethylene sheet to separate the insulation from the soil. An exterior insulation placed below grade is considered to be in an undesirable environment because of moisture gain of the insulation.

Extruded polystyrene boards are acceptable under any condition. They have relatively low water absorption by total immersion (0.3%), their water vapor permeability is 1.1 perm-in., flexural strength is 50 psi, and compressive resistance of 25 psi. It loses some R-value with time but is very stable after an initial "aging" process. The thermal conductivity is usually given as a five year aged value. Insulation sheet thickness is usually limited to less than 4 inches. Another type of insulation that is also suitable for external placement is MEPS insulation. It has similar flexural and compressive strengths as XEPS insulation, but it has a higher permeability to water vapor, and less resistance to moisture absorption. However, MEPS insulation is available in thicker sections (up to 32 inches) than most types of foam insulations, and is less expensive than XEPS insulation (Labs et al., 1988).

5.2 Conclusions

The following conclusions are supported by the results in this study:

1. The results indicate that the response of the system was strongly sensitive to the mat depth. Placing the mats close to the slab surface allows for quick response to changing loads, but it has the disadvantage of allowing the inside air temperature to drop rapidly when the mats are turned off. Deeper mats cannot respond quickly but the storage

capacity is greater which is needed in order to use off-peak electric power.

2. The effect of varying the thickness of the sand bed beneath the mats on the response of the system was found to be insignificant. Since the purpose of providing a sand layer beneath the mats is to protect the heating elements from stones and hard objects that can cut into the mats and cause them to fail, a 2 inch sand layer was found to be sufficient.
3. Determining the optimal insulation thicknesses based on life-cycle costs depends on fuel prices, insulation cost, economic parameters, and climate. The optimal insulation thickness determined in this study may change if different fuel prices, insulation costs, and economic parameters are used.
4. The mathematical model for determining the optimal insulation thickness developed in Section 3.2, is more expensive (regarding computer time) than the parametric study. The optimal solution given by this model depends on the terminal time P and the grid size. The optimal solution must be obtained for P equal to at least one year. And to achieve accurate results the grid size must be small.
5. For foundation heat-flux calculations the appropriate soil thermal properties must be selected. The response of the system is greatly influenced by the soil thermal properties. The thermal resistivity of soil changes with moisture content. It increases with moisture content

up to the critical moisture content. Beyond that, the thermal resistivity tends to remain constant.

6. Because of the difficulty to control the temperature of the air in the heated space, this heating system may not be suitable for heating residential or office buildings. However, it may be suitable for heating storage and maintenance facilities.
7. When the heating mats are installed a predetermined distance below the concrete slab, there is a considerable time lag between thermostat demand and heat delivery to the space. Hence, controls that can detect load changes early must be provided for this type of slab-heating.
8. A load prediction algorithm is needed to predict load changes 24 hours in advance in order to determine the start time of energizing the mats, the period of charging, and whether a continuous or intermittent heating strategy should be deployed.
9. The increased below-grade heat loss for slab heating results in a higher energy usage than for direct systems. Nevertheless, since off-peak power is used exclusively, the energy cost for slab heating could be less.
10. Slab-heating systems share the advantage of other radiant heating methods in that the air temperature can be lower than for convective-type systems. In addition, they are quiet and clean.

5.3 Recommendations for Future Work

- 1. Analysis of earth contact systems that (1) realistically couple the earth contact facets of a building to the other building elements including above grade roofs and walls, (2) model the effect of changes in the internal loads due to people, lights, equipment, and direct solar gain, on earth contact heat transfer, and (3) account for the interaction between various passive design strategies are needed.**
- 2. To make more useful predictions of the energy performance of common earth contact configurations (basements, crawl spaces, floor slabs) more attention is needed on modeling three-dimensional heat flow from the floor, from corners, and from the building as a whole.**
- 3. Detailed measurements of foundation heat transfer in buildings is needed. Because soil thermal properties are strongly influenced by moisture content, soil moisture retention characteristics, water table movement, and coupled heat and mass transfer which affect the moisture distribution around foundations, and associated heat transfer, more understanding of the above factors is needed.**
- 4. Soil thermal conductivity is the primary variable that influences heat loss or gain from earth contact surfaces and underground electric cables. Also, the impact of moisture in and around foundations on heat transfer is not completely understood. The biggest uncertainty in modeling heat and mass transfer around building foundations is the soil condition. Some systematic testing of soils is needed to better**

select the soil thermal properties for foundation heat-flux calculations. In addition, studies of the influence of moisture on the heat transfer are also needed to determine when the moisture content is significant and should be included in the heat loss calculation, and when it can be ignored.

5. Because optimization methods using economic analysis depend on fuel prices, insulation costs, and economic parameters, knowledge of fuel prices, insulation costs, and interest rates in the different cities of the United States is needed to determine optimal insulation levels for buildings in each city.

TABLES

TABLE 1
List of Climate Cities

City, State	HDD (based on 65F)	Min. Temp (F)	Max. Temp (F)
Minneapolis, MN	8,400	-22.5	92.5
Chicago, IL	6,600	-2.5	92.5
Washington DC	4,200	12.5	87.5
Las Vegas, NV	2,700	17.5	112.5

TABLE 2
Description of Prototype Building in Washington, DC

Building Type	:	Warehouse
Building gross floor area	:	100,000 ft²
Building net conditioned area	:	100,000 ft²
Number of zones	:	5
Building Location		
North latitude	:	38.5 deg
West longitude	:	77 deg
Time Zone Number	:	5
Daylight Savings Time	:	No
Typical Weekday Operating Schedule		
Occupancy start hour	:	8
Operating hours/day	:	10
Summer Thermostat Schedule		
Beginning month	:	May
Ending month	:	September
Typical Occupied Schedule		
Weekdays from	:	800 to 1700
Saturdays from	:	900 to 1600
Sundays from	:	0 to 0
Thermostat Set Point Temperatures		
Summer occupied temperature	:	80 deg F
Winter occupied temperature	:	70 deg F
Winter unoccupied temperature	:	70 deg F
Daylighting analysis	:	No
Lighting system type	:	Sus-Fluor
Percent light heat to space	:	100
Wall U-Factor (Btu/hr-ft²- F)	:	0.087
Wall construction group	:	E
Color correction	:	Medium
Roof U-Factor (Btu/hr-ft²- F)	:	0.056
Roof construction code	:	9
Color correction	:	Light
Shading coefficient	:	0.55
Window U-Factor (Btu/hr-ft²- F)	:	0.68
Space mass code	:	Medium
Leakage coefficient	:	3
Occupied air change rate	:	0.5 air changes per hour

TABLE 3
Description of Prototype Building in Chicago, IL

Building Type	: Warehouse
Building gross floor area	: 100,000 ft ²
Building net conditioned area	: 100,000 ft ²
Number of zones	: 5
Building Location	
North latitude	: 42 deg
West longitude	: 87.5 deg
Time Zone Number	: 6
Daylight Savings Time	: No
Typical Weekday Operating Schedule	
Occupancy start hour	: 8
Operating hours/day	: 10
Summer Thermostat Schedule	
Beginning month	: May
Ending month	: September
Typical Occupied Schedule	
Weekdays from	: 800 to 1700
Saturdays from	: 900 to 1600
Sundays from	: 0 to 0
Thermostat Set Point Temperatures	
Summer occupied temperature	: 80 deg F
Winter occupied temperature	: 70 deg F
Winter unoccupied temperature	: 70 deg F
Daylighting analysis	: No
Lighting system type	: Sus-Fluor
Percent light heat to space	: 100
Wall U-Factor (Btu/hr-ft²- F)	: 0.087
Wall construction group	: E
Color correction	: Medium
Roof U-Factor (Btu/hr-ft²- F)	: 0.056
Roof construction code	: 9
Color correction	: Light
Shading coefficient	: 0.55
Window U-Factor (Btu/hr-ft²- F)	: 0.68
Space mass code	: Medium
Leakage coefficient	: 3
Occupied air change rate	: 0.5 air changes per hour

TABLE 4
Description of Prototype Building in Minneapolis, MN

Building Type	:	Warehouse
Building gross floor area	:	100,000 ft²
Building net conditioned area	:	100,000 ft²
Number of zones	:	5
Building Location		
North latitude	:	44.5 deg
West longitude	:	93.1 deg
Time Zone Number	:	6
Daylight Savings Time	:	No
Typical Weekday Operating Schedule		
Occupancy start hour	:	8
Operating hours/day	:	10
Summer Thermostat Schedule		
Beginning month	:	June
Ending month	:	August
Typical Occupied Schedule		
Weekdays	from	: 800 to 1700
Saturdays	from	: 900 to 1600
Sundays	from	: 0 to 0
Thermostat Set Point Temperatures		
Summer occupied temperature	:	80 deg F
Winter occupied temperature	:	70 deg F
Winter unoccupied temperature	:	70 deg F
Daylighting analysis	:	No
Lighting system type	:	Sus-Fluor
Percent light heat to space	:	100
Wall U-Factor (Btu/hr-ft²- F)	:	0.07
Wall construction group	:	E
Color correction	:	Medium
Roof U-Factor (Btu/hr-ft²- F)	:	0.047
Roof construction code	:	9
Color correction	:	Light
Shading coefficient	:	0.55
Window U-Factor (Btu/hr-ft²- F)	:	0.45
Space mass code	:	Medium
Leakage coefficient	:	3
Occupied air change rate	:	0.5 air changes per hour

TABLE 5
Description of Prototype Building in Las Vegas, NV

Building Type	:	Warehouse
Building gross floor area	:	100,000 ft²
Building net conditioned area	:	100,000 ft²
Number of zones	:	5
Building Location		
North latitude	:	36.1 deg
West longitude	:	115.1 deg
Time Zone Number	:	8
Daylight Savings Time	:	No
Typical Weekday Operating Schedule		
Occupancy start hour	:	8
Operating hours/day	:	10
Summer Thermostat Schedule		
Beginning month	:	May
Ending month	:	October
Typical Occupied Schedule		
Weekdays from	:	800 to 1700
Saturdays from	:	900 to 1600
Sundays from	:	0 to 0
Thermostat Set Point Temperatures		
Summer occupied temperature	:	80 deg F
Winter occupied temperature	:	70 deg F
Winter unoccupied temperature	:	70 deg F
Daylighting analysis		
Lighting system type	:	Sus-Fluor
Percent light heat to space	:	100
Wall U-Factor (Btu/hr-ft²- F)		
Wall construction group	:	E
Color correction	:	Medium
Roof U-Factor (Btu/hr-ft²- F)		
Roof construction code	:	9
Color correction	:	Light
Shading coefficient		
Window U-Factor (Btu/hr-ft²- F)	:	0.81
Space mass code	:	Medium
Leakage coefficient		
Occupied air change rate	:	0.5 air changes per hour

TABLE 6
 Characteristics of Eq. (2.8) for three Values of the Weighting Factor γ

γ	Number of unknowns	Solution Method	Truncation error	Name of Method	Stability
0	1	Explicit	$O[\Delta t, (\Delta x)^2, (\Delta y)^2]$	Forward-time, central space (FTCS), Euler Method.	Conditional
1/2	5	Implicit	$O[(\Delta t)^2, (\Delta x)^2, (\Delta y)^2]$	Midpoint-time, central space, (MTCS); Crank-Nicolson.	Unconditional
1	5	Implicit	$O[\Delta t, (\Delta x)^2, (\Delta y)^2]$	Backward-time, central space, (BTCS); Laasonen Method.	Unconditional

TABLE 7
 Properties of Materials Used

Material	Thermal conductivity (Btu/hr-ft-F)	ρc (Btu/ft ³ -F)	Moisture content (Percent)
Concrete	.54	22.0	
Sand	.16	18.9	0
	.36	22.0	5
	.59	25.1	10
	.86	31.4	20
	.91	37.6	30
	.92	43.8	40
Soil	.50	20.0	
Insulation	.017	2.1	

TABLE 8
Peak Load Summary for Prototype
Building in Washington, DC

	COOLING		HEATING
Time of Peak	Jul hour = 17		Jan hour = 6
Outside Temp	87.5 deg F		12.5 deg F
	Sensible (Btu/hr)	Latent (Btu/hr)	Sensible (Btu/hr)
Glass Solar	105,532		0
Glass Conduction	37,128		-121,992
Wall Conduction	19,001		-62,431
Roof Conduction	98,000		-322,000
Opaque Solar	84,737		0
Door Conduction	0		0
Misc Conduction	0		0
Occupants	153,491	217,368	0
Lights	94,690		0
Equipment	30,711		0
Misc Sensible	0		0
Infiltration	77,880		-277,956
Total	701,169		-784,379
Total Load/Area	7.0	(Btu/hr-ft ²)	-7.0

TABLE 9
Peak Load Summary for Prototype
Building in Chicago, IL

	COOLING		HEATING
Time of Peak	Apr hour = 17		Feb hour = 5
Outside Temp	87.5 deg F		-2.5 deg F
	Sensible (Btu/hr)	Latent (Btu/hr)	Sensible (Btu/hr)
Glass Solar	106,387		0
Glass Conduction	37,128		-153,816
Wall Conduction	19,001		-78,718
Roof Conduction	98,000		-406,000
Opaque Solar	86,288		0
Door Conduction	0		0
Misc Conduction	0		0
Occupants	153,491	217,368	0
Lights	94,690		0
Equipment	30,711		0
Misc Sensible	0		0
Infiltration	86,589		-364,306
Total	712,284		-1,002,839
Total Load/Area	7.1	(Btu/hr-ft ²)	-10.0

TABLE 10
Peak Load Summary for Prototype
Building in Minneapolis, MN

	COOLING		HEATING
Time of Peak	Jul hour = 17		Jan hour = 6
Outside Temp	92.5 deg F		-22.5 deg F
	Sensible (Btu/hr)	Latent (Btu/hr)	Sensible (Btu/hr)
Glass Solar	108,335		0
Glass Conduction	31,590		-129,870
Wall Conduction	19,656		-80,808
Roof Conduction	105,750		-434,750
Opaque Solar	63,218		0
Door Conduction	0		0
Misc Conduction	0		0
Occupants	153,491	217,368	0
Lights	94,690		0
Equipment	30,711		0
Misc Sensible	0		0
Infiltration	117,465		-401,941
Total	724,905		-1,047,369
Total Load/Area	7.2	(Btu/hr-ft ²)	-10.5

TABLE 11
Peak Load Summary for Prototype
Building in Las Vegas, NV

	COOLING		HEATING
Time of Peak	Jul hour = 17		Jan hour = 5
Outside Temp	112.5 deg F		17.5 deg F
	Sensible (Btu/hr)	Latent (Btu/hr)	Sensible (Btu/hr)
Glass Solar	89,853		0
Glass Conduction	82,134		-132,678
Wall Conduction	89,232		-144,144
Roof Conduction	172,250		-278,250
Opaque Solar	126,253		0
Door Conduction	0		0
Misc Conduction	0		0
Occupants	153,491	217,368	0
Lights	94,690		0
Equipment	30,711		0
Misc Sensible	0		0
Infiltration	166,471		-232,713
Total	1,005,086		-787,785
Total Load/Area	10.1	(Btu/hr-ft ²)	-7.9

TABLE 12
Building Energy Consumption for Various Insulation Levels

Insulation (hr-ft ² -F/Btu)	Annual Energy Consumption (KWH)			
	Las Vegas	Washington DC	Chicago	Minneapolis
R-0	411,460	575,225	851,132	856,519
R-5	356,790	498,796	738,044	742,715
R-10	333,771	466,616	690,429	694,798
R-20	313,630	438,458	648,765	652,871
R-30	304,998	426,390	630,910	634,902
R-40	302,121	422,368	624,957	628,912

TABLE 13
Fuel Cost Savings

Insulation (hr-ft ² -F/Btu)	Annual Fuel Cost Savings (\$/lineal ft)			
	Las Vegas	Washington DC	Chicago	Minneapolis
R-0	-	-	-	-
R-5	1.49	2.08	3.07	3.09
R-10	2.16	3.02	4.47	4.50
R-20	2.67	3.73	5.51	5.55
R-30	2.98	4.16	6.15	6.19
R-40	3.01	4.20	6.21	6.25

TABLE 14
Insulation Costs

Inulation Level (R-value) (F-ft ² -hr/Btu)	Total Cost (\$/Lineal Foot)
5	15.4
10	26.2
20	40.0
30	66.2
40	92.3

TABLE 15
Economic Parameters Used in the Analysis

Inflation Rate (i)	5%
Fuel Price Inflation Rate (i_F)	7%
After Tax Discount Rate (d)	10%
Finance Rate (m)	12%
State and Federal Tax Bracket (\bar{i})	30%
Down Payment Percentage (DP)	10%
Property Tax Rate (t_p)	1%
Analysis Period in Years (N_E)	30
Mortgage Period in Years (N_L)	30
O&M Fraction (M_S)	0%
Resale Value (R_v)	0%

TABLE 16
Life-Cycle cost Analysis

Insulation Level (R-value) F-ft ² -hr/Btu	Fuel Life-Cycle Cost				Fuel Life-Cycle Cost Savings				Total Life-Cycle Cost			
	LasV	Wash	Chic	Minn	LasV	Wash	Chic	Minn	LasV	Wash	Chic	Minn
0	214	299	443	445	-	-	-	-	-	-	-	-
5	186	260	385	387	27.9	39.0	57.7	58.1	202	276	401	403
10	173	242	359	361	40.6	56.8	84.0	84.5	200	268	385	387
20	164	229	339	341	50.1	70.0	104	104	204	269	379	381
30	158	221	327	329	55.9	78.1	116	116	224	287	393	395
40	157	220	326	328	56.5	78.9	117	118	249	312	418	420

All costs are in dollars per lineal foot.

LasV=Las Vegas

Chic=Chicago

Wash=Washington DC

Minn=Minneapolis

TABLE 17
Annual Energy End-Use of Prototype
Building in Washington, DC

	Electric (KWH)	Site (MBtu)
Heating Energy		
Electric Resistance	402,255	1,372.89
Cooling Energy	0	0
Domestic Hot Water Energy	0	0
Building Miscellaneous		
Lights	77,589	264.81
Equipment	3,524	12.03
Consumption Totals	483,367	
Unit Cost	\$0.036	
Dollar Cost	\$17,401	\$17,401
Site Energy (MBtu)	1,649.7	1,649.7
Source Energy (MBtu)	5,607.1	5,607.1

TABLE 18
Annual Energy End-Use for Prototype
Building in Chicago, IL

	Electric (KWH)	Site (MBtu)
Heating Energy Electric Resistance	595,197	2,031.41
Cooling Energy	0	0
Domestic Hot Water Energy	0	0
Building Miscellaneous Lights	77,589	264.81
Equipment	3,524	12.03
Consumption Totals	676,309	
Unit Cost	\$0.036	
Dollar Cost	\$24,347	\$24,347
Site Energy (MBtu)	2,308.2	2,308.2
Source Energy (MBtu)	7,845.2	7,845.2

TABLE 19
Annual Energy End-Use of Prototype
Building in Minneapolis, MN

	Electric (KWH)	Site (MBtu)
Heating Energy		
Electric Resistance	598,964	2,044.26
Cooling Energy	0	0
Domestic Hot Water Energy	0	0
Building Miscellaneous		
Lights	77,589	264.81
Equipment	3,524	12.03
Consumption Totals	680,077	
Unit Cost	\$0.036	
Dollar Cost	\$24,483	\$24,483
Site Energy (MBtu)	2,321.1	2,321.1
Source Energy (MBtu)	7,888.9	7,888.9

TABLE 20
Annual Energy End-Use of Prototype
Building in Las Vegas, NV

	Electric (KWH)	Site (MBtu)
Heating Energy Electric Resistance	287,734	982.03
Cooling Energy	0	0
Domestic Hot Water Energy	0	0
Building Miscellaneous Lights	77,589	264.81
Equipment	3,524	12.03
Consumption Totals	368,846	
Unit Cost	\$0.036	
Dollar Cost	\$13,278	\$13,278
Site Energy (MBtu)	1,258.9	1,258.9
Source Energy (MBtu)	4,278.6	4,278.6

TABLE 21
Monthly Energy Consumption for Prototype
Building in Washington, DC

Month	Electricity (KWH)	Totals Through Month (KWH)
Jan	89,631	89,631
Feb	72,638	162,269
Mar	58,313	220,581
Apr	30,946	251,528
May	28,905	280,433
Jun	11,264	291,696
Jul	8,960	300,656
Aug	9,064	309,720
Sep	18,969	328,689
Oct	25,050	353,739
Nov	49,381	403,120
Dec	80,247	483,367

TABLE 22
Monthly Energy Consumption for Prototype
Building in Chicago, IL

Month	Electricity (KWH)	Totals Through Month (KWH)
Jan	114,188	114,188
Feb	98,583	212,771
Mar	83,523	296,294
Apr	47,996	344,290
May	42,668	386,958
Jun	20,695	407,653
Jul	12,437	420,090
Aug	13,215	433,304
Sep	29,669	462,973
Oct	35,034	498,007
Nov	71,662	569,669
Dec	106,641	676,309

TABLE 23
Monthly Energy Consumption for Prototype
Building in Minneapolis, MN

Month	Electricity (KWH)	Totals Through Month (KWH)
Jan	125,159	125,159
Feb	100,846	226,005
Mar	82,925	308,930
Apr	46,151	355,081
May	23,205	378,286
Jun	19,941	398,227
Jul	13,291	411,518
Aug	16,499	428,018
Sep	20,763	448,780
Oct	40,828	489,608
Nov	77,199	566,807
Dec	113,269	680,077

TABLE 24
Monthly Energy Consumption for Prototype
Building in Las Vegas, NV

Month	Electricity (KWH)	Totals Through Month (KWH)
Jan	69,095	69,095
Feb	46,498	115,593
Mar	35,546	151,139
Apr	18,655	169,794
May	18,785	188,579
Jun	9,488	198,067
Jul	6,937	205,004
Aug	7,139	212,144
Sep	11,042	223,185
Oct	34,618	257,803
Nov	44,675	302,478
Dec	66,368	368,846

TABLE 25
Sensitivity of Objective Function to Design
Variable ω for Various Values of ω and ϕ

$\phi \backslash \omega$	0.2	0.4	0.8	1.2	1.6
2	-39.56509	-39.58174	-8.530717	6.603876	14.13012
4	-33.46498	-24.79936	-7.683368	8.939914	23.37762
8	-22.19187	-16.70038	-5.917057	4.476792	14.37560

TABLE 26
Sensitivity of Objective Function to Design
Variable ϕ for Various Values of ω and ϕ

$\omega \backslash \phi$	1	2	4	6	8
0.2	0.651563	0.646303	0.632301	0.612745	0.585630
0.4	0.455344	1.052629	1.032117	1.003699	0.964971
0.8	-1.713885	0.940619	1.141854	1.128383	1.112934

TABLE 27
Sensitivity* of Objective Function to Design Variable ω

ω	$f(\omega+\Delta\omega)$	$f(\omega-\Delta\omega)$	Approximate	Exact	Relative Error %
0.2	17.883556	18.000122	-29.141500	-39.565090	35.768
0.4	12.764373	12.938846	-21.809125	-39.581740	81.492
0.8	7.023667	7.136330	-7.041438	-8.530717	21.150
1.2	6.759366	6.661518	4.077000	6.603876	61.980
1.6	9.789231	9.471698	9.922906	14.130120	42.399

* $\phi = 2$

TABLE 28
Sensitivity* of Objective Function to Design Variable ϕ

ϕ	$f(\phi+\Delta\phi)$	$f(\phi-\Delta\phi)$	Approximate	Exact	Relative Error %
1	12.256743	12.252656	2.043500	0.455344	-77.718
2	12.864738	12.838117	0.665525	1.052629	58.165
4	14.229255	14.174500	0.684438	1.032117	50.798
6	15.629166	15.545157	0.700075	1.003699	43.371
8	17.056112	16.942379	0.710831	0.964971	35.753

* $\omega = 0.4$

TABLE 29
Sensitivity of Maximum Slab-Surface Temperature to Design
Variable ω for Various Values of ω and ϕ

$\phi \backslash \omega$	0.2	0.4	0.8	1.2	1.6
2	8.047215	8.047573	7.552066	6.026809	4.840493
4	8.041915	8.037479	7.999564	7.871912	7.361530
8	8.047216	8.042663	7.994562	7.923996	7.826599

TABLE 30
Sensitivity of Maximum Heating-Element Temperature to Design
Variable ω for Various Values of ω and ϕ

$\phi \backslash \omega$	0.2	0.4	0.8	1.2	1.6
2	43.39164	32.73029	25.38326	18.78799	14.32776
4	43.39164	31.72807	26.87849	24.34707	21.54462
8	43.39162	31.72807	26.87870	24.48542	22.73963



*
0



*
0

TABLE 31
Sensitivity* of Maximum Slab-Surface Temperature to Design Variable ω

ω	$g_1(\omega+\Delta\omega)$	$g_1(\omega-\Delta\omega)$	Approximate	Exact	Relative Error %
0.2	71.349380	71.322769	6.652500	8.047215	20.966
0.4	72.696212	72.642937	6.659125	8.047573	20.850
0.8	75.336128	75.236053	6.254688	7.552066	20.742
1.2	77.618996	77.496712	5.095167	6.026809	18.284
1.6	79.475533	79.340271	4.226938	4.840493	14.515

* $\phi = 2$

TABLE 32
Sensitivity* of Maximum Heating-Element Temperature to Design Variable ω

ω	$g_2(\omega+\Delta\omega)$	$g_2(\omega-\Delta\omega)$	Approximate	Exact	Relative Error %
0.2	85.88414	85.71233	42.95250	43.39164	1.022
0.4	93.17790	92.92178	32.01463	32.73029	2.236
0.8	104.65557	104.25001	25.34769	25.38326	0.140
1.2	113.42435	112.97691	18.64338	18.78799	0.776
1.6	119.93759	119.47914	14.32659	14.32776	0.008

* $\phi = 2$

TABLE 33
Sensitivity* of Maximum Slab-Surface Temperature to Design Variable ϕ

ϕ	$g_1(\phi+\Delta\phi)$	$g_1(\phi-\Delta\phi)$	Approximate	Exact	Relative Error %
1	73.250633	73.248657	0.098800	0.121303	22.776
2	73.242897	73.243866	-0.024225	-0.029616	22.254
4	73.199142	73.199509	-0.018350	-0.021529	17.326
6	73.158585	73.158928	-0.017150	-0.020670	20.522
8	73.121185	73.121658	-0.023650	-0.028735	21.499

* $\omega = 0.4$

TABLE 34
Sensitivity* of Maximum Heating-Element Temperature to Design Variable ϕ

ϕ	$g_2(\phi+\Delta\phi)$	$g_2(\phi-\Delta\phi)$	Approximate	Exact	Relative Error %
1	95.224998	95.213409	0.579450	0.609339	5.158
2	95.222610	95.226059	-0.086225	-0.089710	4.042
4	95.057800	95.059402	-0.080100	-0.080896	0.994
6	94.905006	94.906502	-0.074800	-0.076326	2.040
8	94.764351	94.765762	-0.070550	-0.074035	4.940

* $\omega = 0.4$

TABLE 35
Life-Cycle Cost Analysis for Prototype
Building in Washington ,DC

Insulation Level (R-value) (F-ft ² -hr/Btu)	Fuel Life Cycle Cost	Fuel Life Cycle Cost Savings	Total Life Cycle Cost
0	403	-	403
5	322	81	337
10	295	108	321
20	262	141	301
30	249	153	314
40	238	165	329

All costs are in dollars per lineal foot.

TABLE 36
Life-Cycle Cost Analysis for Prototype
Building in Chicago, IL

Insulation Level (R-value) (F-ft ² -hr/Btu)	Fuel Life Cycle Cost	Fuel Life Cycle Cost Savings	Total Life Cycle Cost
0	596	-	596
5	477	119	492
10	436	159	562
20	387	209	426
30	369	227	434
40	352	244	443

All costs are in dollars per lineal foot.

TABLE 37
Life-Cycle Cost Analysis for Prototype
Building in Minneapolis, MN

Insulation Level (R-value) (F-ft ² -hr/Btu)	Fuel Life Cycle Cost	Fuel Life Cycle Cost Savings	Total Life Cycle Cost
0	600	-	600
5	480	120	495
10	440	160	465
20	390	210	429
30	371	228	435
40	354	245	445

All costs are in dollars per lineal foot.

TABLE 38
Life-Cycle Cost Analysis for Prototype
Building in Las Vegas, NV

Insulation Level (R-value) (F-ft ² -hr/Btu)	Fuel Life Cycle Cost	Fuel Life Cycle Cost Savings	Total Life Cycle Cost
0	288	-	288
5	230	58	246
10	211	77	237
20	187	101	224
30	178	110	243
40	170	118	261

All costs are in dollars per lineal foot.

FIGURES

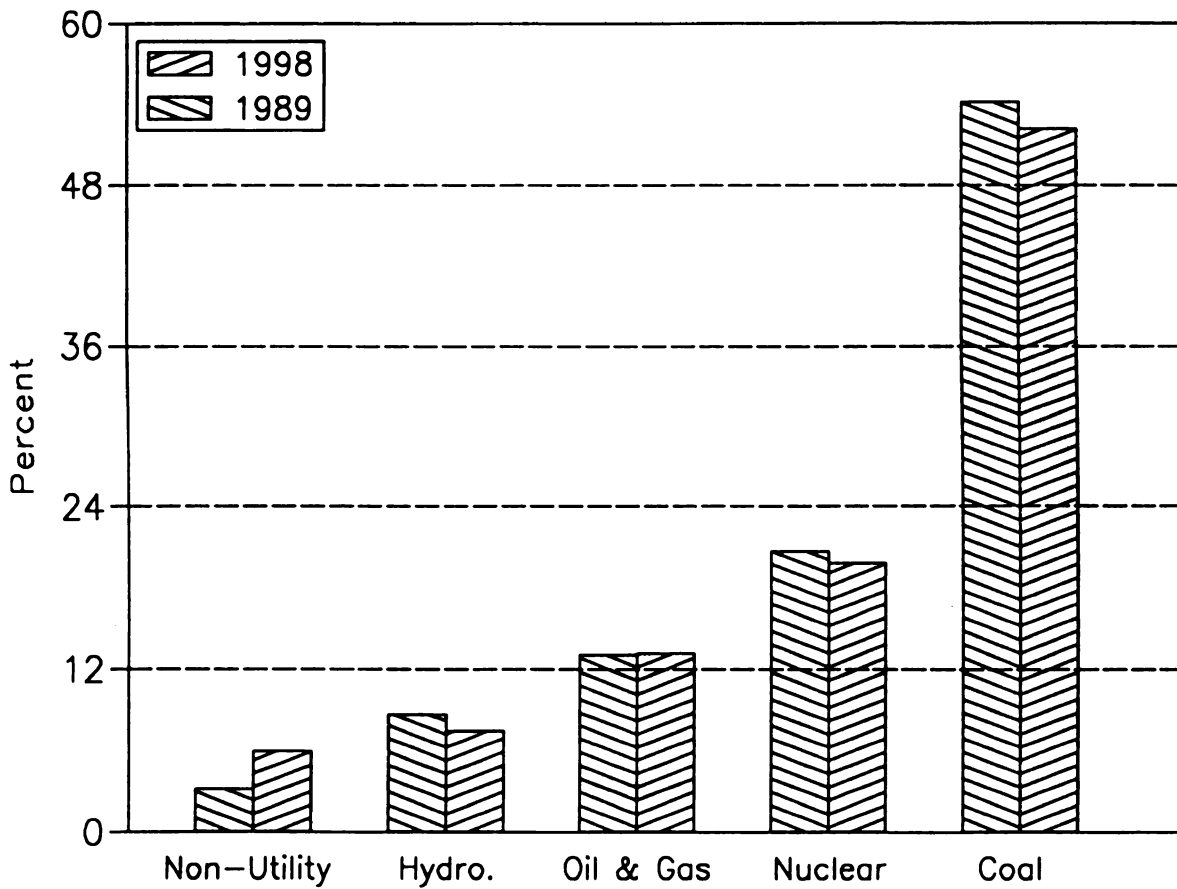


Figure 1. Electrical energy production by fuel in the U.S.

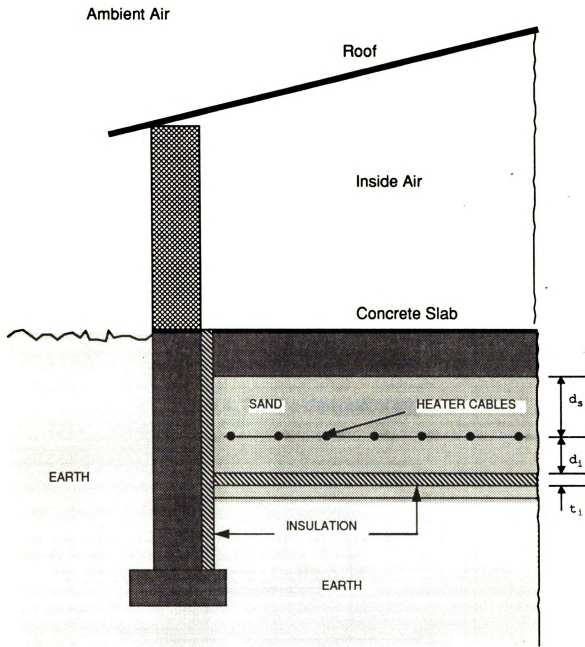


Figure 3. The deepheat concept.

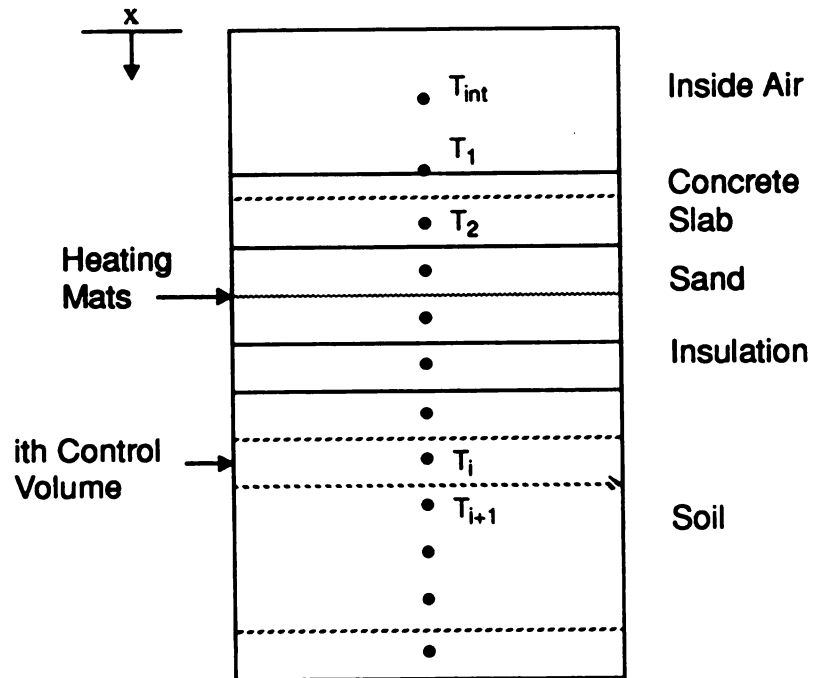


Figure 4. The one-dimensional grid.

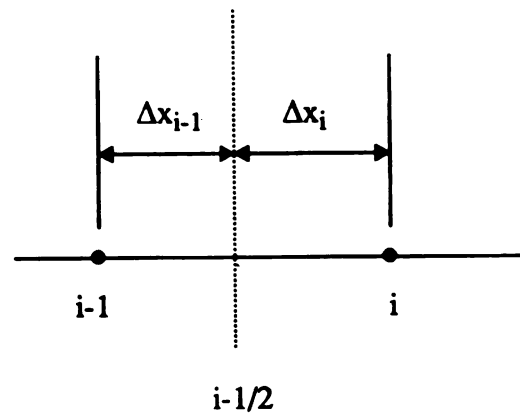


Figure 5. The interface conductivity.

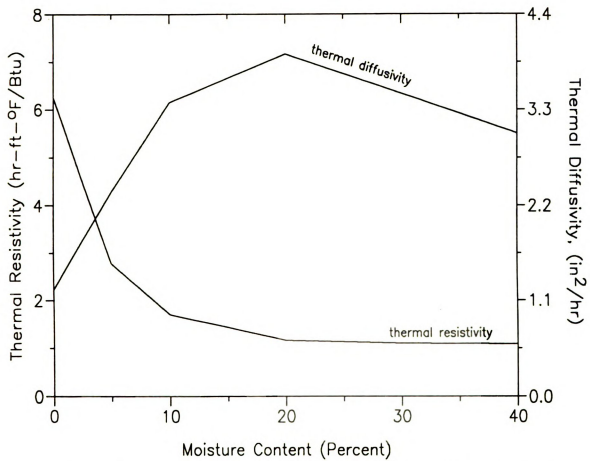


Figure 6. Variation of sand thermal properties with moisture content.

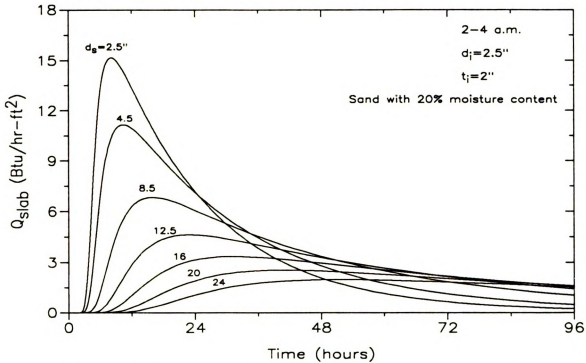


Figure 7. Slab heat-flux as a function of mat depth.

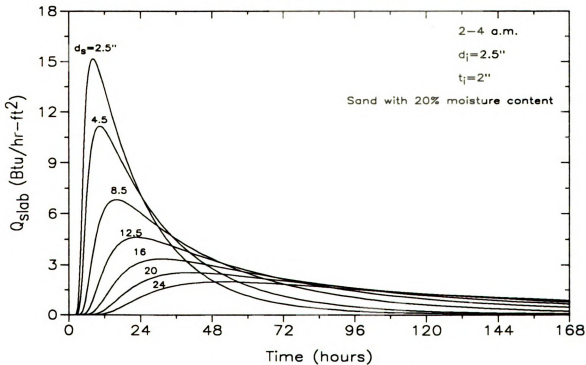


Figure 8. Slab heat-flux as a function of mat depth.

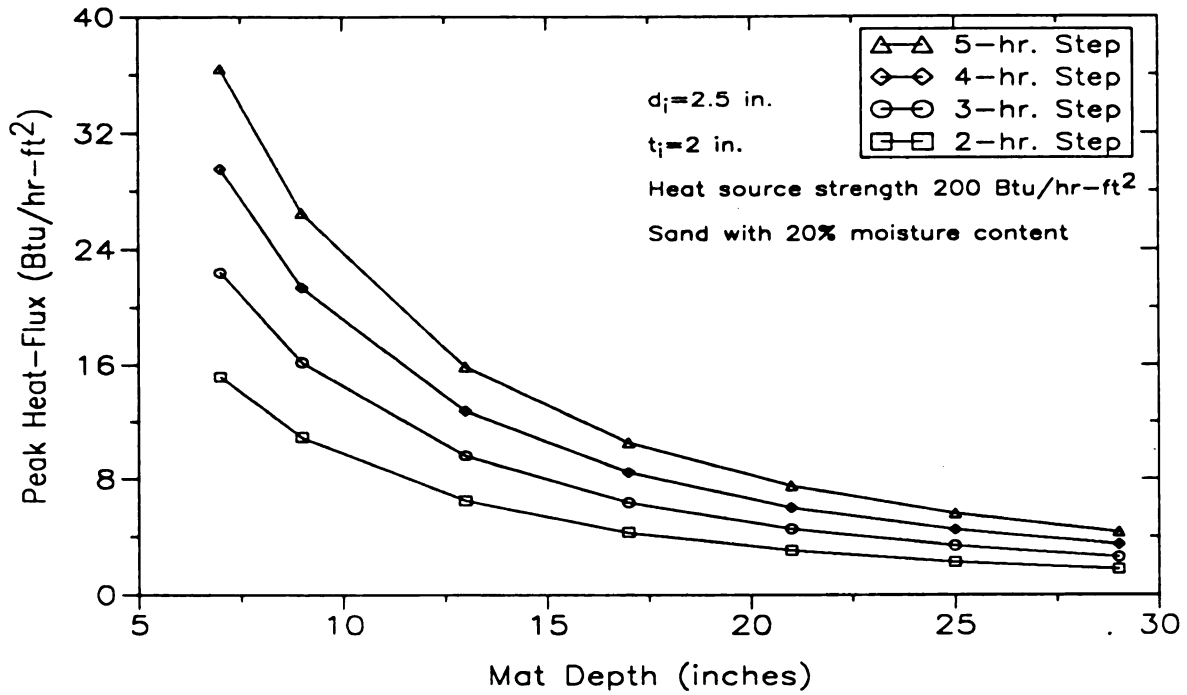


Figure 9. Peak slab heat-flux versus mat depth for various energy inputs.

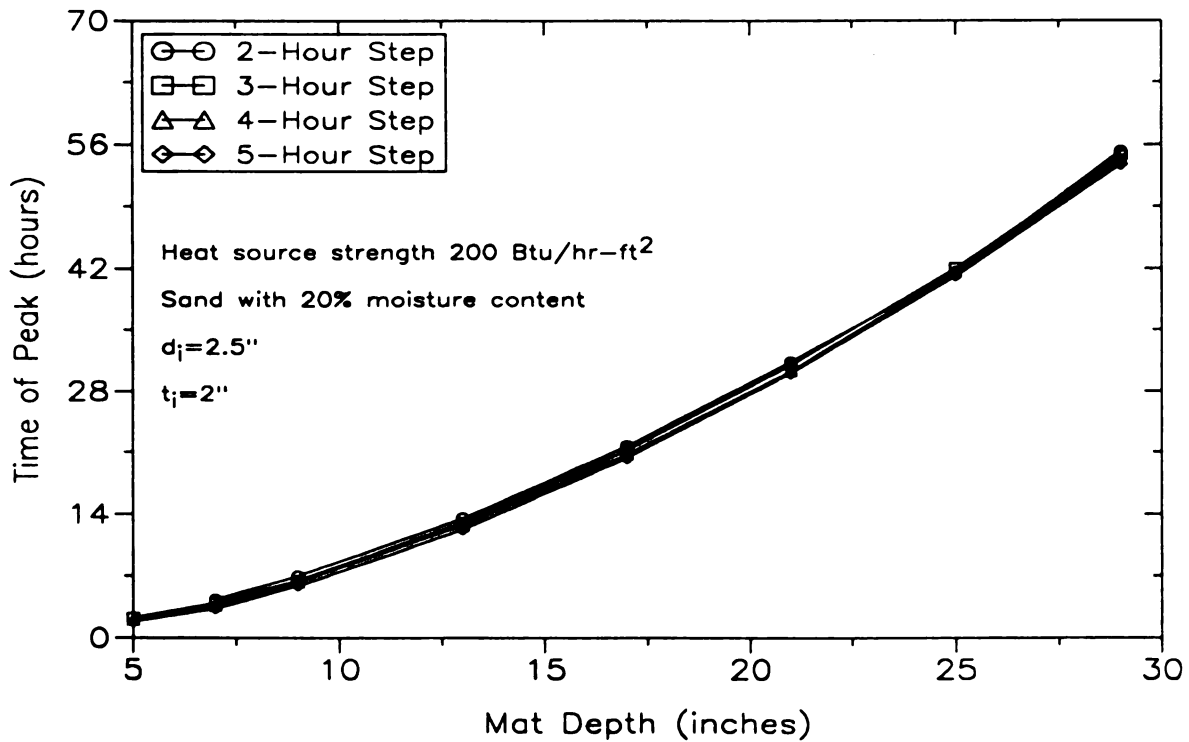


Figure 10. Time of peak heat-flux as a function of mat depth.

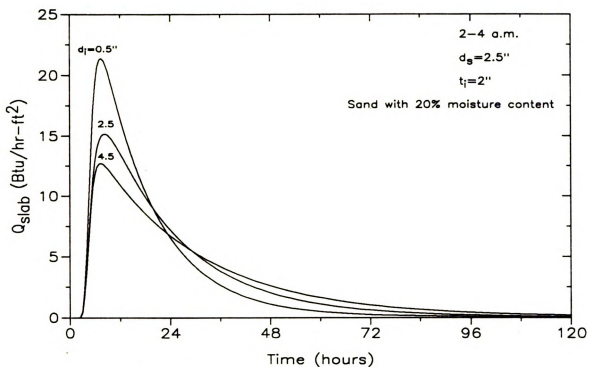


Figure 11. Slab heat-flux for various sand layer thicknesses.

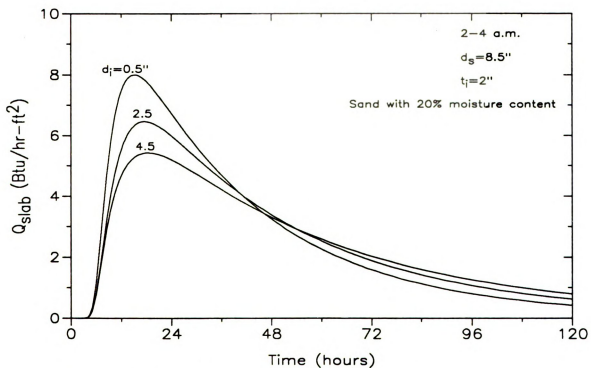


Figure 12. Slab heat-flux for various sand layer thicknesses.

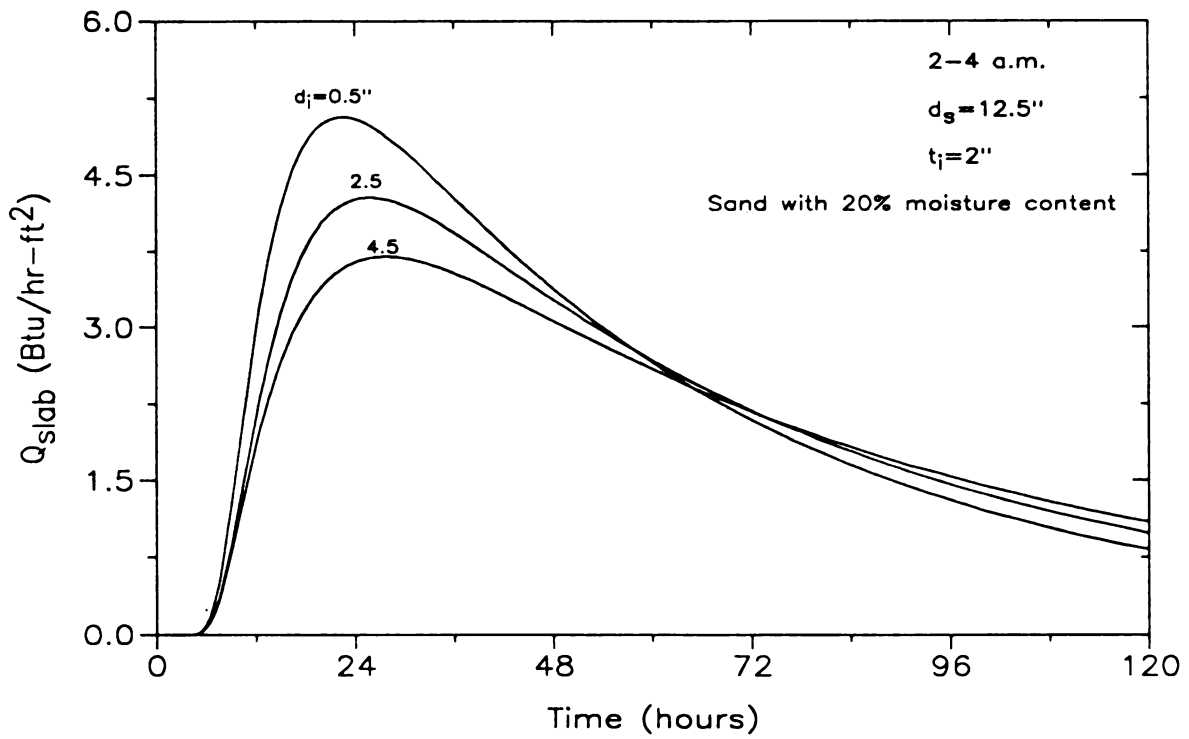


Figure 13. Slab heat-flux for various sand layer thicknesses.

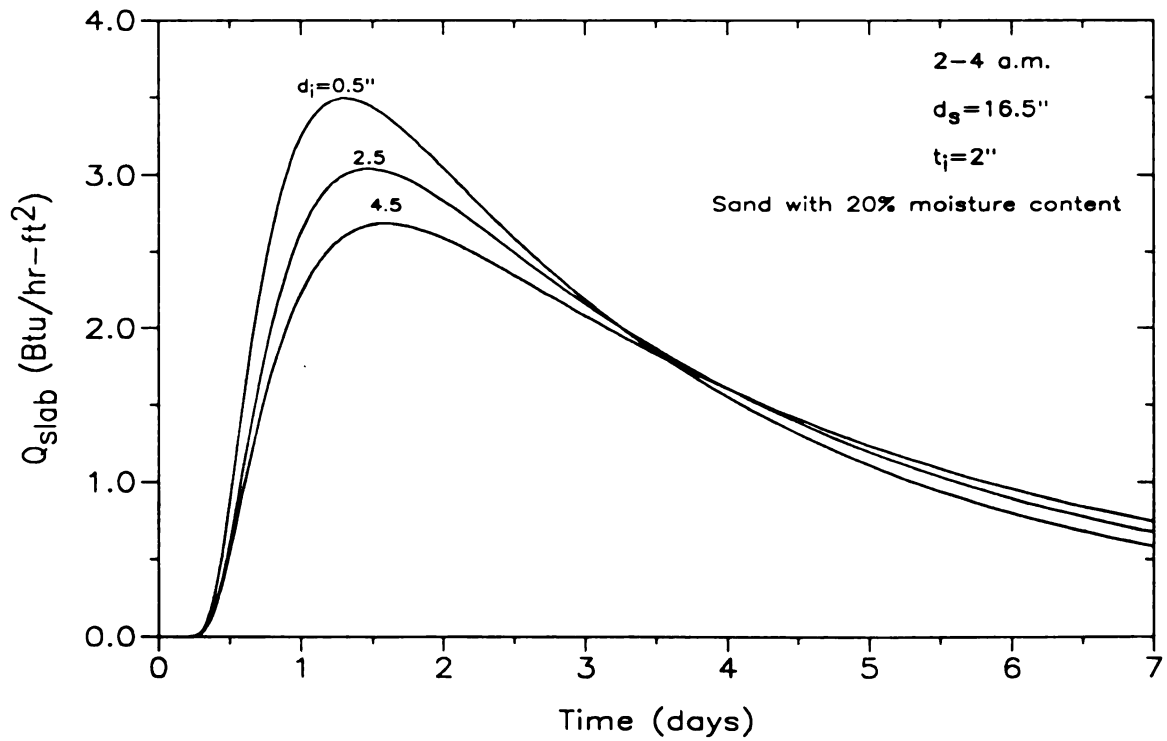


Figure 14. Slab heat-flux for various sand layer thicknesses.

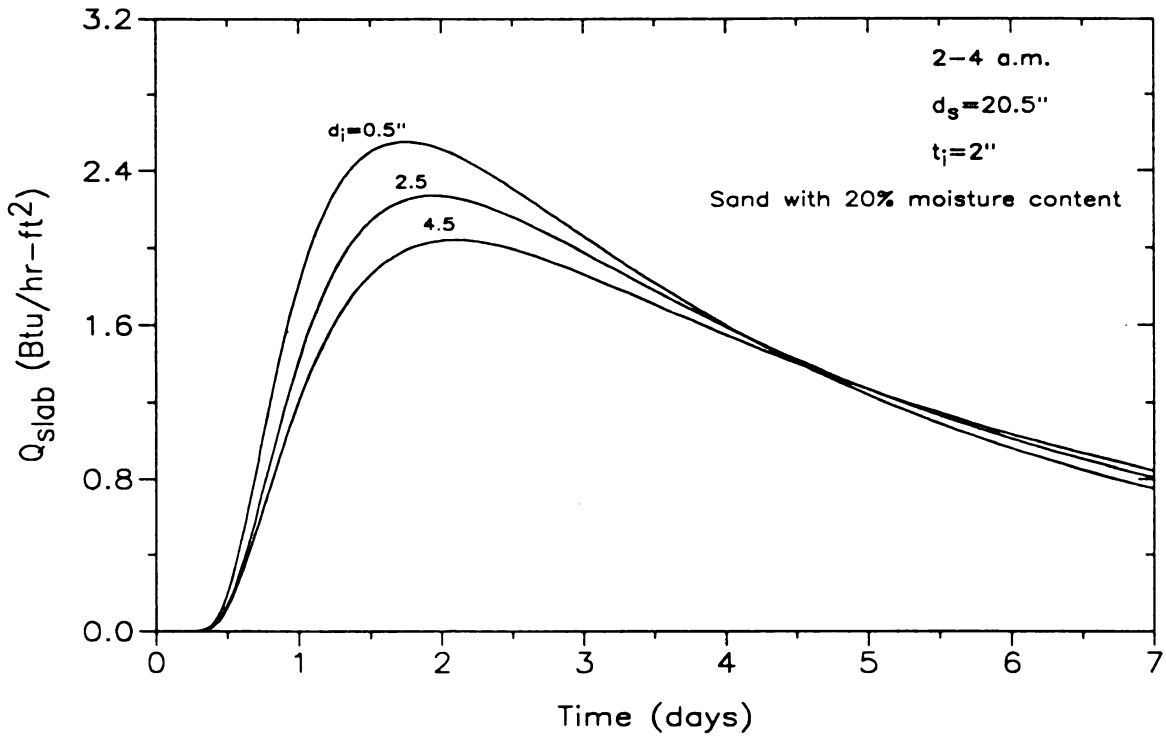


Figure 15. Slab heat-flux for various sand layer thicknesses.

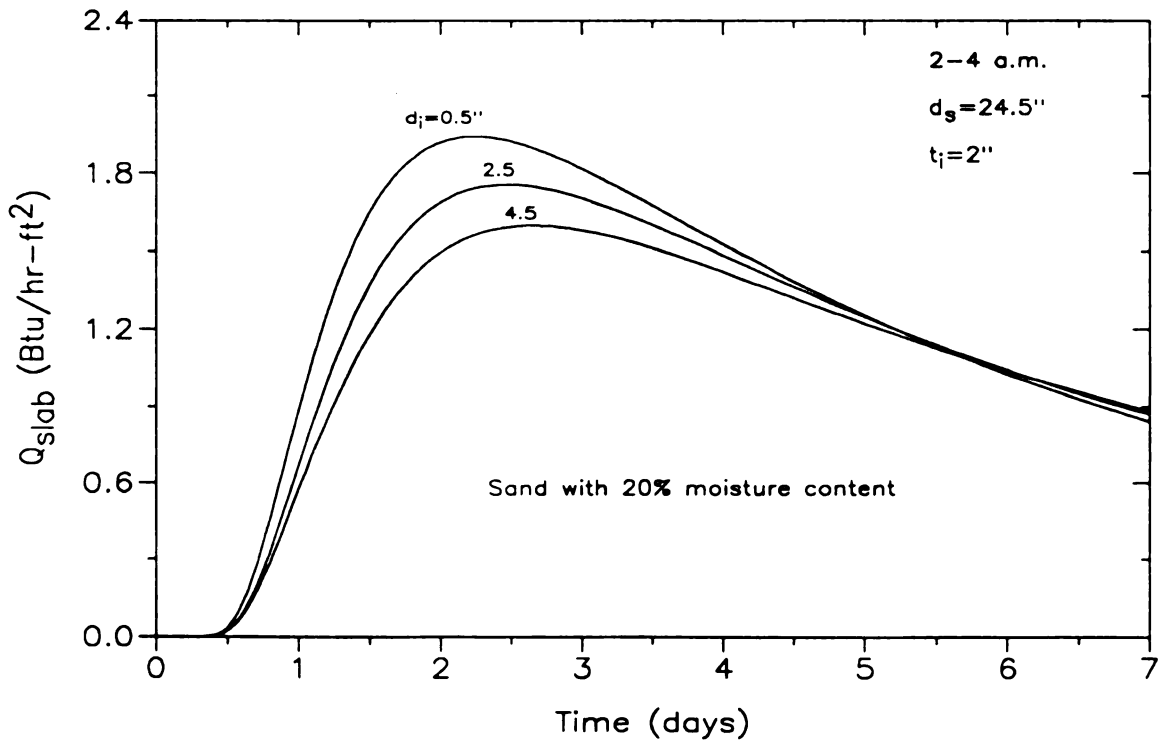


Figure 16. Slab heat-flux for various sand layer thicknesses.

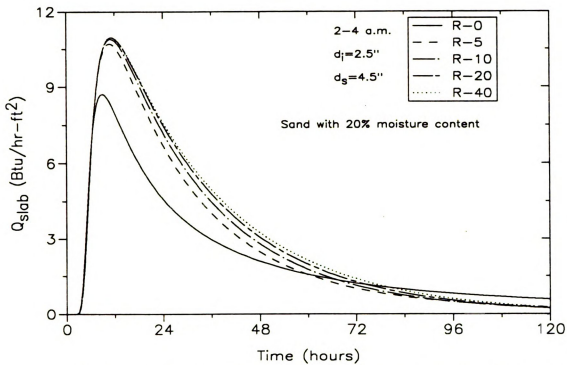


Figure 17. Variation of slab heat-flux for various insulation levels.

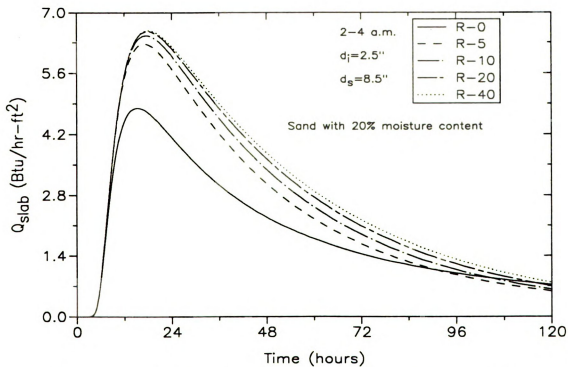


Figure 18. Variation of slab heat-flux for various insulation levels.

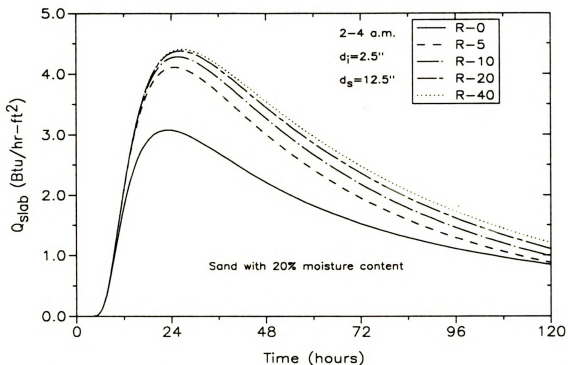


Figure 19. Variation of slab heat-flux for various insulation levels.

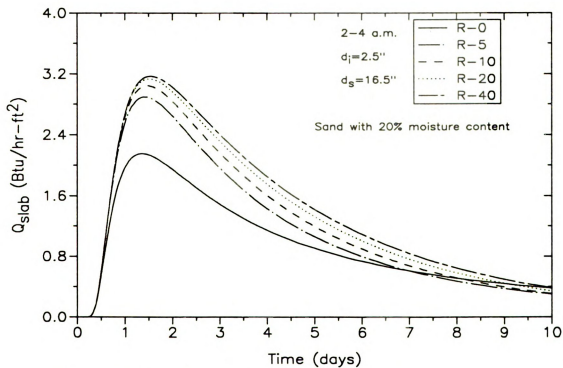


Figure 20. Variation of slab heat-flux for various insulation levels.

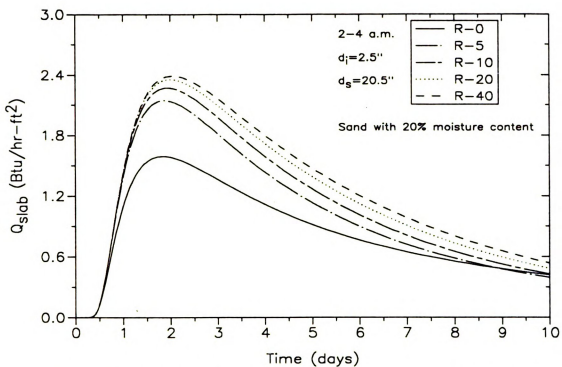


Figure 21. Variation of slab heat-flux for various insulation levels.

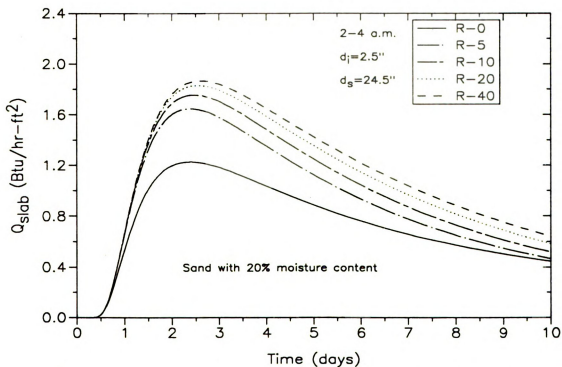


Figure 22. Variation of slab heat-flux for various insulation levels.

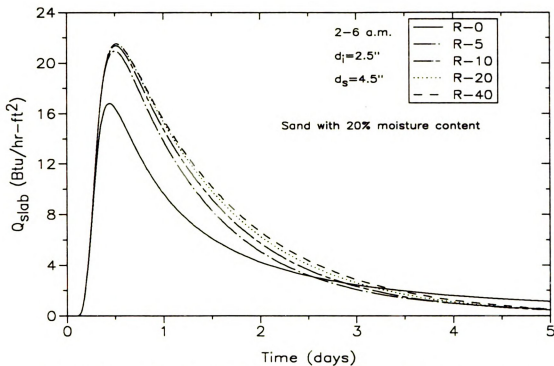


Figure 23. Variation of slab heat-flux for various insulation levels.

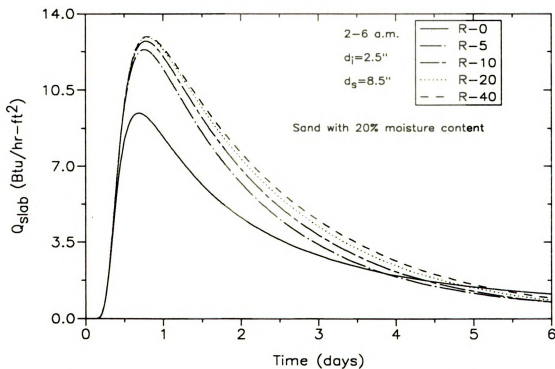


Figure 24. Variation of slab heat-flux for various insulation levels.

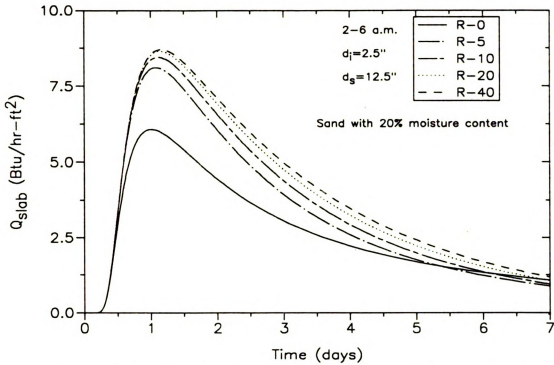


Figure 25. Variation of slab heat-flux for various insulation levels.

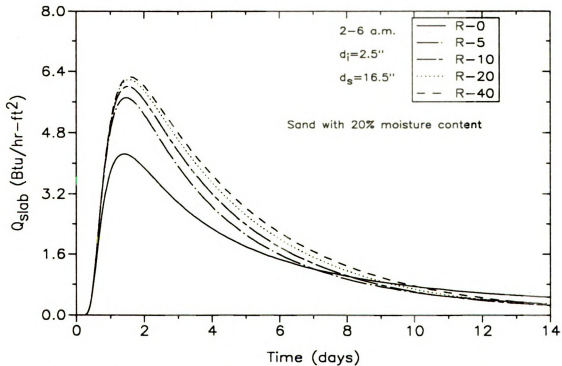


Figure 26. Variation of slab heat-flux for various insulation levels.

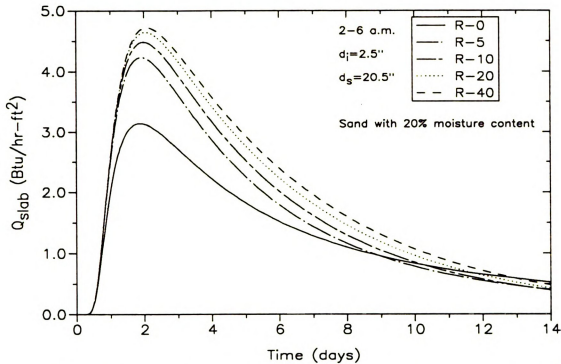


Figure 27. Variation of slab heat-flux for various insulation levels.

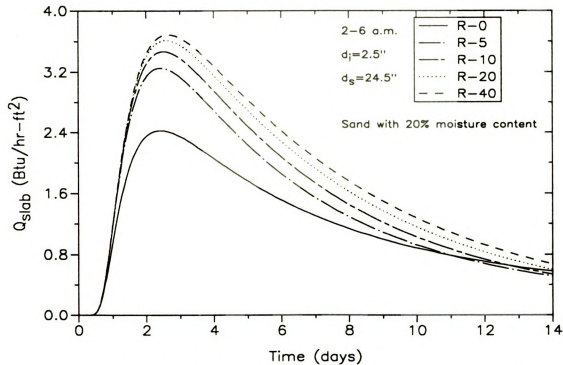


Figure 28. Variation of slab heat-flux for various insulation levels.

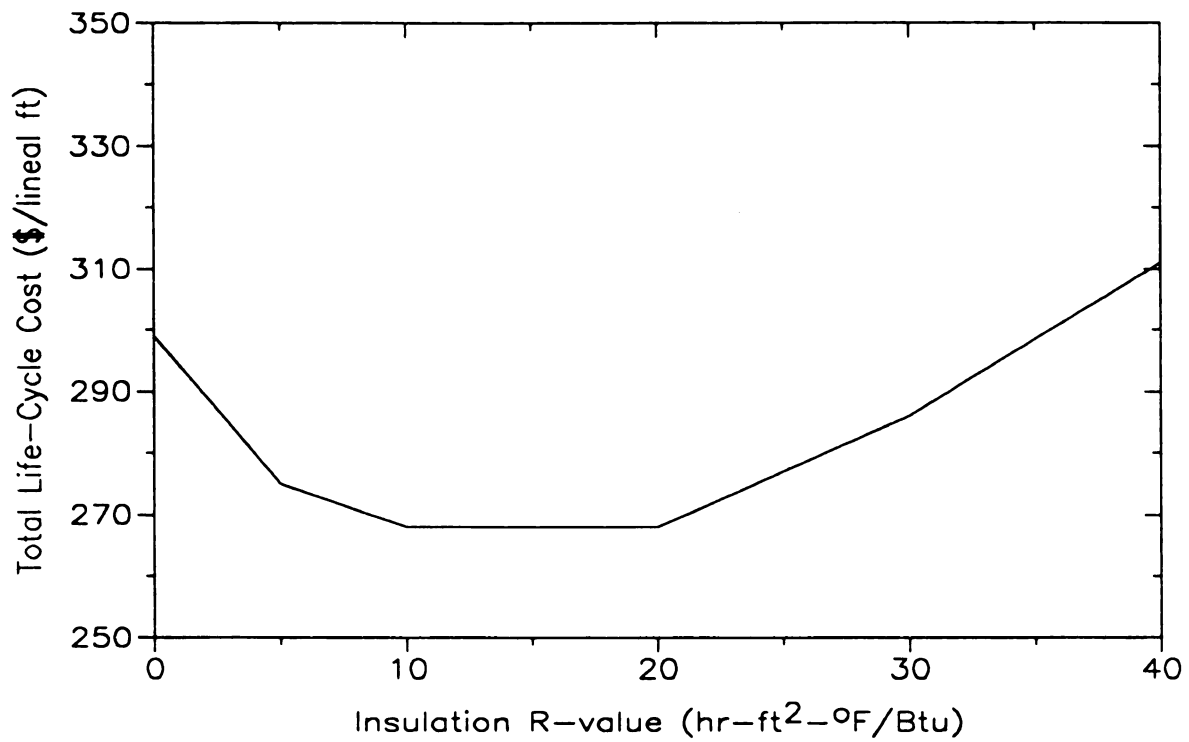


Figure 29. Life-Cycle cost of insulation options for Washington DC.

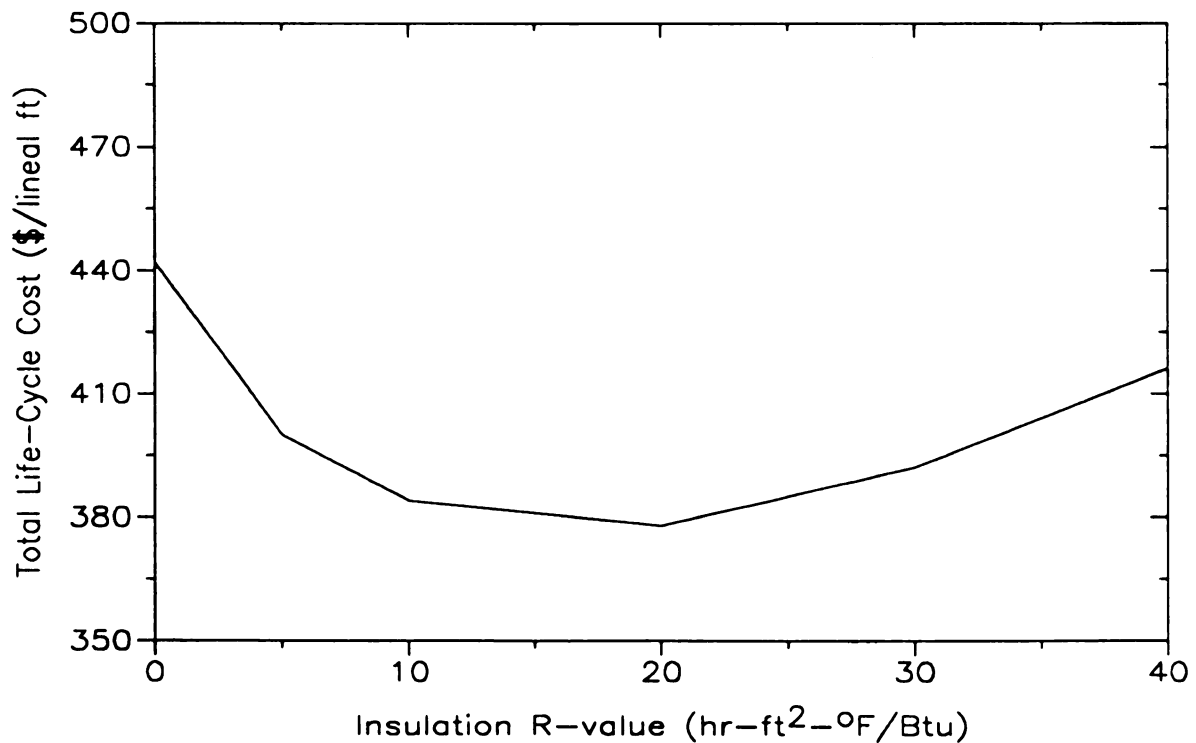


Figure 30. Life-cycle cost of insulation options for Chicago, IL.

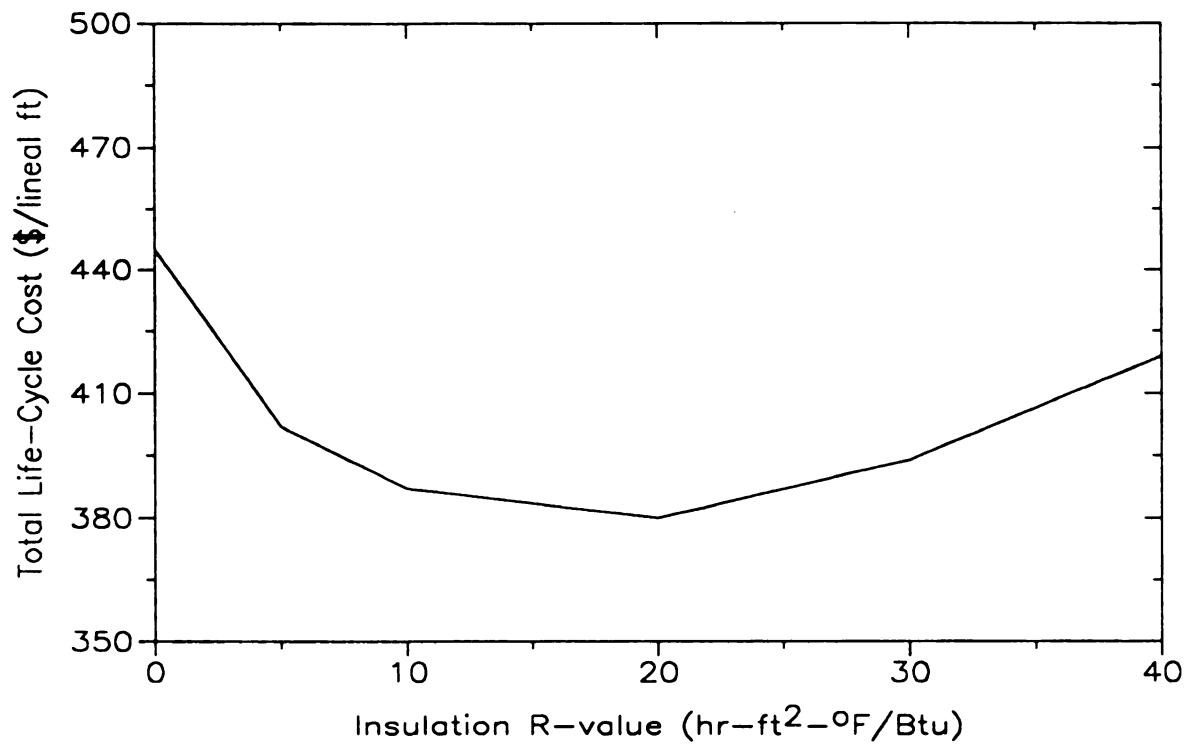


Figure 31. Life-cycle cost of insulation options for Minneapolis, MN.

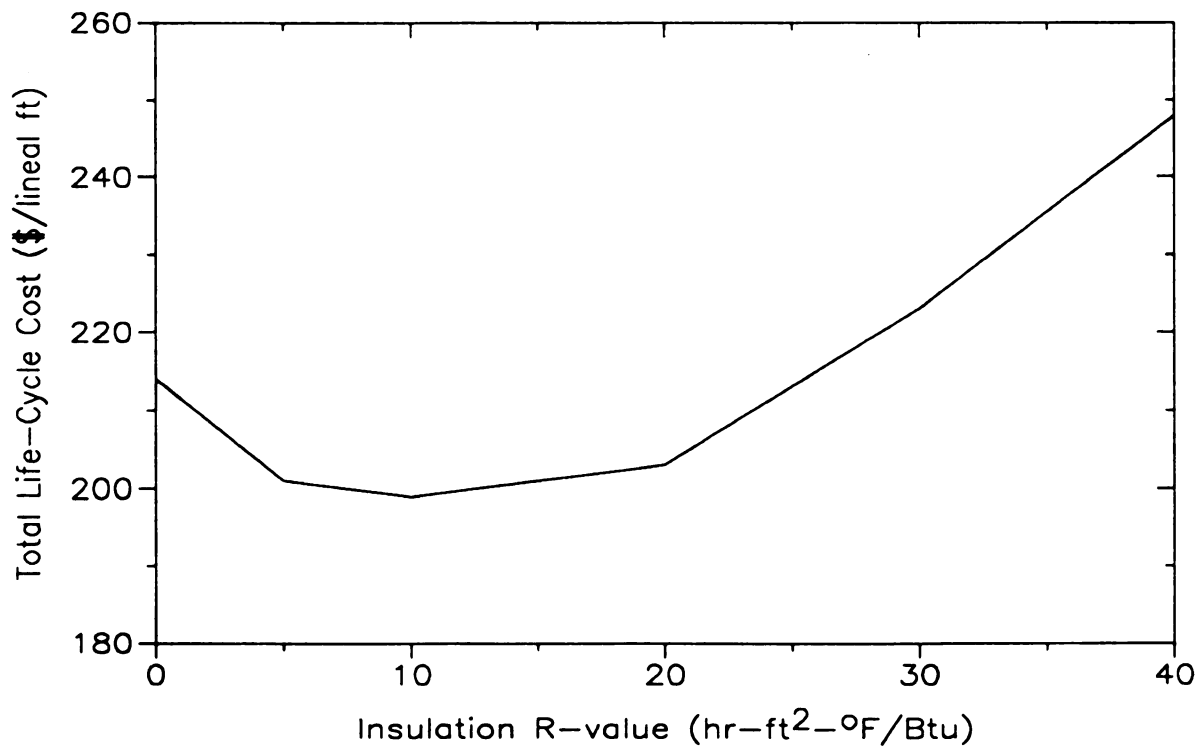


Figure 32. Life-cycle cost of insulation options for Las Vegas, NV.

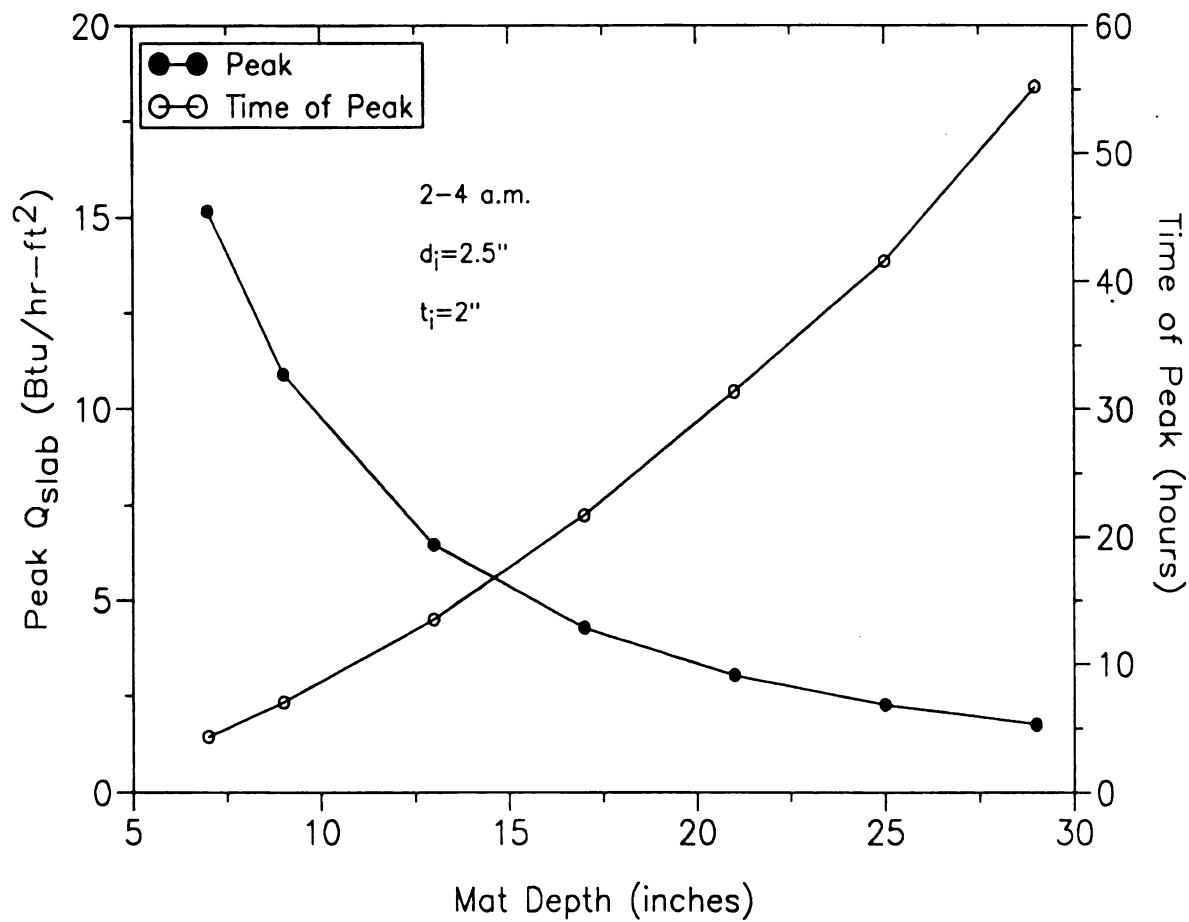


Figure 33. Variation of slab heat-flux with mat depth.

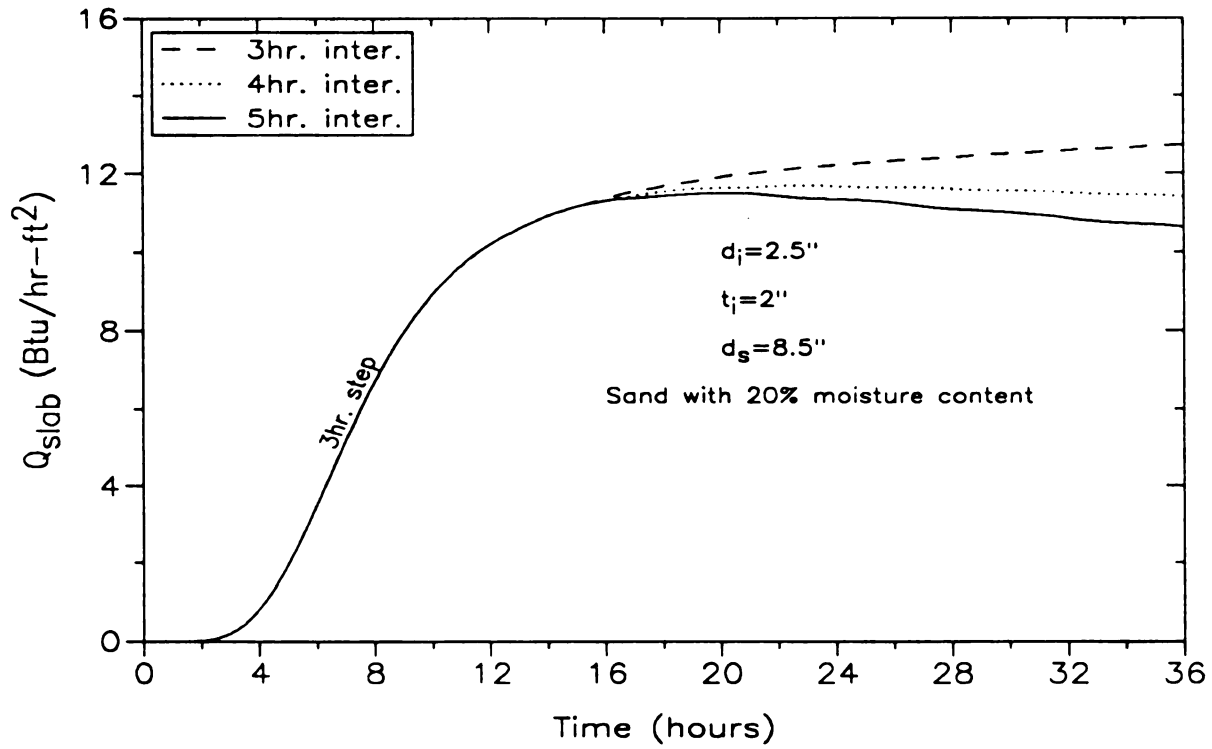


Figure 34. Slab heat-flux with intermittent heating.

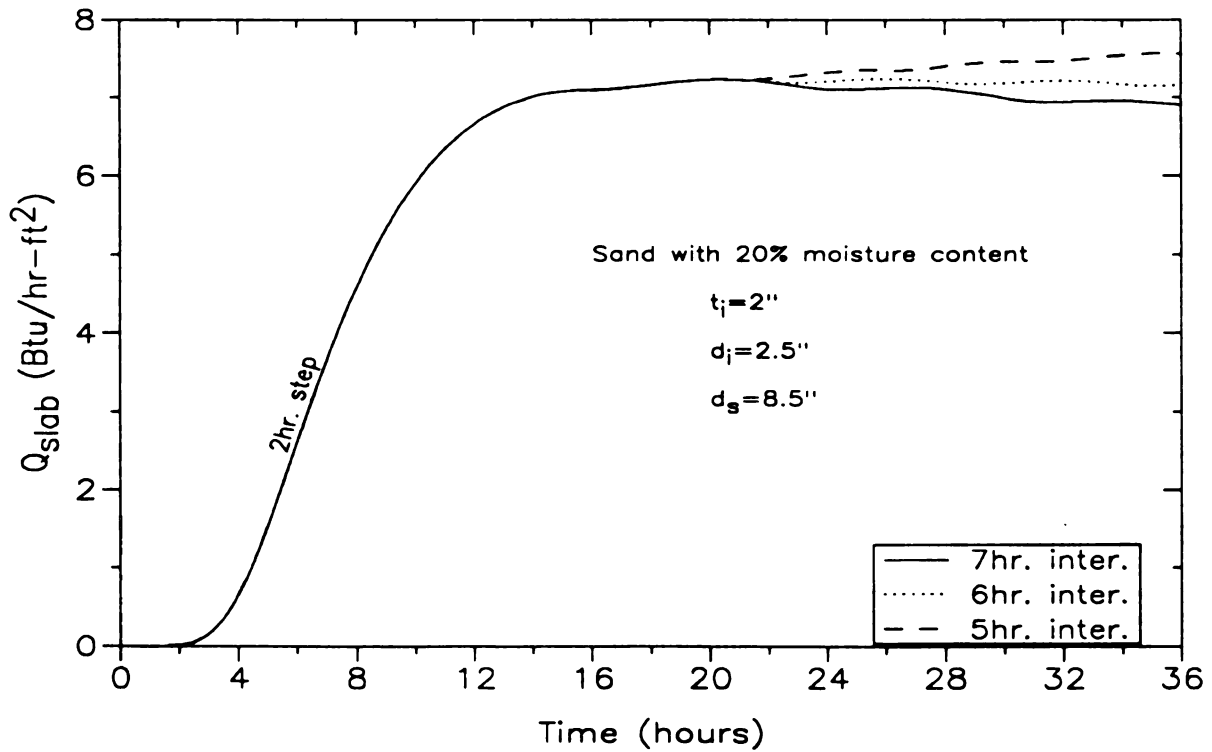


Figure 35. Slab heat-flux with intermittent heating.

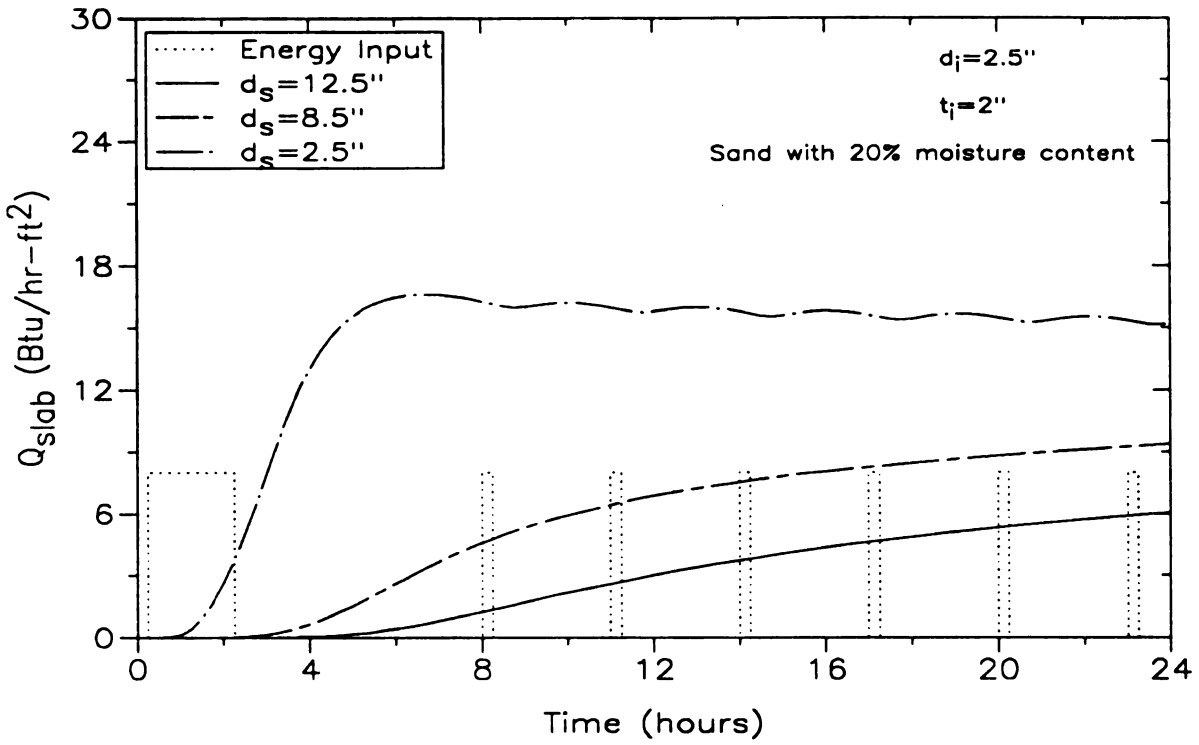


Figure 36. Slab heat-flux with intermittent heating.

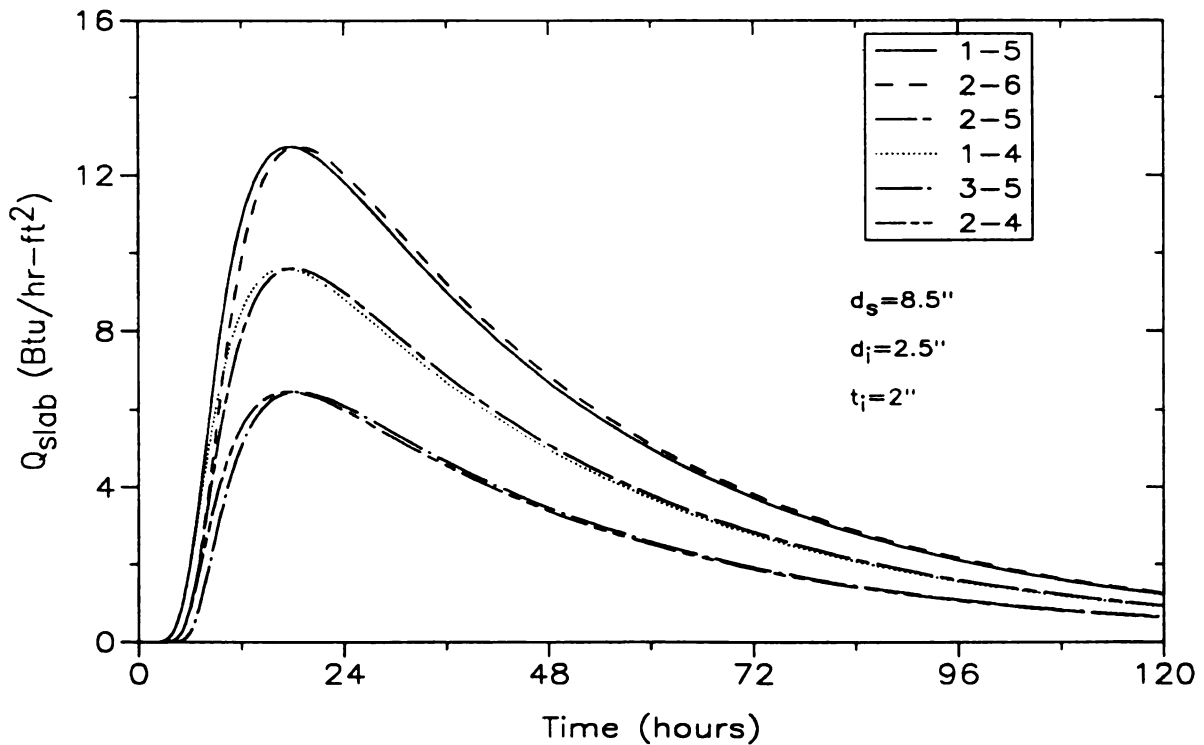


Figure 37. Slab heat-flux for various energy inputs.

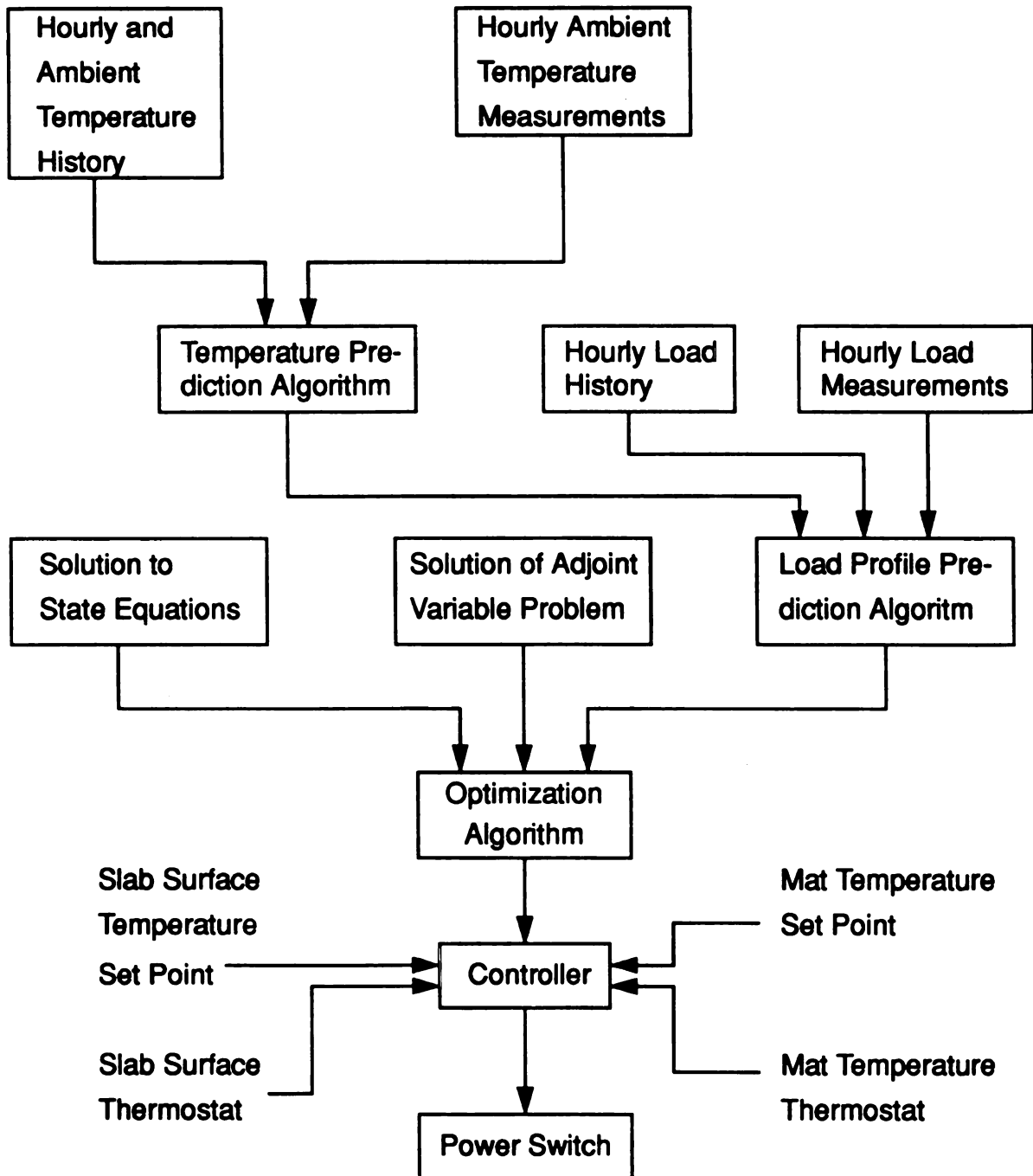


Figure 38. Block diagram of controller functions.

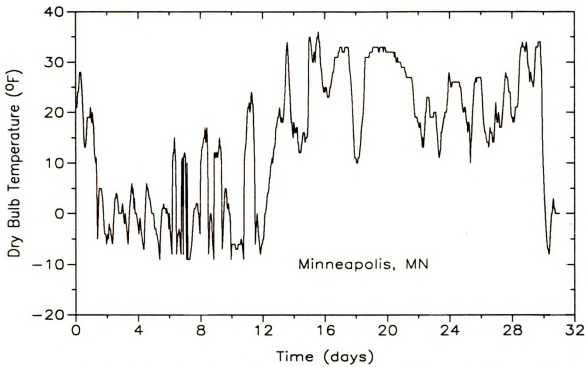


Figure 39. Outside air temperature fluctuations in January.

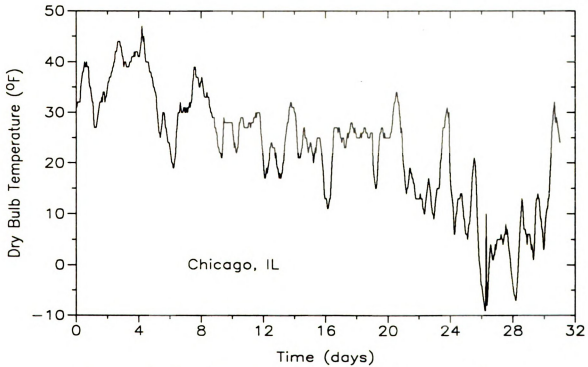


Figure 40. Outside air temperature fluctuations in January.

Dry Bulb Temperature (°F)
5
4
3
2
1
-
-1

Dry Bulb Temperature (°F)
60
50
40
30
20
10

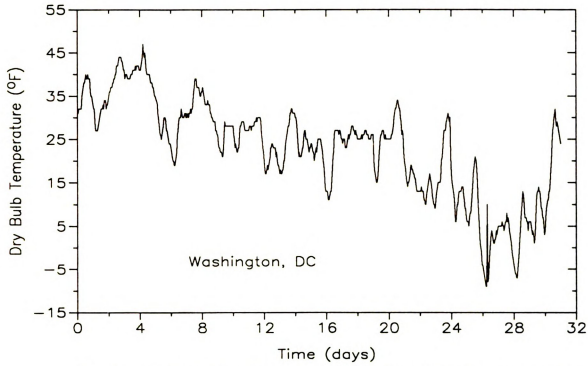


Figure 41. Outside air temperature fluctuations in January.

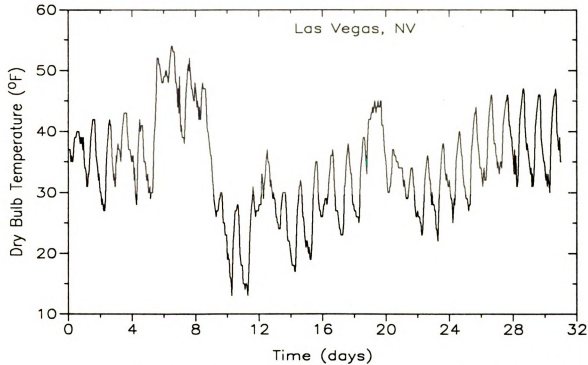


Figure 42. Outside air temperature fluctuations in January.

10-
8
6
4
2
0

Load (Btu/hr-ft²)

10
8
6
4
2
0

Load (Btu/hr-ft²)

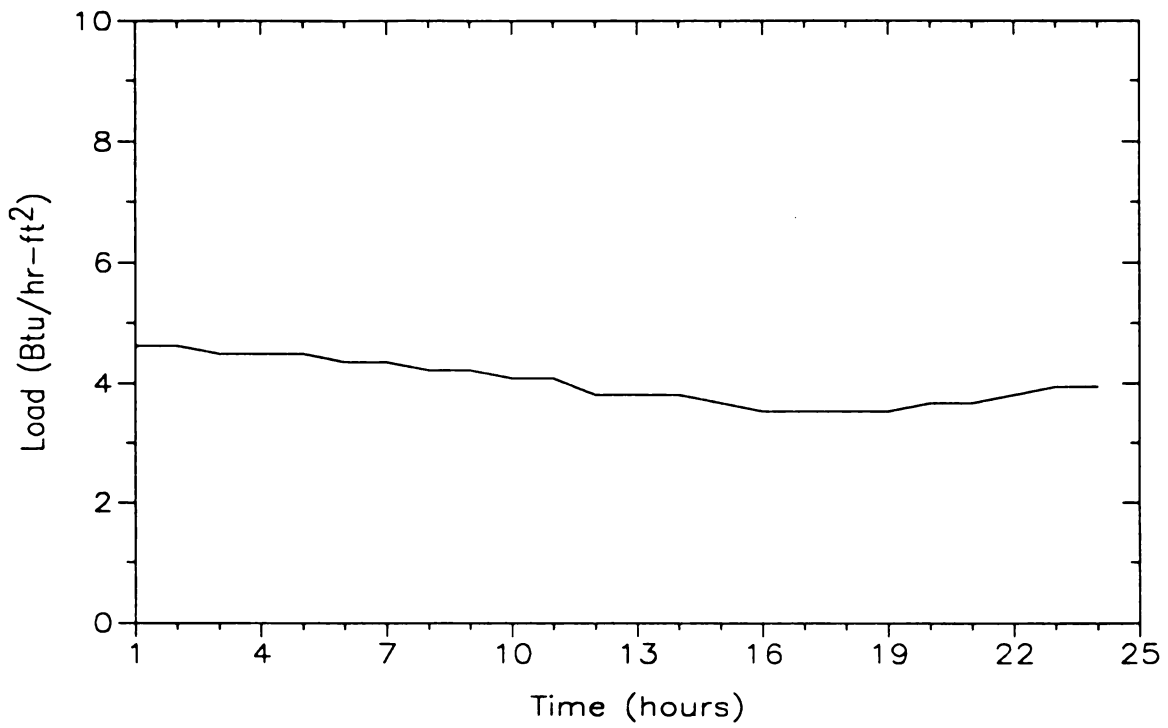


Figure 43. Load profile for day 3 in January; Chicago, IL.

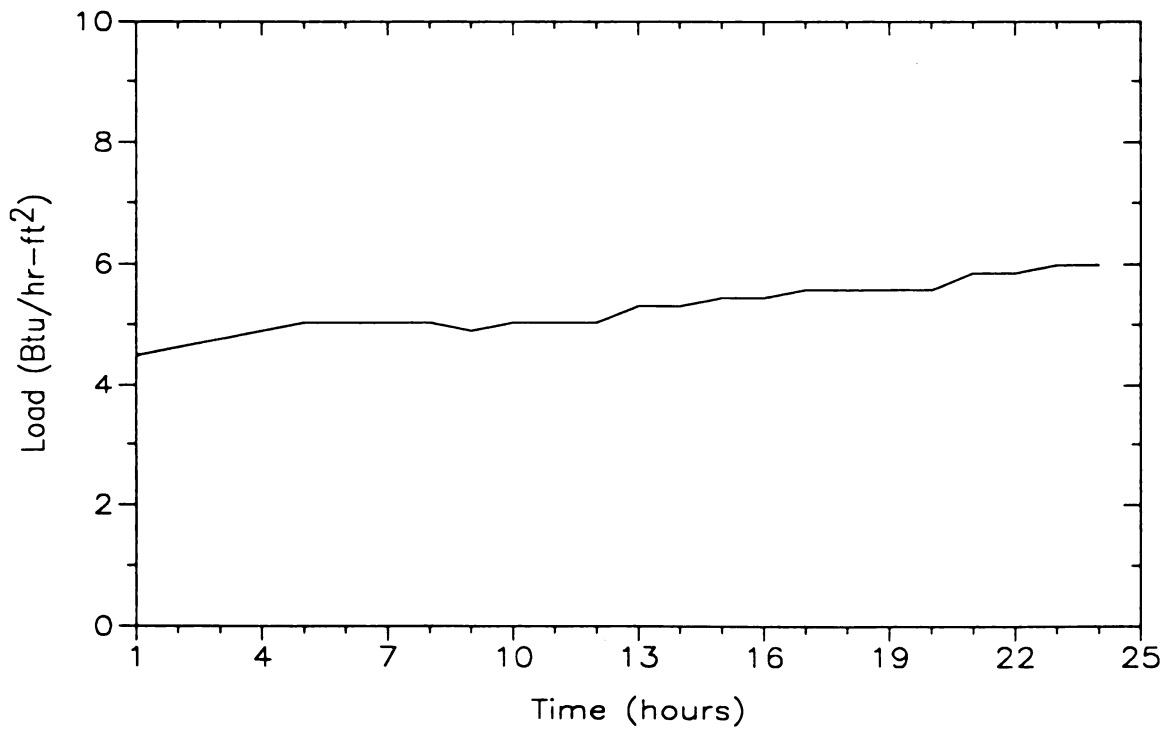


Figure 44. Load profile for day 9 in January; Chicago, IL.

10
8
6
4
2
0
Load (Btu/hr-ft²)

12
10
8
6
4
2
0
Load (Btu/hr-ft²)

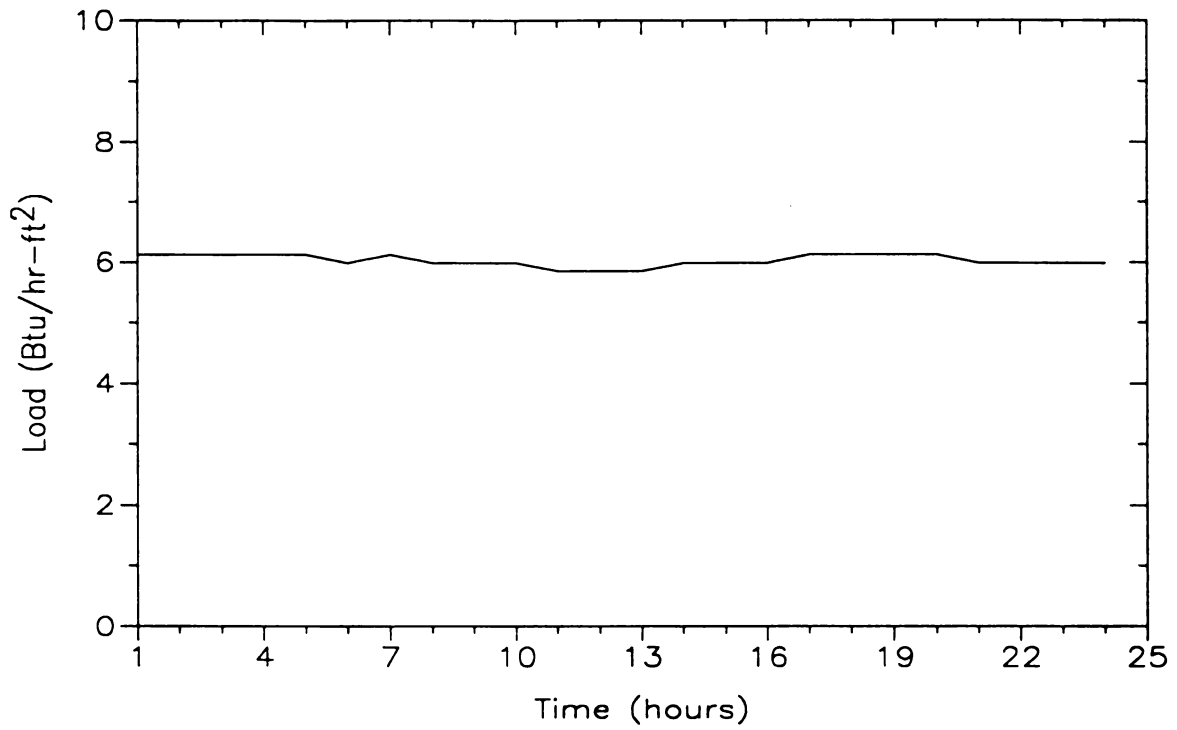


Figure 45. Load profile for day 19 in January; Chicago, IL.

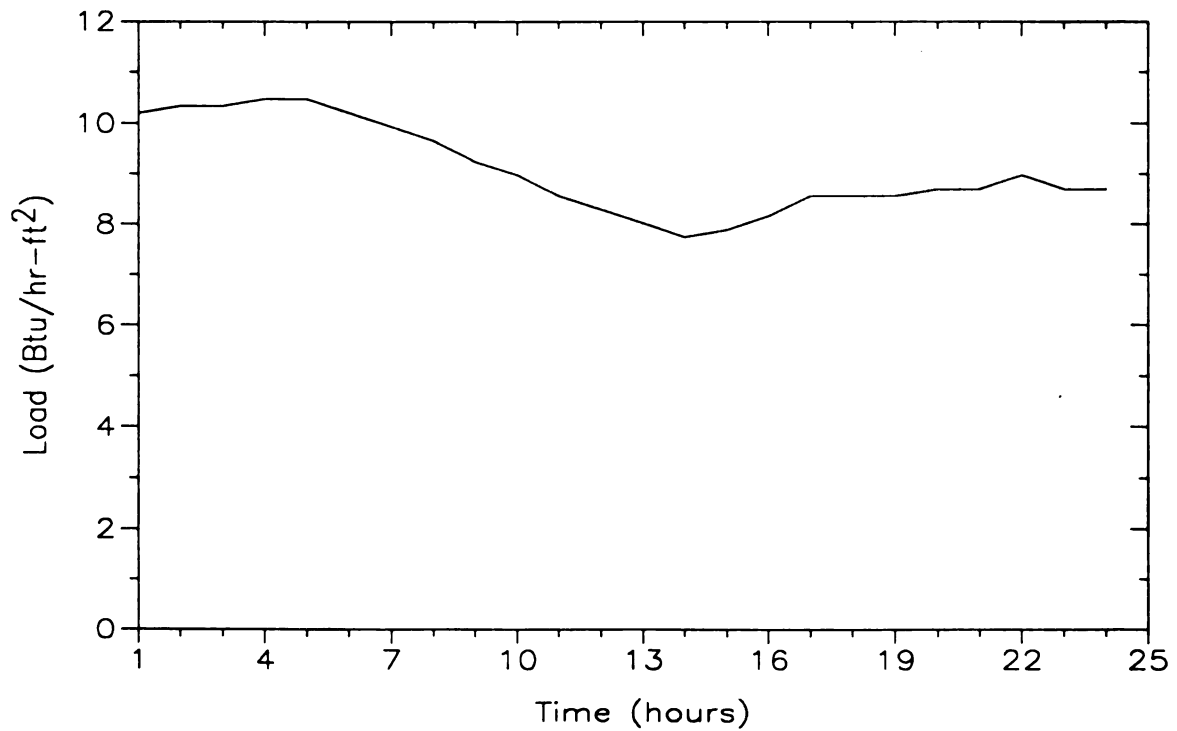


Figure 46. Load profile for day 29 in January; Chicago, IL.

8
6
4
2
0
F
8
6
4
2
0
F

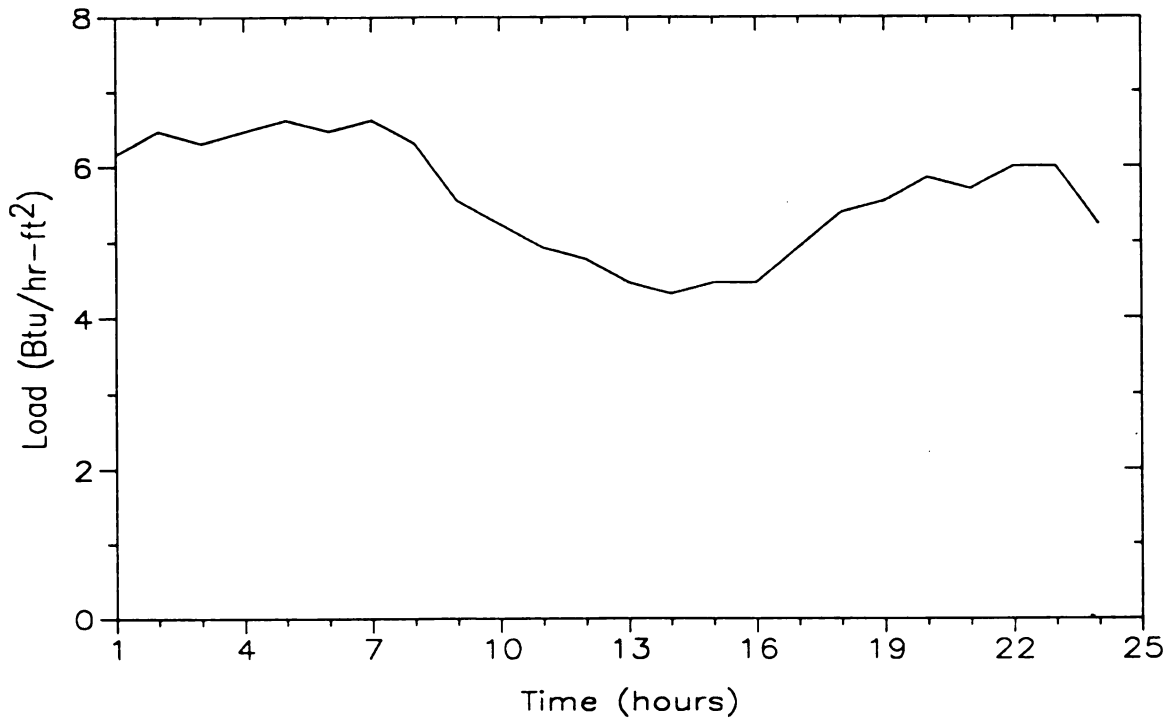


Figure 47. Load profile for day 3 in January; Las Vegas, NV.

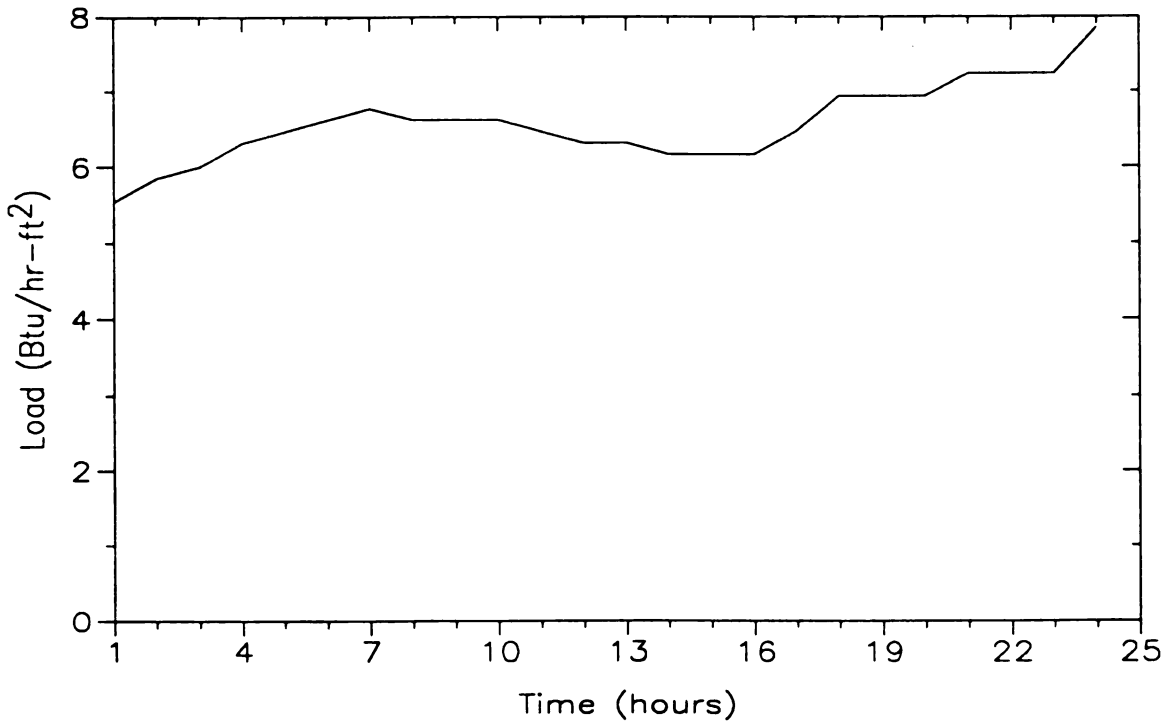


Figure 48. Load profile for day 10 in January; Las Vegas, NV.

Load (Btu/hr-ft²)

8
6
4
2
0

F

Load (Btu/hr-ft²)

8
6
4
2
0

F

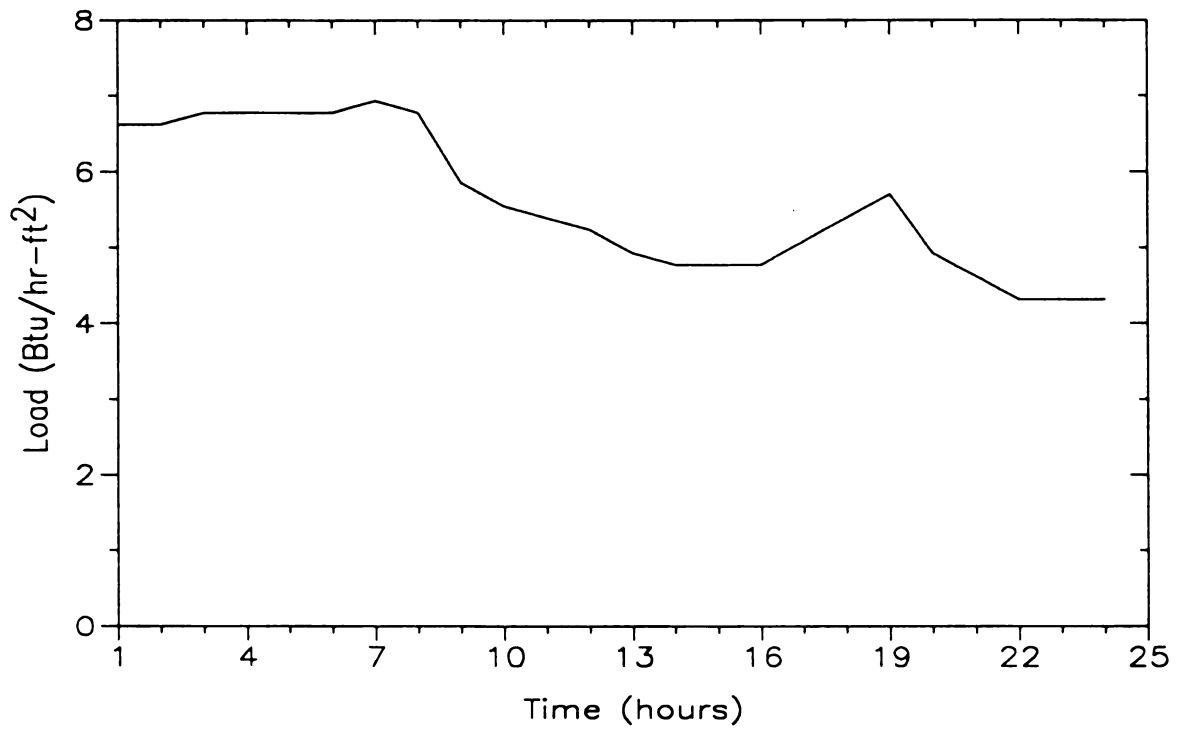


Figure 49. Load profile for day 19 in January; Las Vegas, NV.

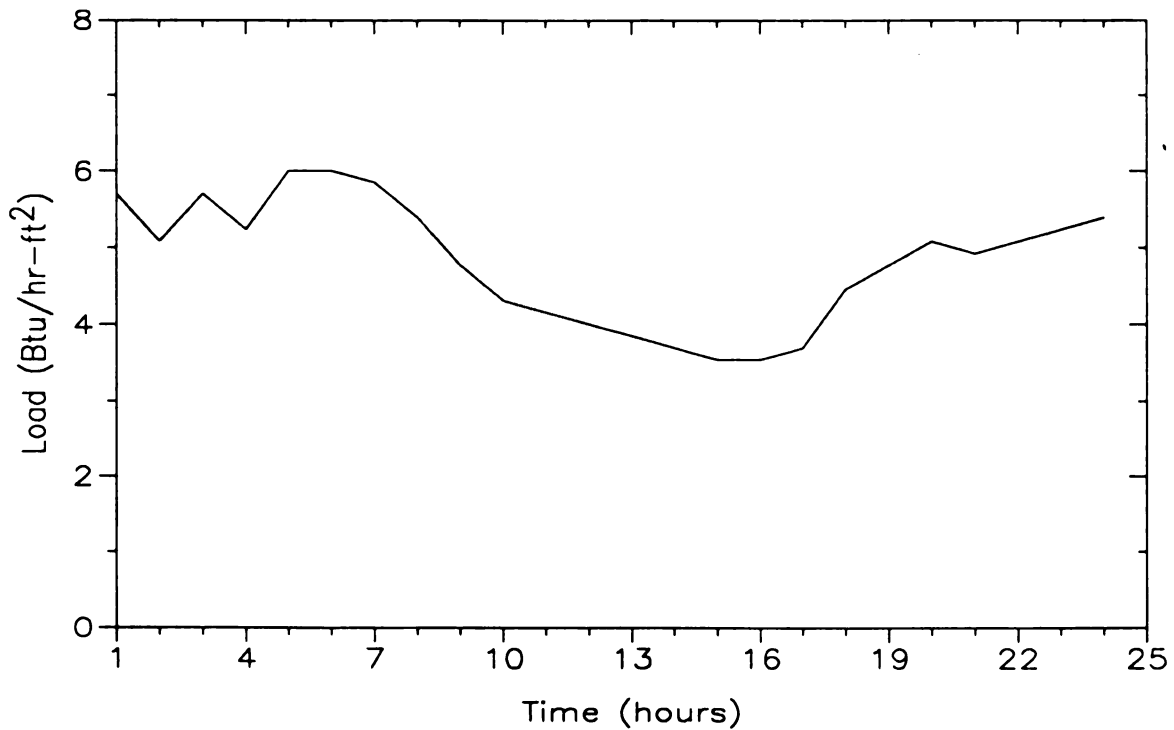


Figure 50. Load profile for day 29 in January; Las Vegas, NV.

10-
8-
6-
4-
2-
0-
7

Load (Btu/hr-ft²)

10-
8-
6-
4-
2-
0-
7

Load (Btu/hr-ft²)

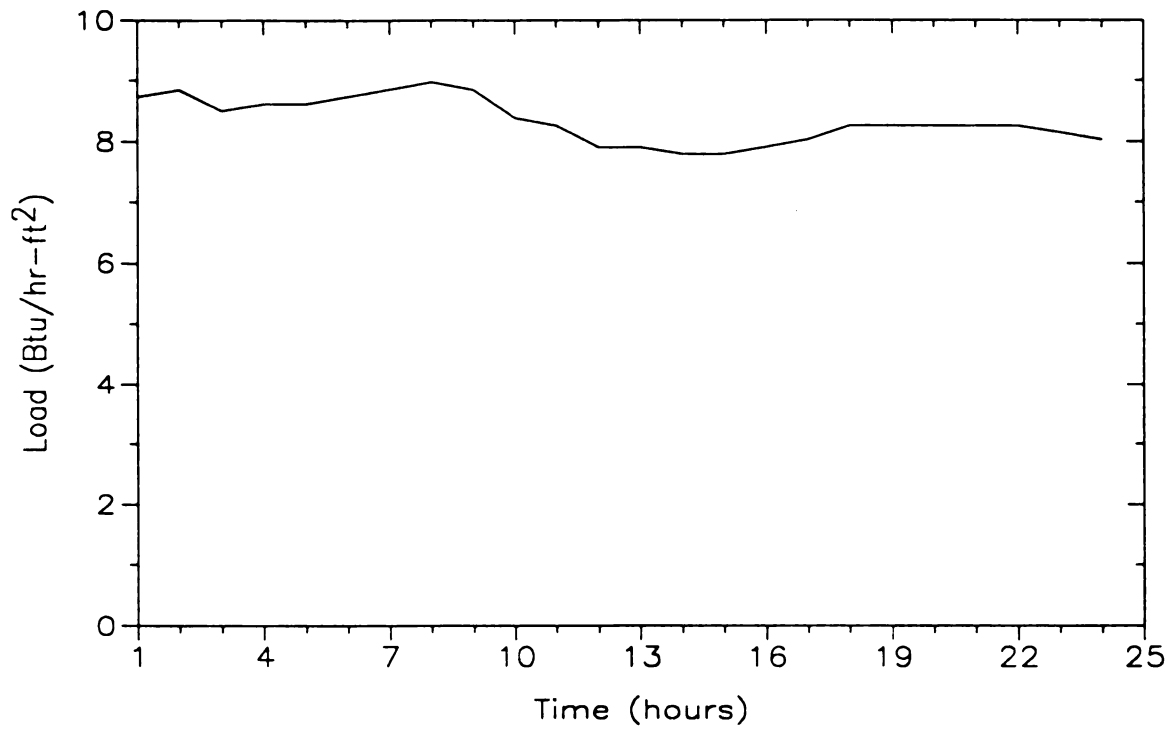


Figure 51. Load profile for day 3 in January; Minneapolis, MN.

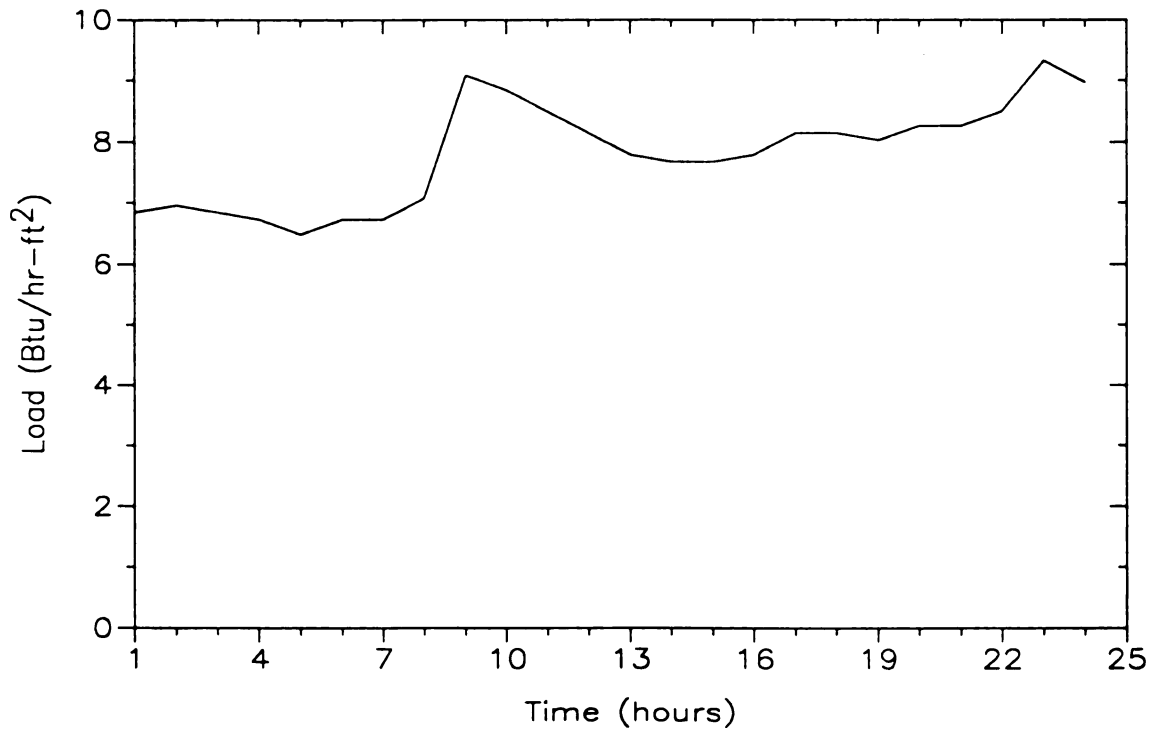


Figure 52. Load profile for day 10 in January; Minneapolis, MN.

Load (Btu/hr-ft²)

10

8

6

4

2

0

7

10

8

6

4

2

0

7

Load (Btu/hr-ft²)

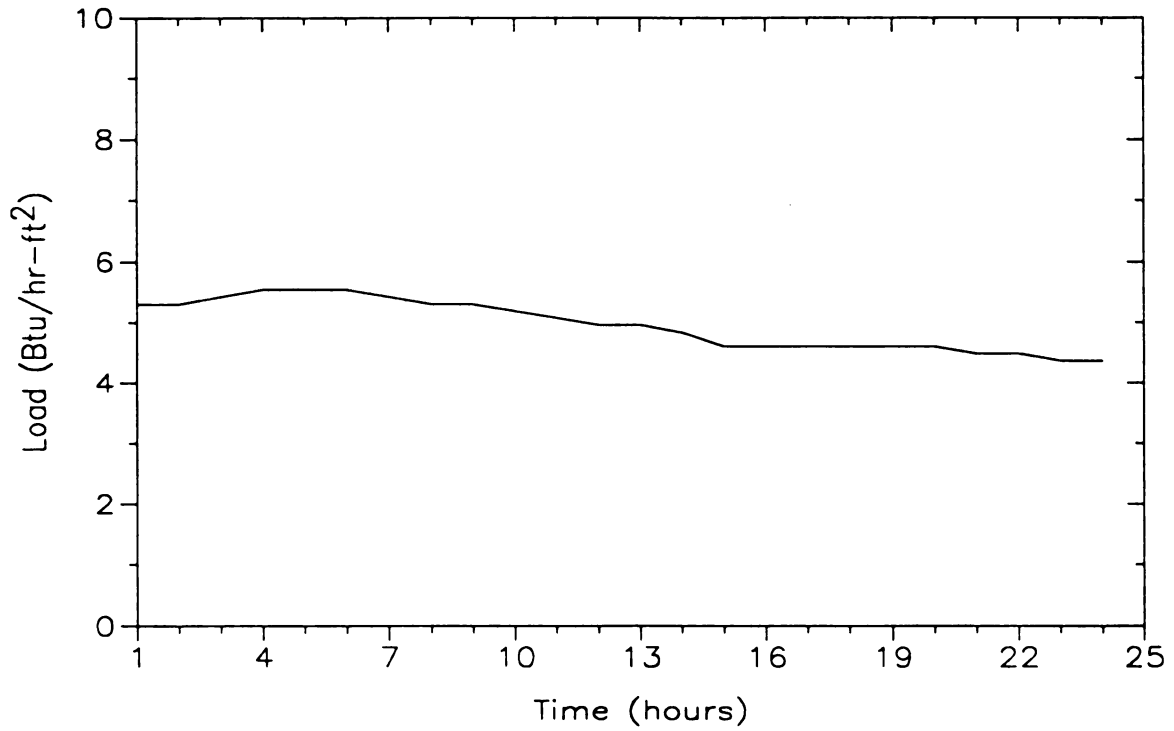


Figure 53. Load profile for day 17 in January; Minneapolis, MN.

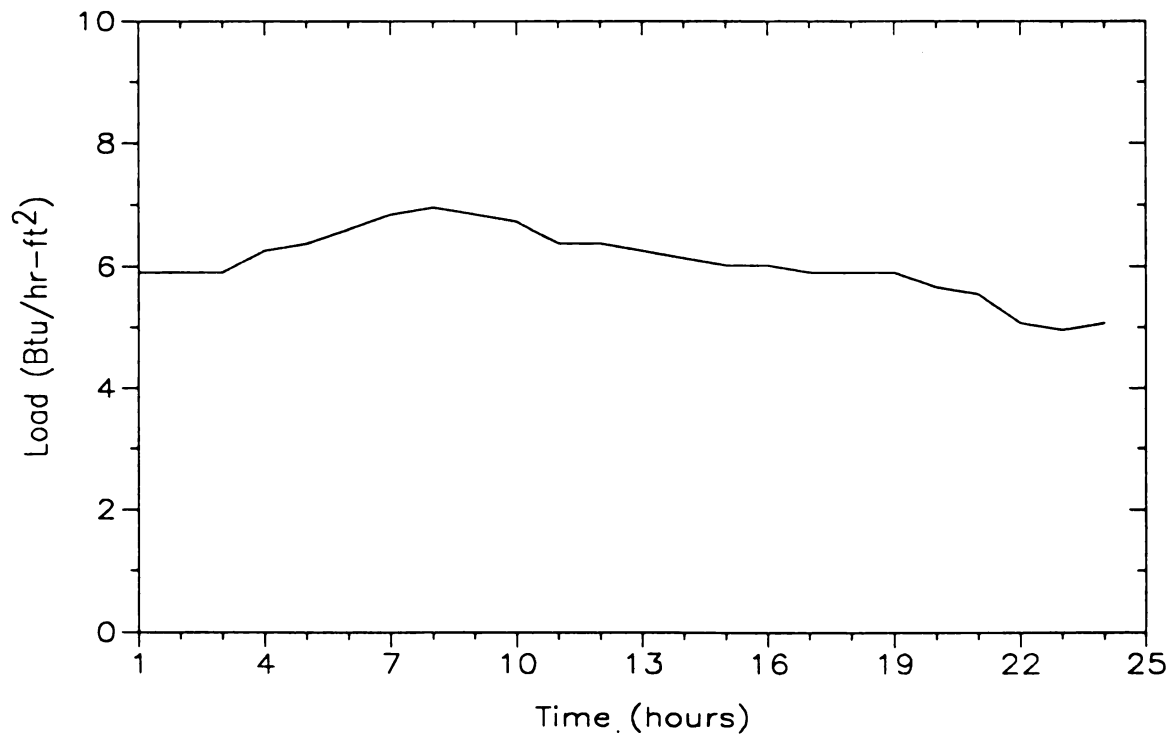


Figure 54. Load profile for day 24 in January; Minneapolis, MN.

8
6
4
2
0

Load (Btu/hr-ft²)

8
6
4
2
0

Load (Btu/hr-ft²)

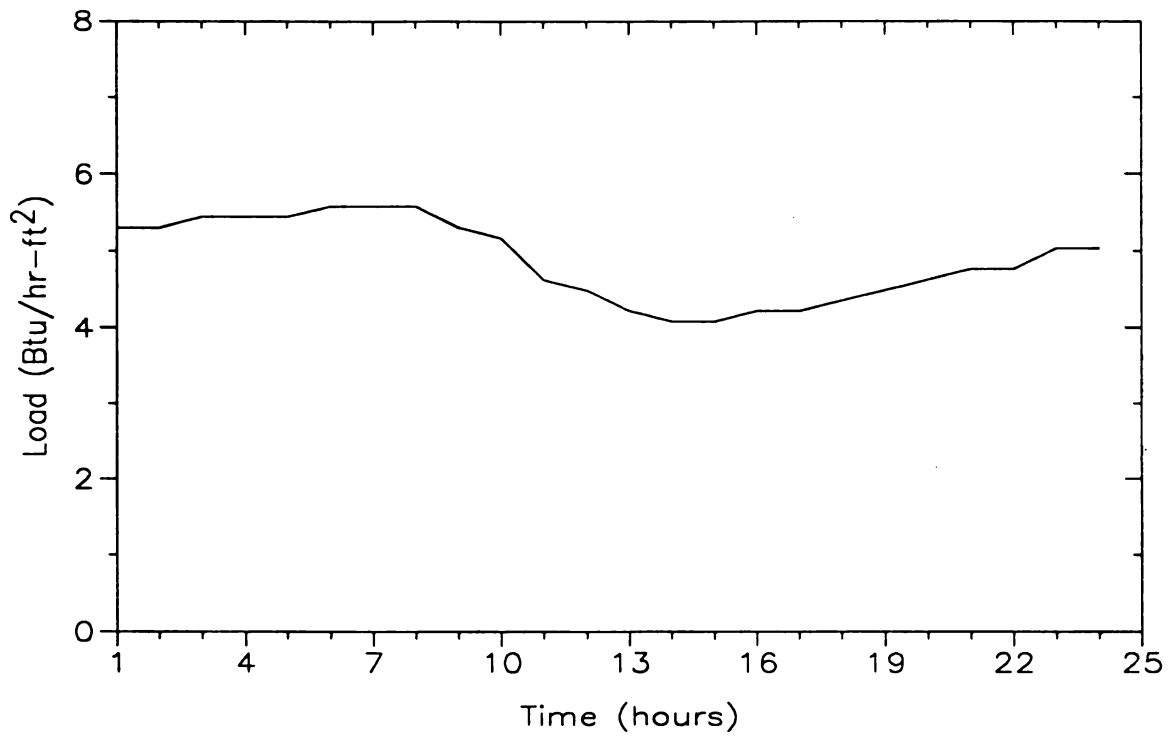


Figure 55. Load profile for day 3 in January; Washington DC.

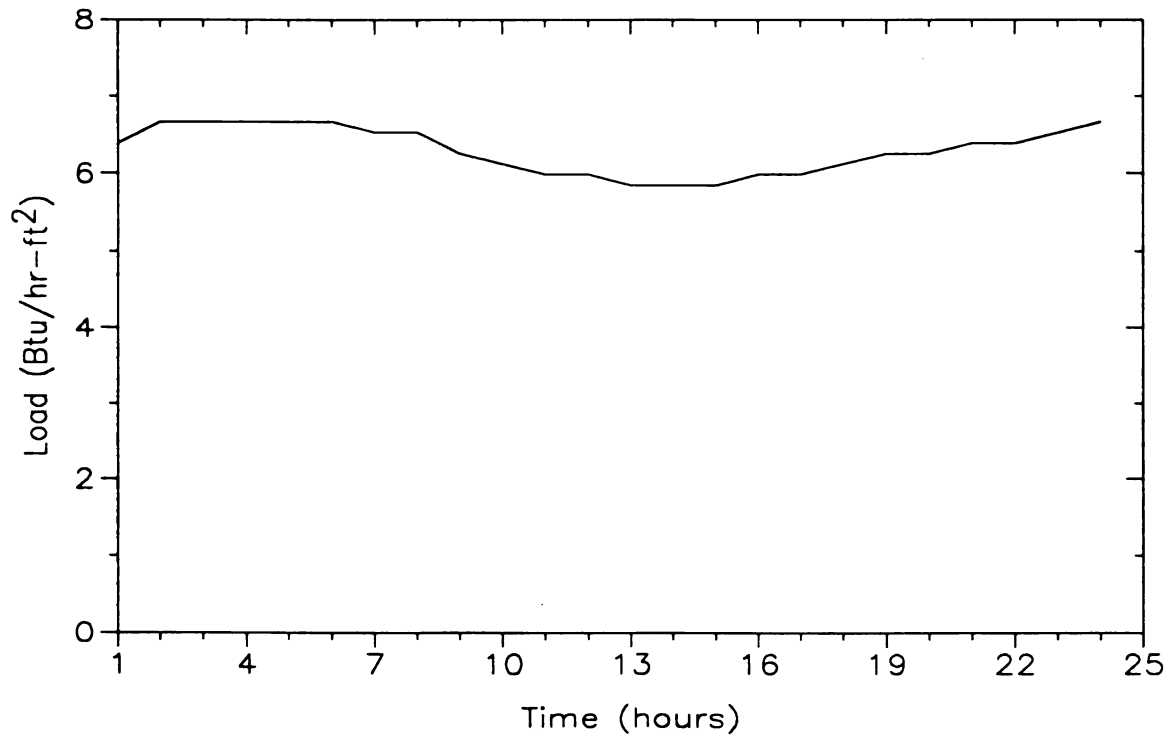


Figure 56. Load profile for day 9 in January; Washington DC.

Load (Btu/hr-ft²)

0

2

4

6

8

0

2

4

6

8

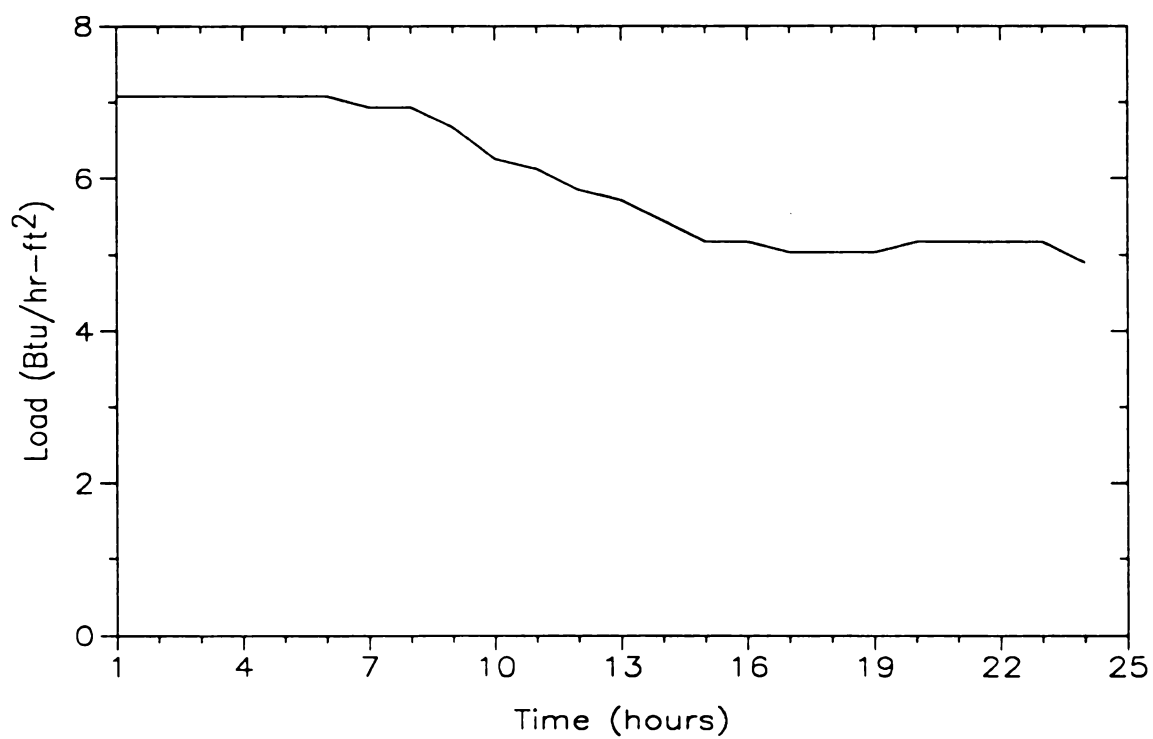


Figure 57. Load profile for day 19 in January; Washington DC.

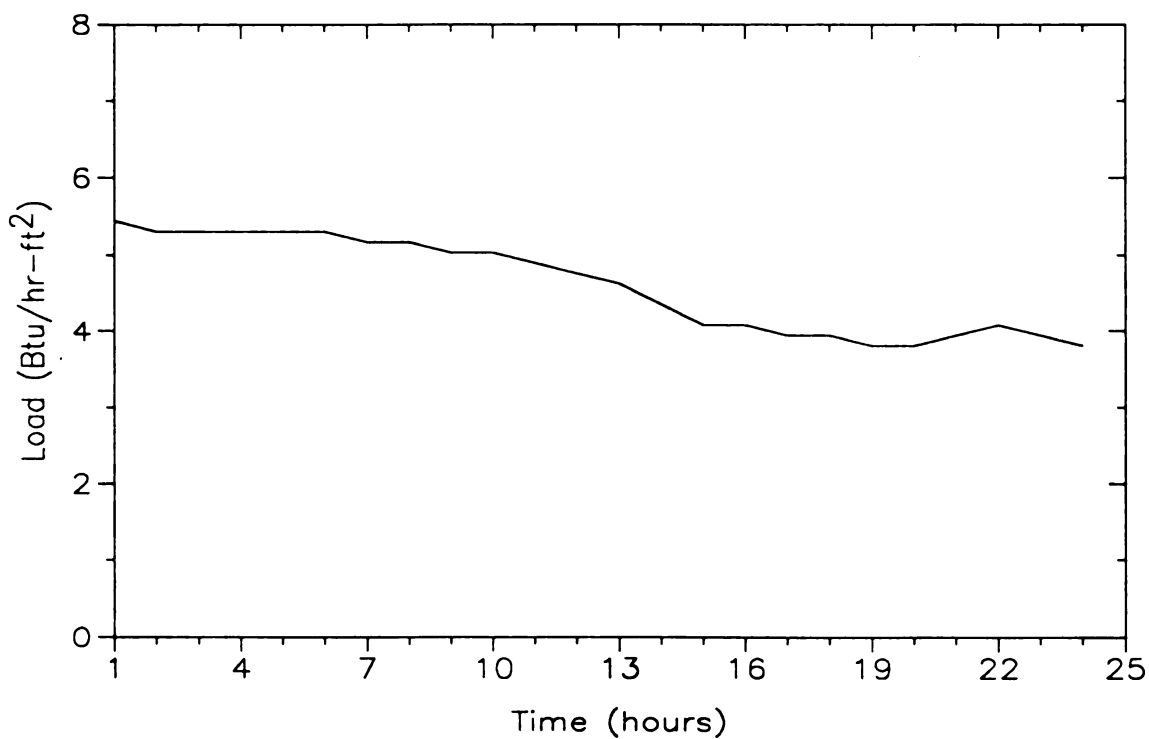


Figure 58. Load profile for day 29 in January; Washington DC.

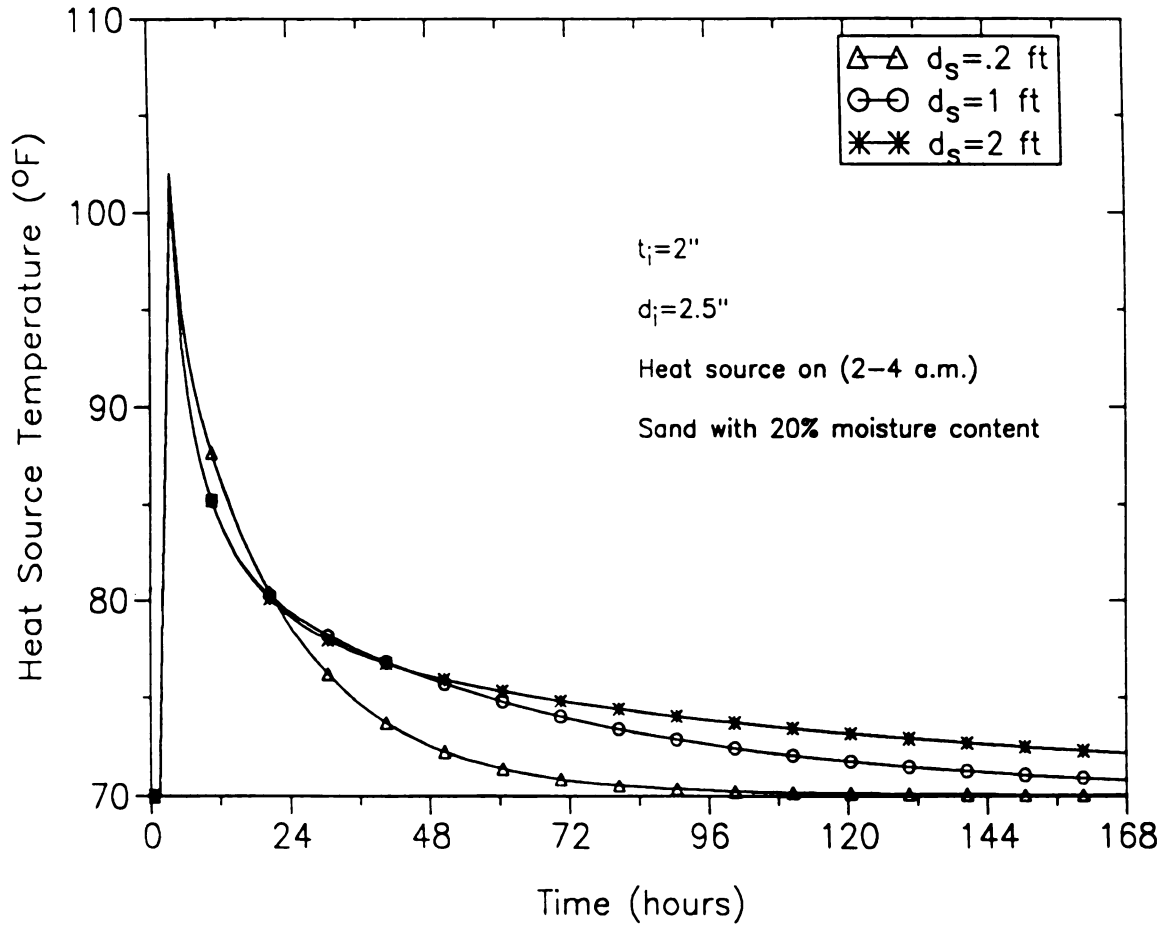


Figure 59. Variation of heating element temperature with mat depth.

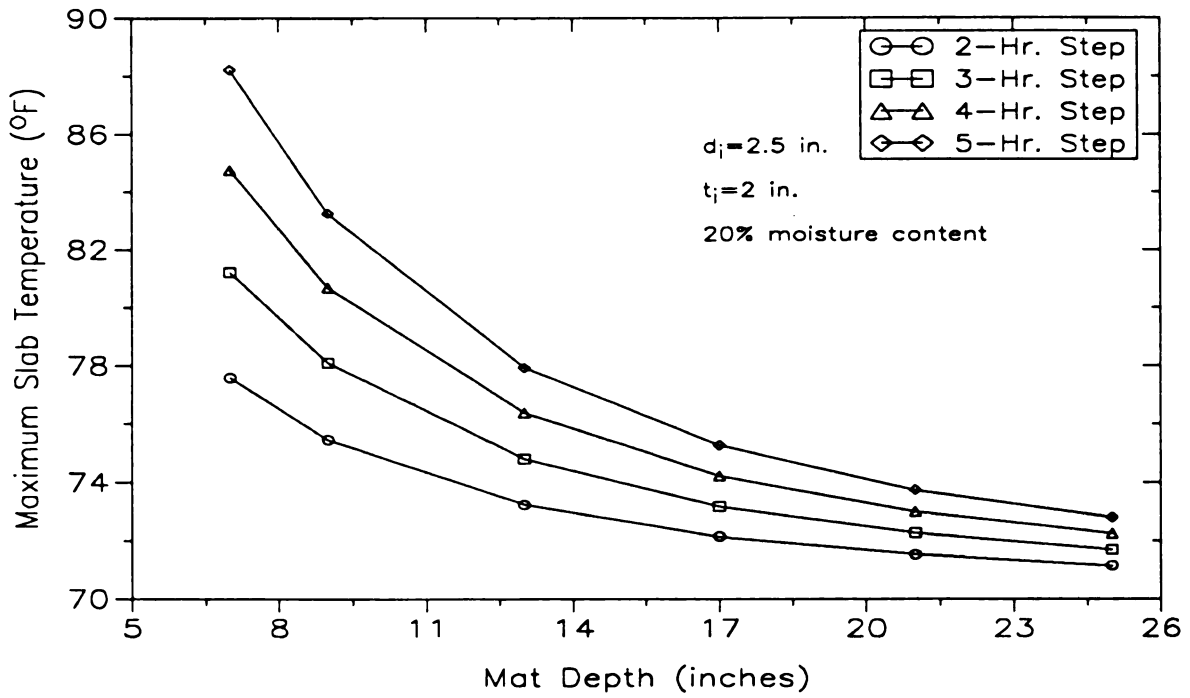


Figure 60. Maximum slab surface temperature as a function of mat depth and energy input.

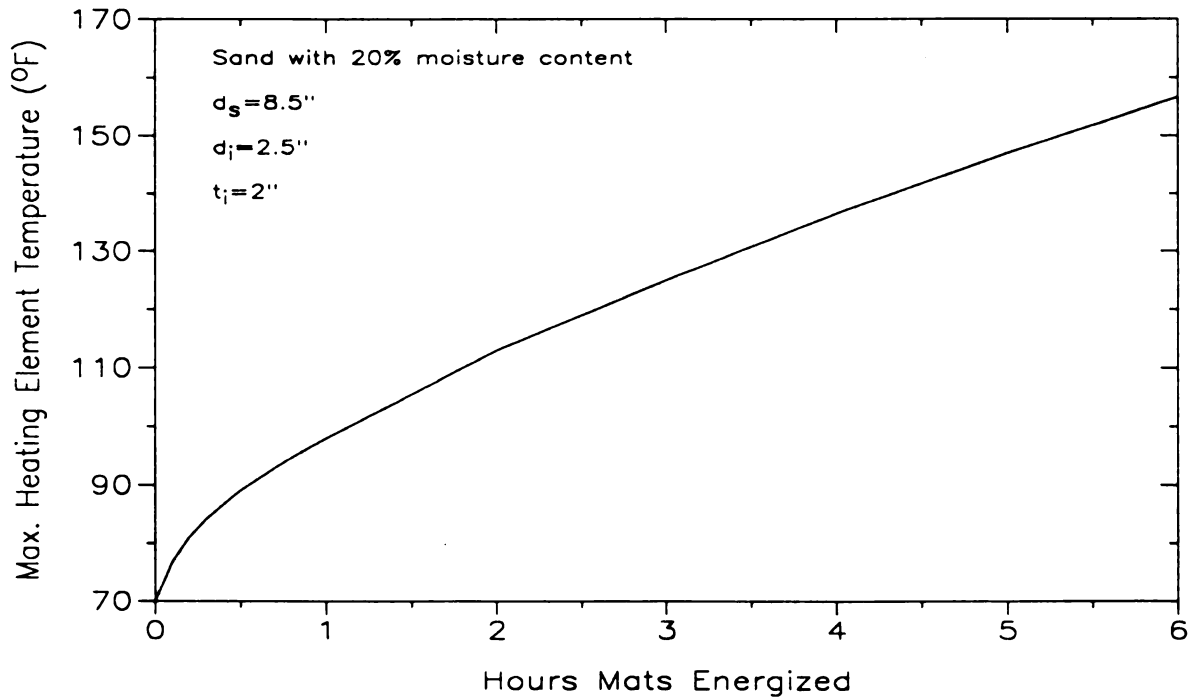


Figure 61. Maximum heating element temperature as a function of energy input.

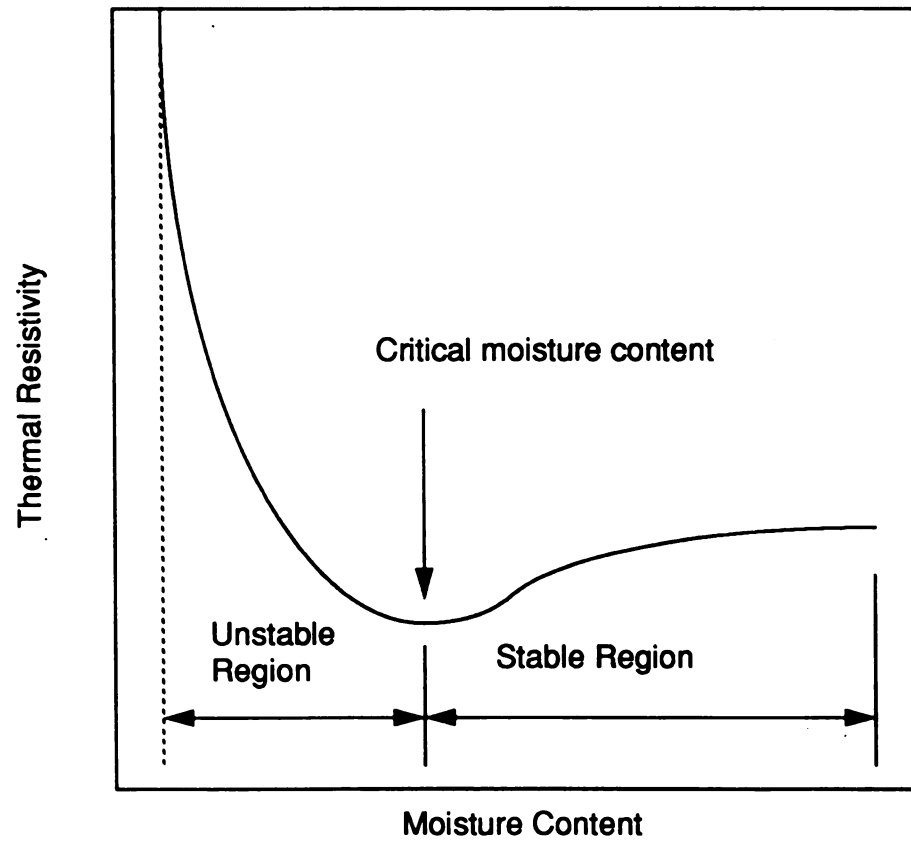


Figure 62. Variation of soil thermal resistivity with moisture content.

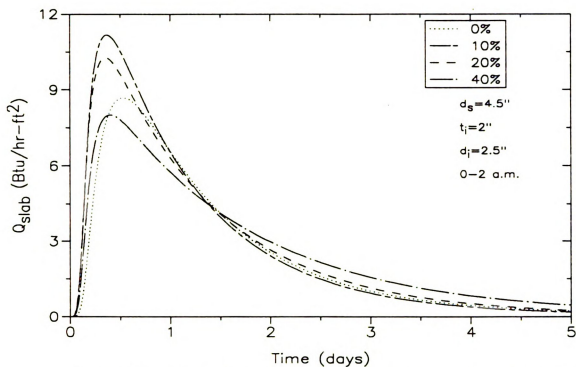


Figure 63. Effect of soil moisture content on slab heat-flux.

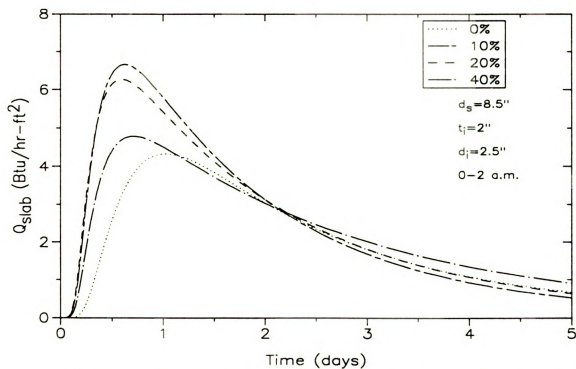


Figure 64. Effect of soil moisture content on slab heat-flux.

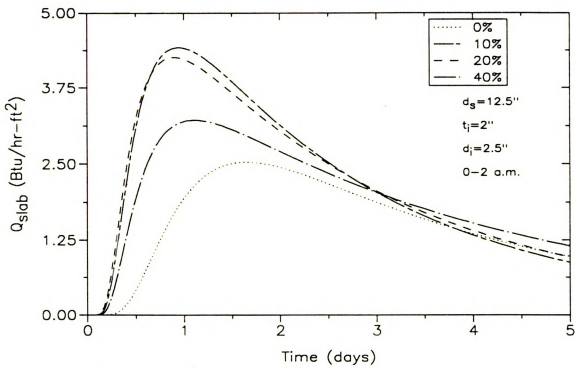


Figure 65. Effect of soil moisture content on slab heat-flux.

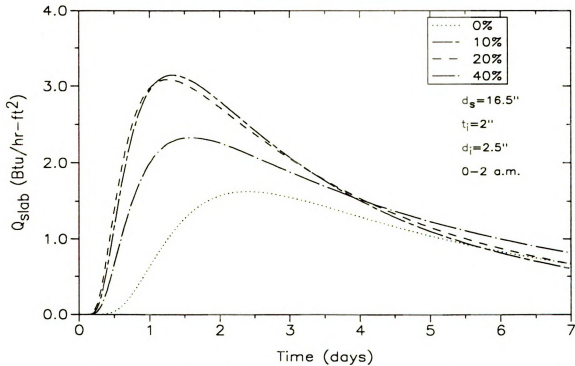


Figure 66. Effect of soil moisture content on slab heat-flux.

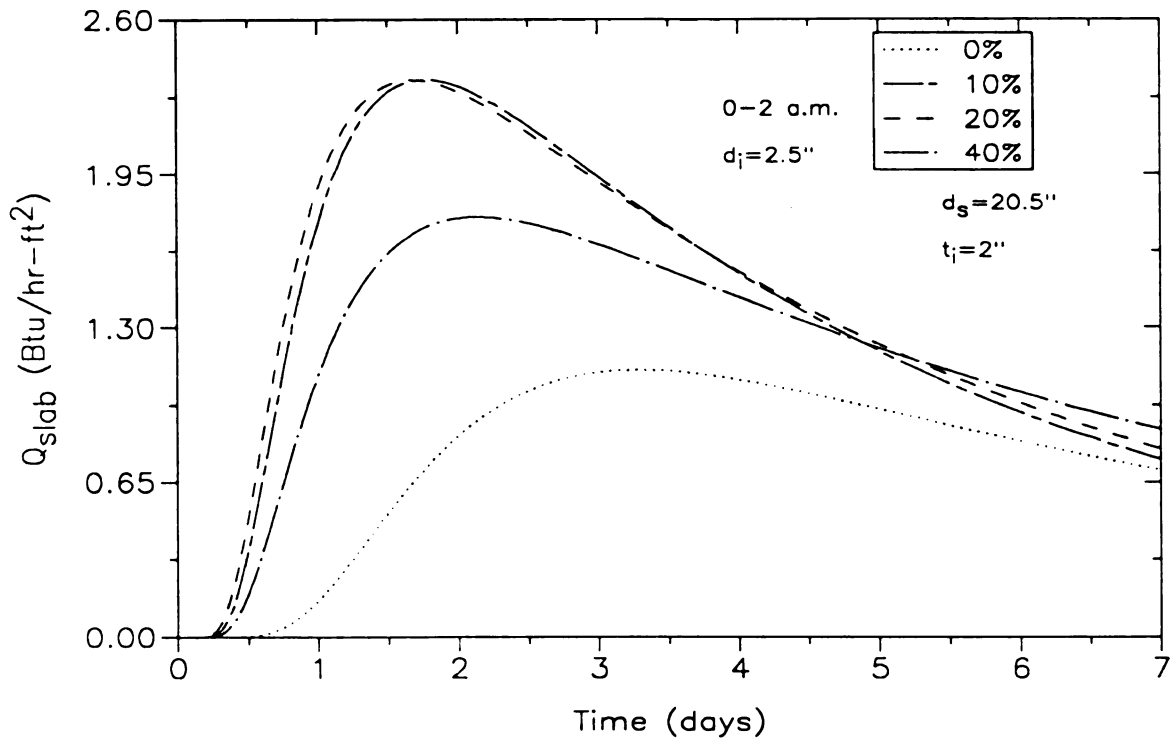


Figure 67. Effect of soil moisture content on slab heat-flux.

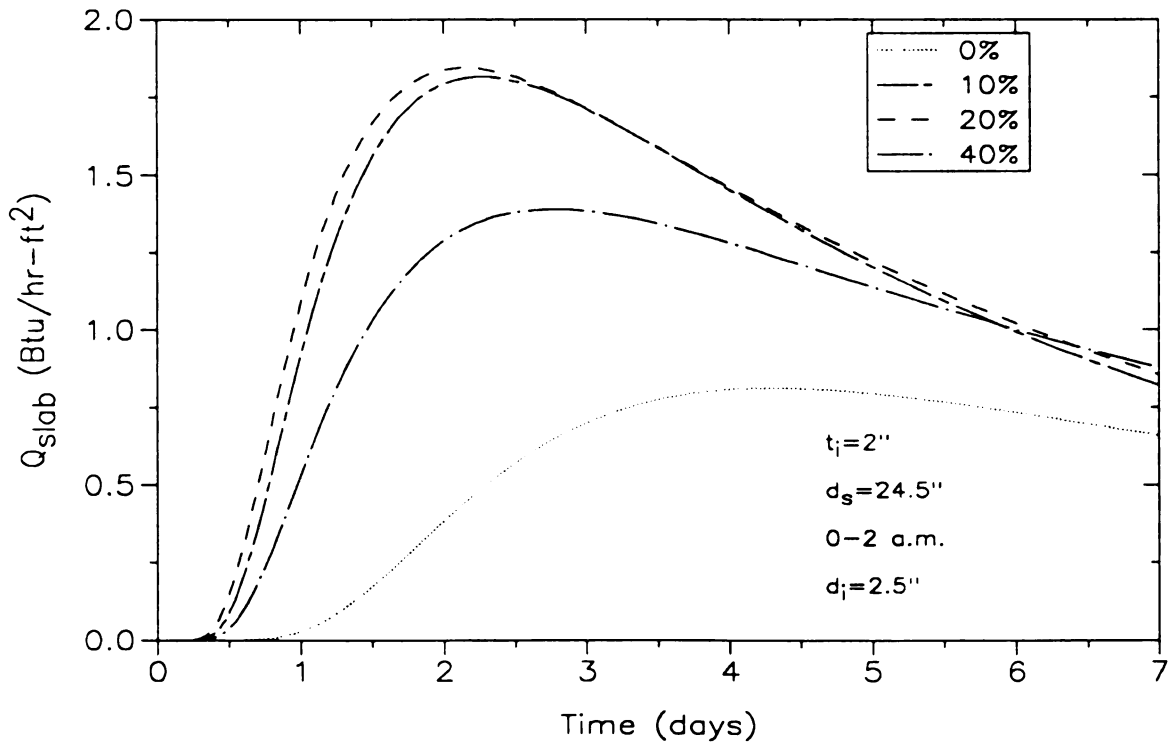


Figure 68. Effect of soil moisture content on slab heat-flux.

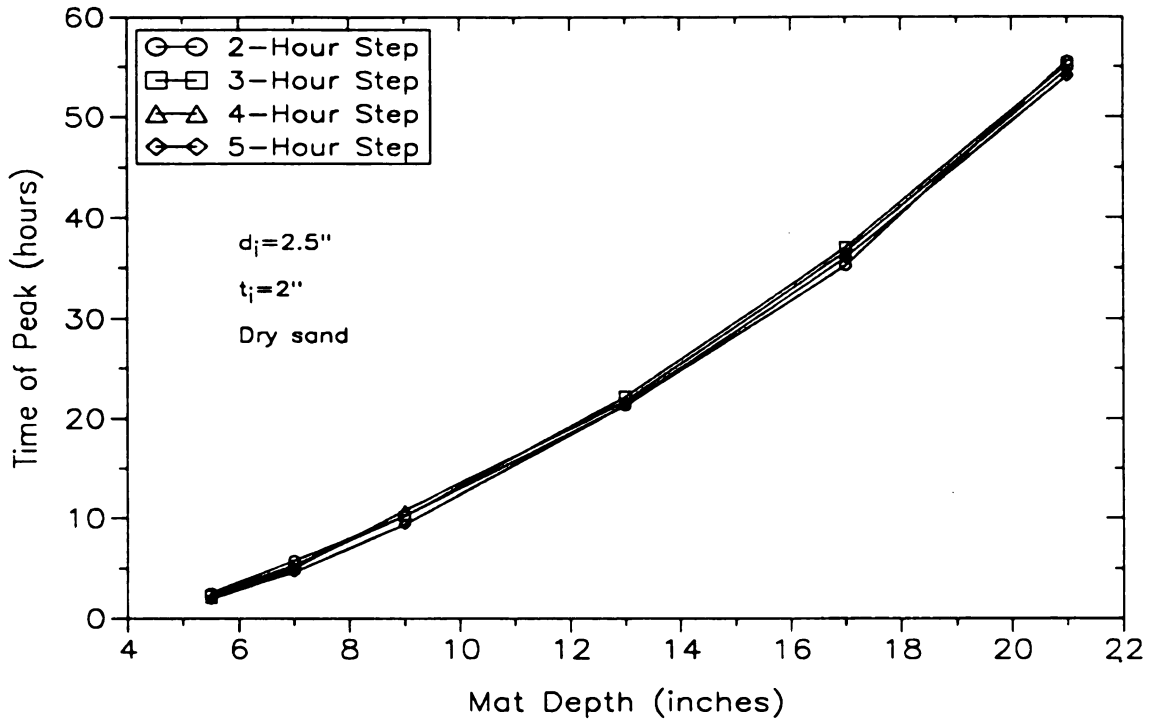


Figure 69. Time of peak heat-flux as a function of mat depth and energy input.

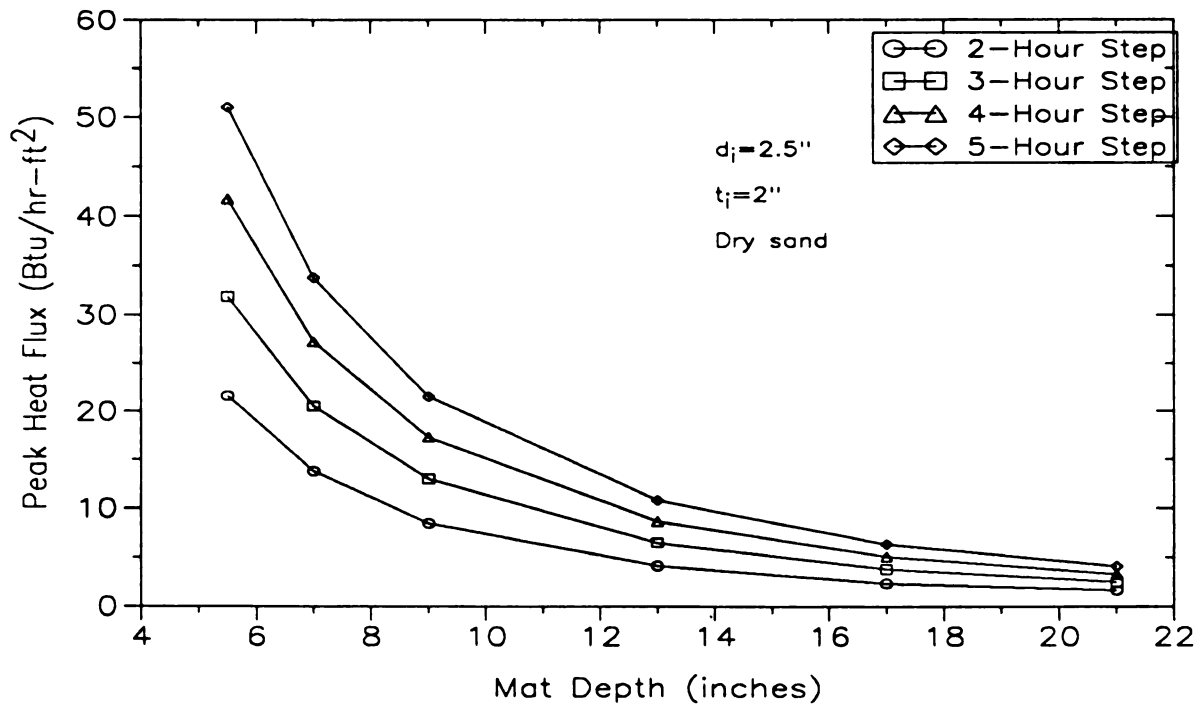


Figure 70. Peak heat-flux as a function of mat depth and energy input.

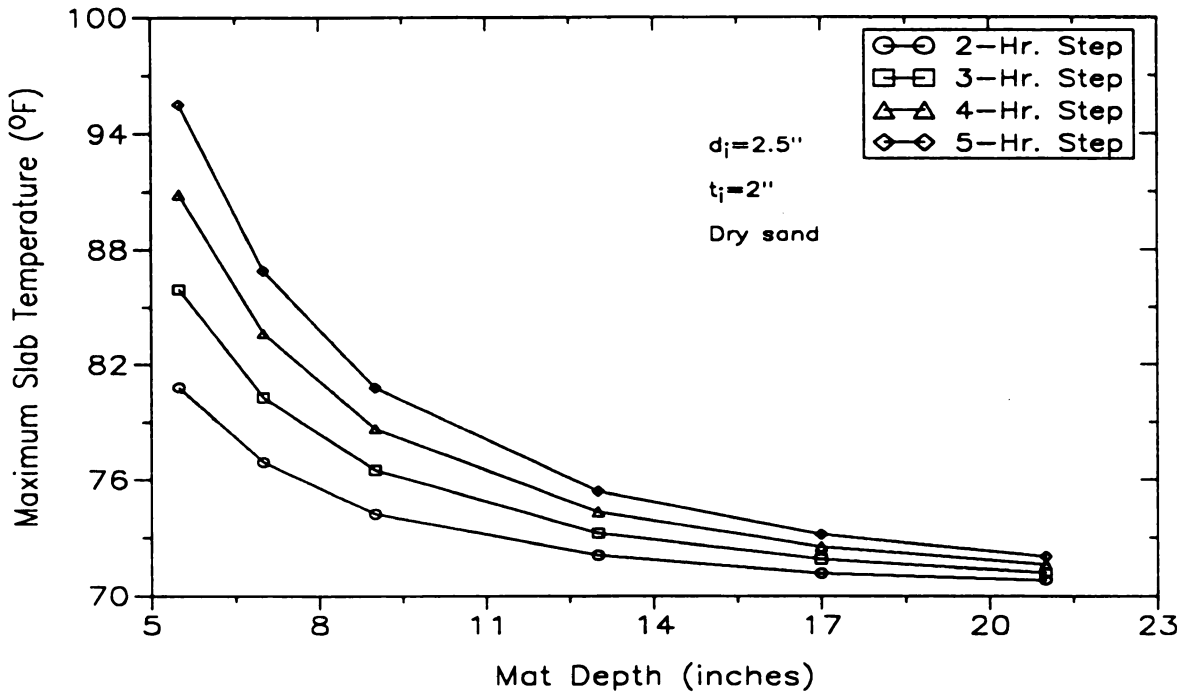


Figure 71. Maximum slab surface temperature as a function of mat depth and energy input.

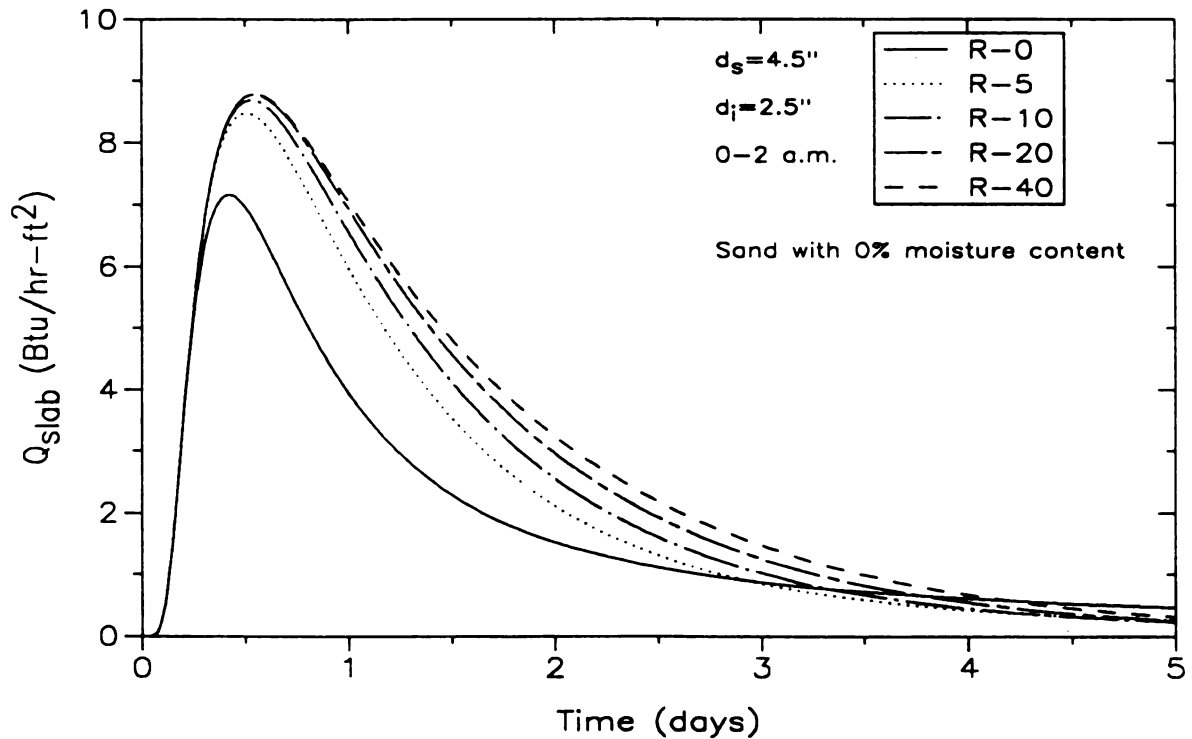


Figure 72. Variation of slab heat-flux with insulation R-value.

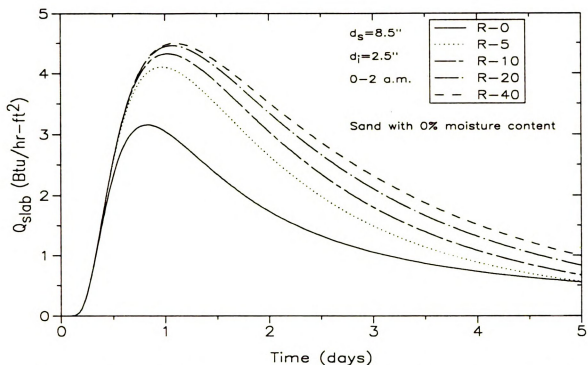


Figure 73. Variation of slab heat-flux with insulation R-value.

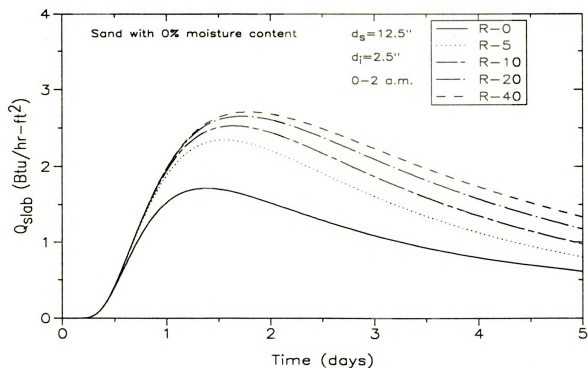


Figure 74. Variation of slab heat-flux with insulation R-value.

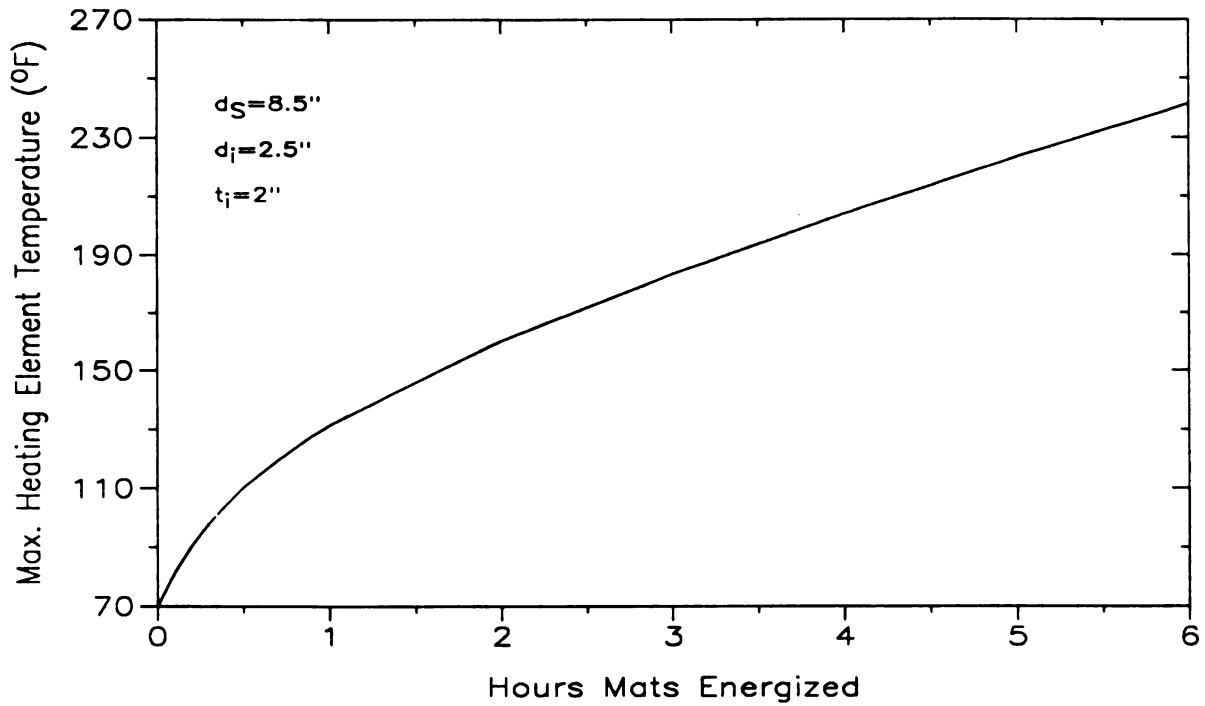


Figure 75. Maximum heating element temperature as a function of energy input for dry sand.

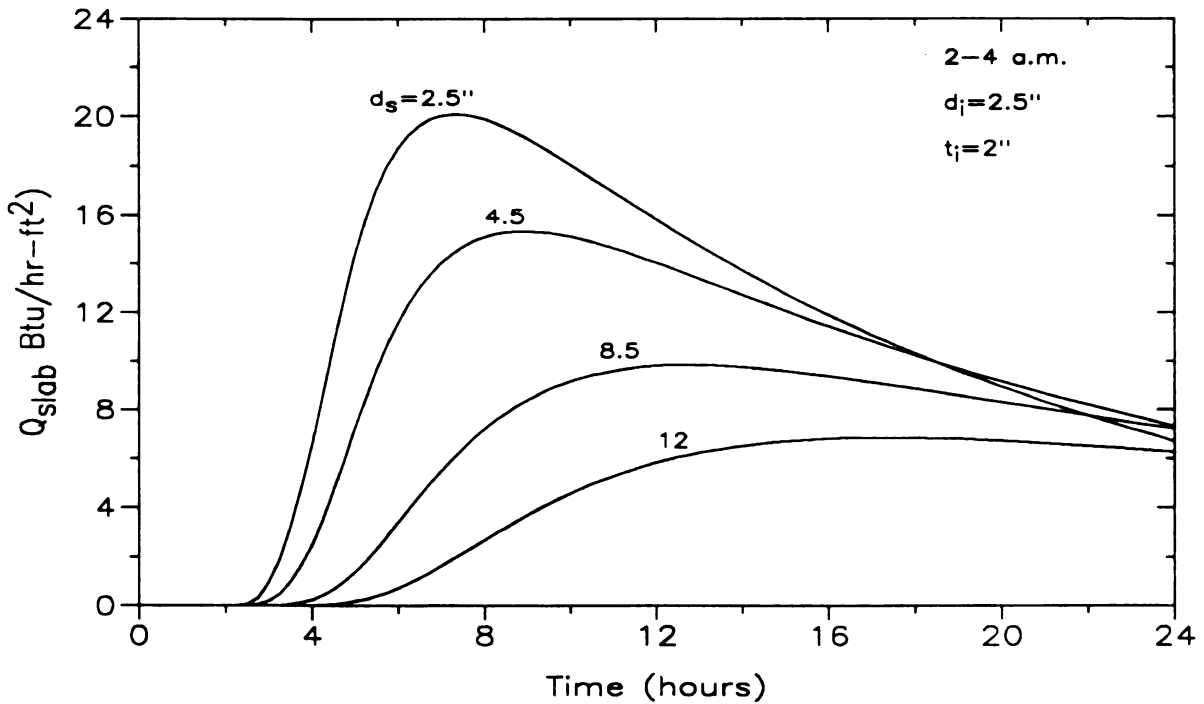


Figure 76. Variation of slab heat-flux with mat depth for $\alpha_{\text{sand}} = 0.044 \text{ ft}^2/\text{hr}$.

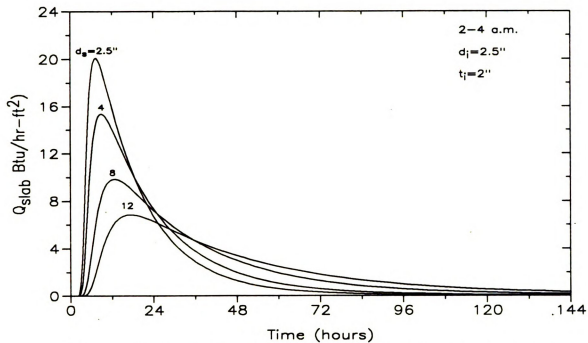


Figure 77. Variation of slab heat-flux with mat depth for $\alpha_{\text{sand}} = 0.044 \text{ ft}^2/\text{hr}$.

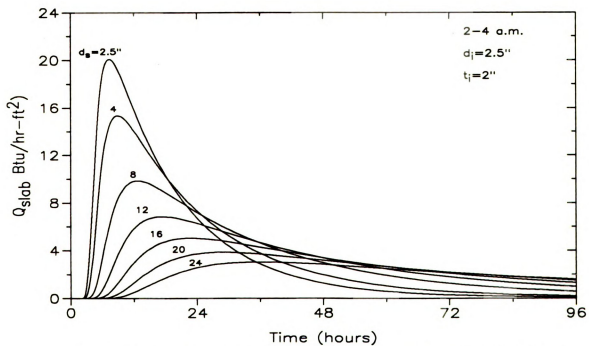


Figure 78. Variation of slab heat-flux with mat depth for $\alpha_{\text{sand}} = 0.044 \text{ ft}^2/\text{hr}$.

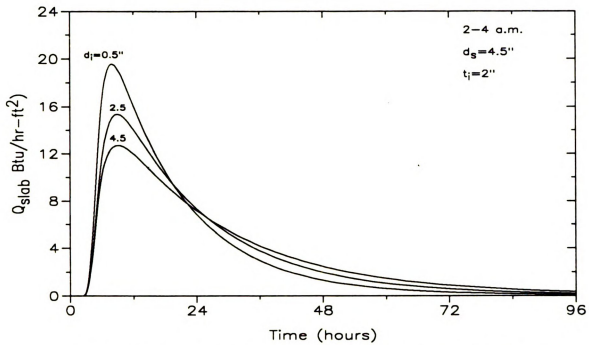


Figure 79. Variation of slab heat-flux for various sand layer thicknesses for $\alpha_{sand} = 0.044 \text{ ft}^2/\text{hr}$.

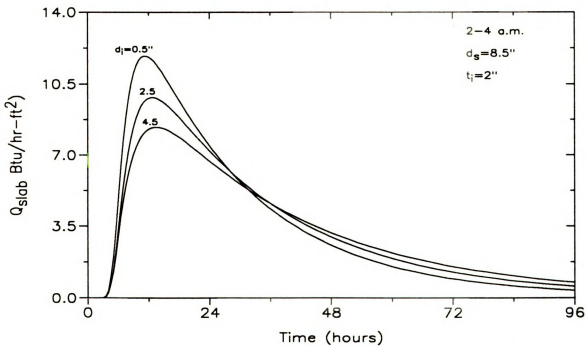


Figure 80. Variation of slab heat-flux for various sand layer thicknesses for $\alpha_{sand} = 0.044 \text{ ft}^2/\text{hr}$.

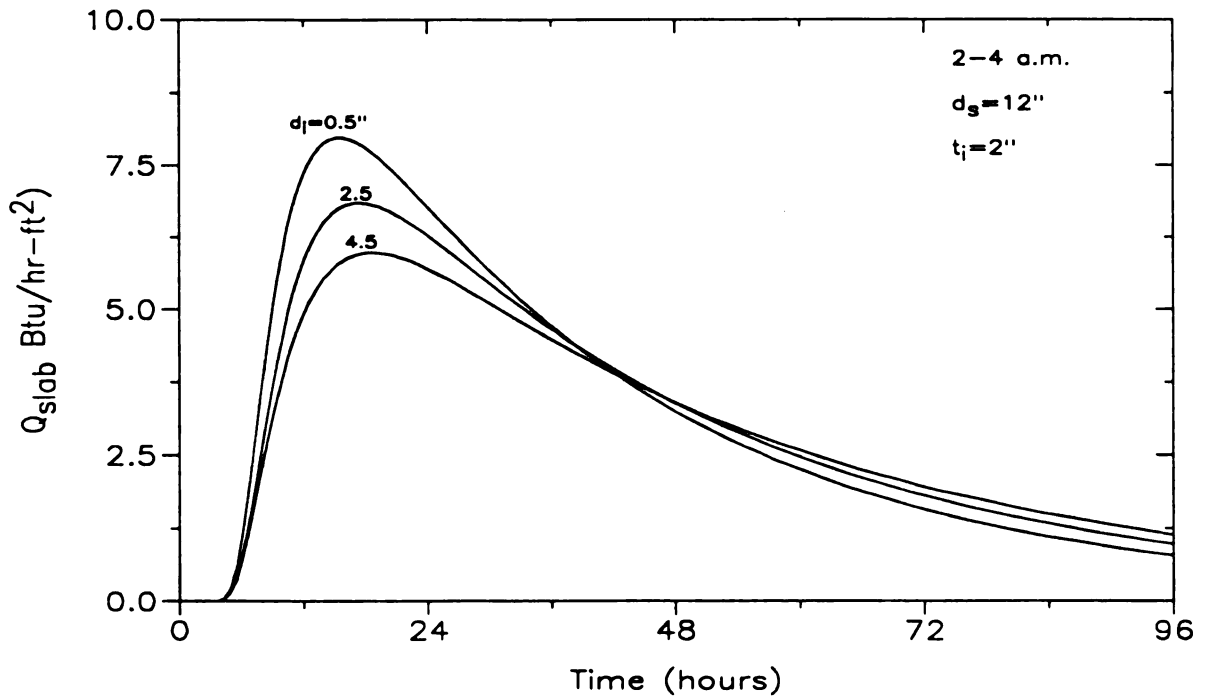


Figure 81. Variation of slab heat-flux for various sand layer thicknesses for $\alpha_{sand} = 0.044$ ft²/hr.

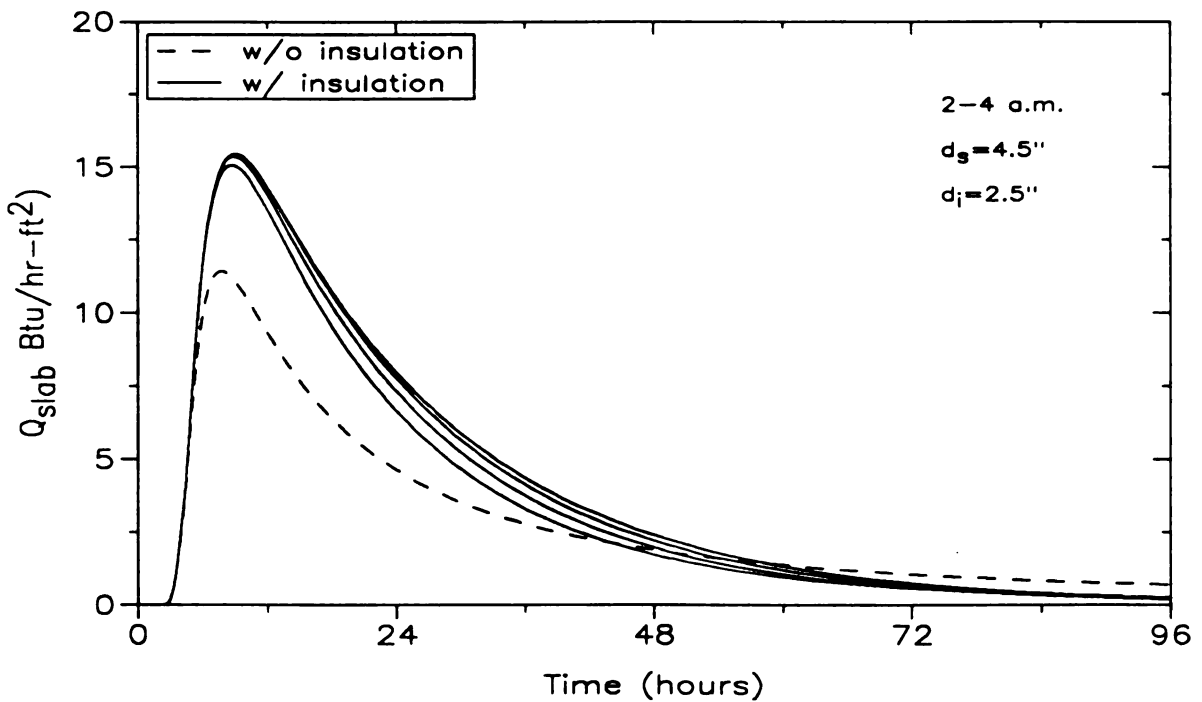


Figure 82. Variation of slab heat-flux for various insulation levels for $\alpha_{sand} = 0.044$ ft²/hr.

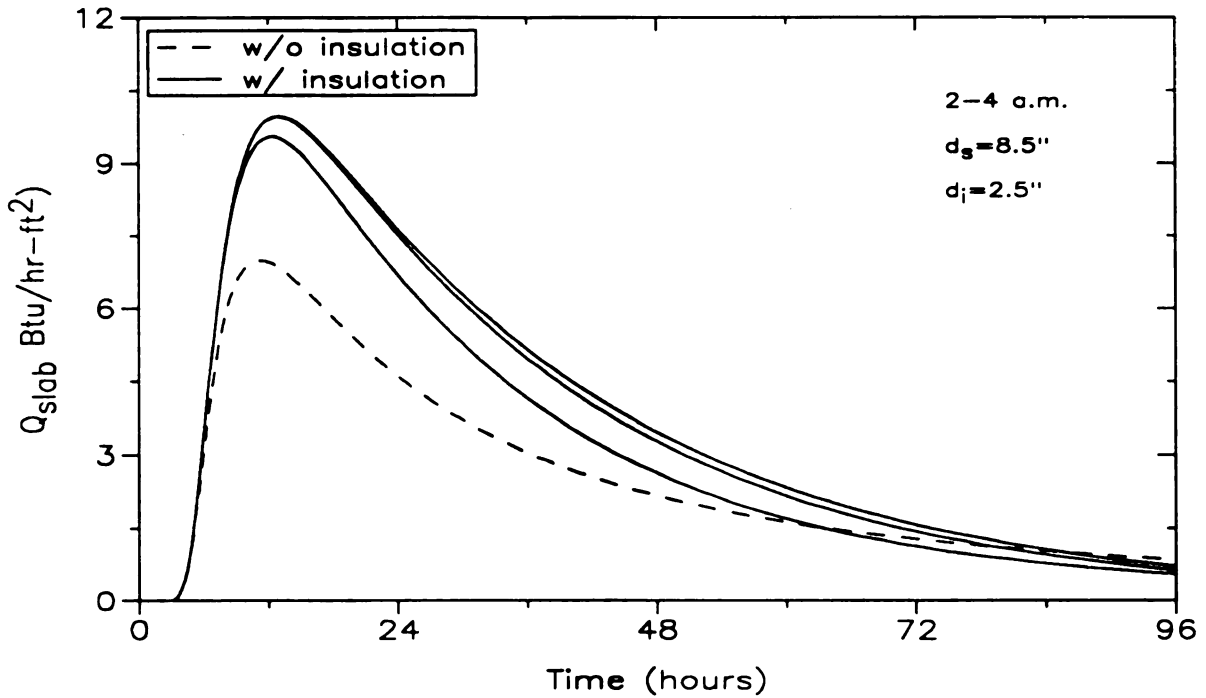


Figure 83. Variation of slab heat-flux for various insulation levels for $\alpha_{sand}=0.044 \text{ ft}^2/\text{hr}$.

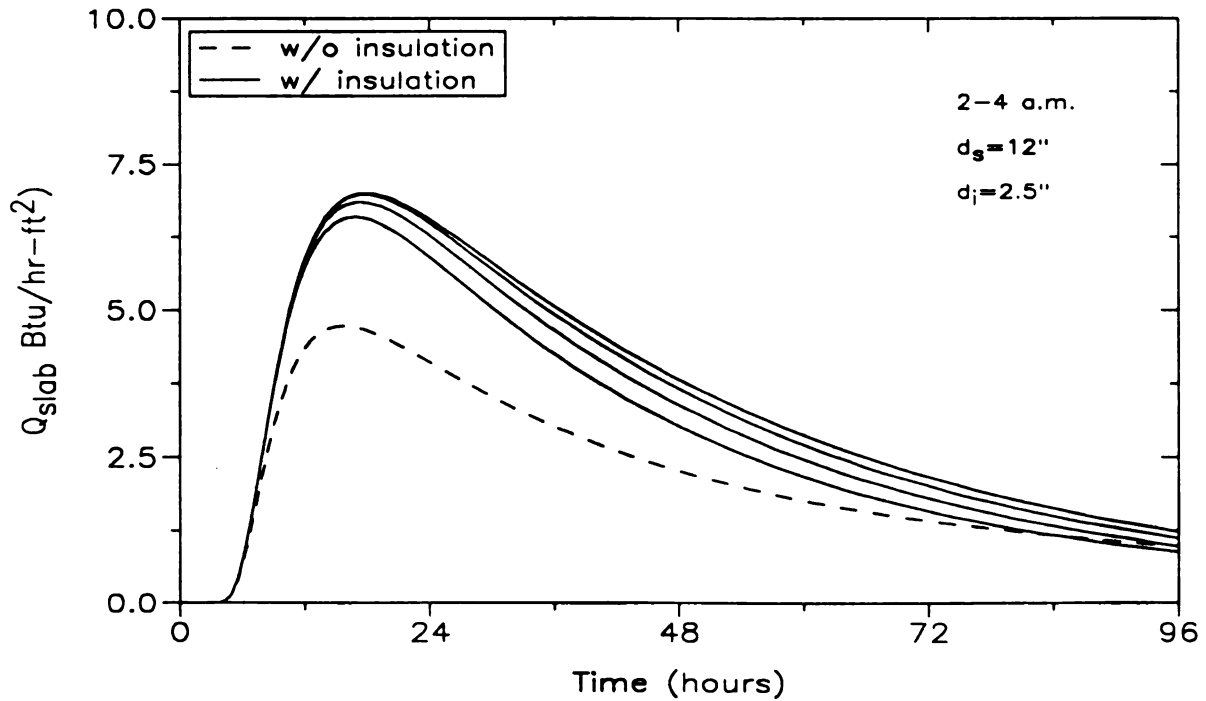


Figure 84. Variation of slab heat-flux for various insulation levels for $\alpha_{sand}=0.044 \text{ ft}^2/\text{hr}$.

REFERENCES

REFERENCES

- ASHRAE 1985. *ASHRAE handbook - 1985 fundamentals*. American Society of Heating, Refrigerating, and Air-Conditioning Engineers, Atlanta, GA.
- ASHRAE 1987. *ASHRAE handbook - HVAC systems and applications*. American Society of Heating, Refrigeration, and Air-Conditioning Engineers, Atlanta, GA.
- Brandemuehl, M.J. and Beckman, W.A. 1979. "Economic evaluation and optimization of solar heating systems." *Solar Energy*, Vol. 23.
- Christian, J.E. and Strzepek, W.R. 1987. "Procedure of determining the optimum foundation insulation levels for new low-rise residential buildings." *ASHRAE Transactions*, Vol. 93, Part 1.
- Class notes, 1990. Applied Energy Conversion, University of Michigan, Ann Arbor, MI.
- DOE2 Engineers Manual Version 2.1A* 1982. Energy and Environmental Division, Building Energy Simulation Group, Lawrence Berkeley Laboratory, Berkeley, CA.
- Green, M.A. 1982. *Solar Cells, Operating Principles, Technology, and System Applications*. Prentice Hall, Inc. Englewood Cliffs, NJ.
- Harrison, E. 1959. "The intermittent heating of buildings by off-peak electricity supplies." *Journal of the Institute of Heating and Ventilating Engineers*, Vol. 27.
- IES 1984. *Lighting Handbook Reference Volume*. Illuminating Engineering Society.
- Kedl, R.J. 1983. "Assessment of energy storage technology." Oak Ridge National Laboratory Report ORNL/TM - 8997.
- Labs, K., Carmody, J., Sterling, R., Shen, L., Huang, Y.J., and Parker, D. 1988. *Building foundation design handbook*. Oak Ridge National Laboratory Report ORNL/Sub 86-72143/1.

MacArthur, J.W., Mathur, A., and Zhao, J. 1989. "On-Line recursive estimation for load profile prediction." *ASHRAE Transactions*, Vol. 95, Part 1.

NBS. *Comprehensive Guide for Least Cost Energy Decisions* (Special publication 709) U.S. Government Printing Office, Washington D.C.

Nevins, R.G., Michaels, K.B., and Feyerherm, A.M. 1964. "The effect of floor surface temperature on comfort: Part I, college age males." *ASHRAE Transactions*, Vol. 70.

Papalambros, P.Y. and Wilde, D.J. 1988 *Principles of Optimal Design: Modeling and Computation*. New York: Cambridge University Press.

Parker, D.S. and Carmody, J.C. 1988. "Economic optimization of building foundation insulation levels." *ASHRAE Transactions*, Vol. 94, Part 2.

Patankar, S.V. 1980. *Numerical Heat Transfer and Fluid Flow*. Hemisphere Publishing Corporation, McGraw-Hill, N.Y.

Radhakrishna, H.S., Chur, F.Y., and Boggs, A.A. 1980. "Thermal instability and its prediction in cable backfill soils." *IEEE Transactions on Power Apparatus and Systems*, Vol. PAS-99, No. 3.

Salomone, L.R. 1988. *Feasibility study for collecting site soil characterization thermal property data for residential construction*. Oak Ridge National Laboratory ORNL/Sub/86-04923/1.

General References

Ackerman, M. and Dale, J.D. 1987. "Measurement and prediction of insulated and uninsulated basement wall heat losses in a heating climate." *ASHRAE Transactions*, Vol. 93, Part 1.

Beck, J.V. and Arnold, K.J. 1977. *Parameter Estimation in Engineering and Science*. John Wiley & Sons, New York.

Beck, J.V., McLain, H.A., Karnitz, M.A., Shonder, J.A., and Segan, E.G. 1988. "Heat losses form underground steam pipelines." *Transactions of the ASME*, Vol. 110.

Bonacina, C. and Comini, G. 1973. "On the solution of the nonlinear heat conduction equations by numerical methods." *International Journal of Heat and Mass Transfer*, Vol. 16.

Borresen, B.A. 1990. "Controllability - Back to Basics." *ASHRAE Transactions*, Vol. 96, Part 2.

Braun, J.E. 1990. "Reducing energy costs and peak electrical demand through optimal control of building thermal storage." *ASHRAE Transactions*, Vol. 96, Part 2.

Brian, P.L.T. 1961. "A finite difference method of high-order accuracy for the solution of three-dimensional transient heat conduction problems." *A.I.Ch.E. Journal*, Vol. 7.

Brodrick, J.R. 1989. "The equipment R&D benefits of characterizing the energy requirements of office buildings and multifamily housing." *ASHRAE Transactions*, Vol. 95.

Campbell, J. 1990. "Calculation of heat requirements with intermittent heating." *ASHRAE Transactions*, Vol. 96, Part 1.

Ceylan, T.H. and Myers, G.E. 1980. "Long-time solutions to heat conduction transients with time-dependant inputs." *Journal of Heat Transfer*, Vol. 96, Part 2.

Christian, J. E. 1988. "Foundation futures: energy saving opportunities offered by ASHRAE Standard 90.2P." *ASHRAE Transactions*, Vol. 96, Part 2.

Cleaveland, J.P. and Akridge, J.M. 1990. "Slab-on-grade thermal loss in hot climates." *ASHRAE Transactions*, Vol. 96, Part 1.

Crawley, D.B. and Huang, Y.J. 1989. "Using the office building and multifamily data bases in the assessment of HVAC equipment performance." *ASHRAE Transactions*, Vol. 95, Part 1.

Douglas, J. and Rachford, H.H. 1956. "On the numerical solution of heat conduction problems in two and three space variables." *Trans. Am. Math. Soc.*, 82.

Huang, Y.J., Ritschard, R.L., and Fay, J. M. 1989. "DOE-2.1D data base of building loads for prototypical multifamily buildings." *ASHRAE Transactions*, Vol. 95, Part 1.

Huang, Y.J., Shen, L.S., Bull, J., and Goldberg, L. 1988. "Whole-house simulation of foundation heat-flows using the DOE-2.1C program." *ASHRAE Transactions*, Vol. 94, Part 2.

Jaluria, Y. and Torrance, K.E. 1986. *Computational Heat Transfer*. Hemisphere Publishing Corporation, A subsidiary of Harper & Row, Publishers, Inc.

Krarti, M. and Claridge, D.E. 1988. "Analytical calculation procedure for underground heat losses." *ASHRAE Transactions*, Vol. 94, Part 2.

Kusuda, T. and Achenbach, P.R. 1965. "Earth temperature and thermal diffusivity at selected stations in the United States." *ASHRAE Transactions*, Vol.96, Part 2.

MacCluer, C.R. 1989. "Temperature variations of flux-modulated radiant slab systems." *ASHRAE Transactions*, Vol. 95, Part 1.

MacCluer, C.R. 1990. "Analysis and simulation of outdoor reset control of radiant slab heating systems." *ASHRAE Transactions*, Vol. 96, Part 1.

MacCluer, C.R., Miklavcic, M., and Chait, Y. 1989. "The temperature stability of a radiant slab-on-grade." *ASHRAE Transactions*, Vol.95, Part 1.

Meixel, G. D. Jr. and Bligh, T.P. 1983. *Earth Contact Systems: Final Report* University of Minnesota, Underground Space Center DOE/SF/11508-TS.

Mitalas, G.P. 1987. "Calculation of below-grade residential heat loss: low-rise residential building." *ASHRAE Transactions*, Vol. 93, Part 1.

Ozisik, M.N. 1980. *Heat Conduction*. A Wiley - Interscience Publication, John Wiley & Sons.

Parker, D.S. 1987. "F-factor correlations for determining earth contact heat loads." *ASHRAE Transactions*, Vol. 93, Part 1.

Perry, E. H., Cunningham, G.T. and Scesa, S. 1985. "Analysis of heat losses through residential floor slabs." *ASHRAE Transactions*, Vol. 91, Part 2A.

Rosenfeld, A. and Moriniere, O. de la, 1985. "The high cost-effectiveness of cool storage in new commercial buildings." *ASHRAE Transactions*, Vol. 91, Part 2.

Smith-Gates Easyheat 1990. *The foundation of a reliable heating system*, Farmington, CT.

Sterling, R., Meixel, G., Shen, L., Labs, K., and Bligh, T. 1985. "Assessment of the energy savings potential of building foundation research." ORNL/Sub/84-002401/1, Oak Ridge National Laboratory.

Thiyagarajan, R and Yovanovich, M.M. 1974. "Thermal resistance of a buried cylinder with constant flux boundary condition." *ASME Journal of Heat Transfer*, Vol. 96.

Walton, G. N. 1987. "Estimating 3-D heat loss from rectangular basements and slabs using 2-D calculations." *ASHRAE Transactions*, Vol. 93, Part 1.

APPENDICES

APPENDIX A

APPENDIX A

Sample Output of ASEAM2.1
(System Energy Requirement
for building in Chicago, IL)

Report	System	Cycle	Month	Bin Temp	Bin Hours	Oper Hours	Baseboard Load
SB	1	1	1	42.5	1.7	1.7	219,632
SB	1	1	1	37.5	35.5	35.5	283,996
SB	1	1	1	32.5	95.2	95.2	348,359
SB	1	1	1	27.5	39.8	39.8	412,723
SB	1	1	1	22.5	20.6	20.6	477,087
SB	1	1	1	17.5	15.5	15.5	541,450
SB	1	1	1	12.5	19.4	19.4	605,814
SB	1	1	1	7.5	1.7	1.7	670,178
SB	1	1	1	2.5	0.8	0.8	734,541
SB	1	1	2	57.5	2.8	2.8	34,303
SB	1	1	2	52.5	11.1	11.1	78,466
SB	1	1	2	47.5	11.3	11.3	143,165
SB	1	1	2	42.5	13.4	13.4	207,864
SB	1	1	2	37.5	32.6	32.6	272,563
SB	1	1	2	32.5	35.4	35.4	337,262
SB	1	1	2	27.5	35.3	35.3	401,961
SB	1	1	2	22.5	30.0	30.0	466,660
SB	1	1	2	17.5	9.0	9.0	531,359
SB	1	1	2	12.5	10.0	10.0	596,058
SB	1	1	2	7.5	8.1	8.1	660,757
SB	1	1	2	2.5	8.3	8.3	725,456
SB	1	1	2	-2.5	0.8	0.8	790,155
SB	1	1	3	67.5	5.3	5.3	0
SB	1	1	3	62.5	5.1	5.1	5,680
SB	1	1	3	57.5	6.2	6.2	24,988
SB	1	1	3	52.5	15.8	15.8	65,439
SB	1	1	3	47.5	16.4	16.4	127,734
SB	1	1	3	42.5	23.7	23.7	192,385
SB	1	1	3	37.5	75.6	75.6	257,036
SB	1	1	3	32.5	61.1	61.1	321,687
SB	1	1	3	27.5	18.2	18.2	386,337
SB	1	1	3	22.5	2.8	2.8	450,988

SB	1	1	3	17.5	0.0	0.0	0
SB	1	1	4	87.5	9.5	9.5	0
SB	1	1	4	82.5	11.9	11.9	0
SB	1	1	4	77.5	7.8	7.8	0
SB	1	1	4	72.5	6.7	6.7	0
SB	1	1	4	67.5	14.2	14.2	0
SB	1	1	4	62.5	8.7	8.7	2,880
SB	1	1	4	57.5	24.0	24.0	19,596
SB	1	1	4	52.5	23.6	23.6	61,837
SB	1	1	4	47.5	47.4	47.4	118,066
SB	1	1	4	42.5	44.1	44.1	182,572
SB	1	1	4	37.5	22.9	22.9	247,079
SB	1	1	4	32.5	2.0	2.0	311,586
SB	1	1	4	27.5	0.0	0.0	0
SB	1	1	5	87.5	1.7	1.7	0
SB	1	1	5	82.5	21.5	21.5	0
SB	1	1	5	77.5	41.6	41.6	0
SB	1	1	5	72.5	39.7	39.7	0
SB	1	1	5	67.5	20.5	20.5	14,543
SB	1	1	5	62.5	11.9	11.9	53,992
SB	1	1	5	57.5	29.0	29.0	103,227
SB	1	1	5	52.5	26.9	26.9	167,123
SB	1	1	5	47.5	30.3	30.3	231,018
SB	1	1	5	42.5	6.9	6.9	294,913
SB	1	1	5	37.5	0.4	0.4	358,809
SB	1	1	6	92.5	24.9	24.9	0
SB	1	1	6	87.5	31.1	31.1	0
SB	1	1	6	82.5	42.6	42.6	0
SB	1	1	6	77.5	28.4	28.4	0
SB	1	1	6	72.5	42.1	42.1	0
SB	1	1	6	67.5	21.1	21.1	10,057
SB	1	1	6	62.5	23.5	23.5	45,753
SB	1	1	6	57.5	9.1	9.1	91,710
SB	1	1	6	52.5	0.0	0.0	0
SB	1	1	6	47.5	0.0	0.0	0
SB	1	1	7	92.5	6.4	6.4	0
SB	1	1	7	87.5	58.3	58.3	0
SB	1	1	7	82.5	74.5	74.5	0
SB	1	1	7	77.5	37.2	37.2	0
SB	1	1	7	72.5	40.7	40.7	0
SB	1	1	7	67.5	11.7	11.7	11,011
SB	1	1	7	62.5	1.6	1.6	42,554
SB	1	1	7	57.5	0.0	0.0	0
SB	1	1	7	52.5	0.0	0.0	0

SB	1	1	8	92.5	16.5	16.5	0
SB	1	1	8	87.5	43.4	43.4	0
SB	1	1	8	82.5	43.6	43.6	0
SB	1	1	8	77.5	62.7	62.7	0
SB	1	1	8	72.5	43.0	43.0	0
SB	1	1	8	67.5	19.2	19.2	13,024
SB	1	1	8	62.5	1.8	1.8	40,913
SB	1	1	8	57.5	0.0	0.0	0
SB	1	1	8	52.5	0.0	0.0	0
SB	1	1	9	92.5	22.6	22.6	0
SB	1	1	9	87.5	13.4	13.4	0
SB	1	1	9	82.5	20.5	20.5	0
SB	1	1	9	77.5	21.5	21.5	0
SB	1	1	9	72.5	35.5	35.5	0
SB	1	1	9	67.5	26.5	26.5	18,630
SB	1	1	9	62.5	47.8	47.8	47,127
SB	1	1	9	57.5	30.5	30.5	106,368
SB	1	1	9	52.5	4.2	4.2	169,764
SB	1	1	9	47.5	0.4	0.4	233,160
SB	1	1	9	42.5	0.0	0.0	0
SB	1	1	10	82.5	6.0	6.0	0
SB	1	1	10	77.5	16.2	16.2	0
SB	1	1	10	72.5	21.9	21.9	0
SB	1	1	10	67.5	23.8	23.8	0
SB	1	1	10	62.5	33.0	33.0	5,556
SB	1	1	10	57.5	61.8	61.8	24,568
SB	1	1	10	52.5	35.9	35.9	57,875
SB	1	1	10	47.5	21.0	21.0	120,609
SB	1	1	10	42.5	9.0	9.0	184,366
SB	1	1	10	37.5	1.7	1.7	248,124
SB	1	1	10	32.5	0.0	0.0	0
SB	1	1	11	62.5	6.0	6.0	11,017
SB	1	1	11	57.5	17.0	17.0	41,474
SB	1	1	11	52.5	45.8	45.8	91,573
SB	1	1	11	47.5	41.9	41.9	155,842
SB	1	1	11	42.5	38.1	38.1	220,111
SB	1	1	11	37.5	33.6	33.6	284,380
SB	1	1	11	32.5	26.0	26.0	348,649
SB	1	1	11	27.5	7.2	7.2	412,918
SB	1	1	11	22.5	4.1	4.1	477,187
SB	1	1	11	17.5	3.3	3.3	541,456
SB	1	1	11	12.5	0.0	0.0	0
SB	1	1	12	57.5	6.7	6.7	46,897
SB	1	1	12	52.5	3.3	3.3	99,819

SB	1	1	12	47.5	8.1	8.1	164,041
SB	1	1	12	42.5	26.3	26.3	228,263
SB	1	1	12	37.5	45.2	45.2	292,484
SB	1	1	12	32.5	43.2	43.2	356,706
SB	1	1	12	27.5	28.9	28.9	420,928
SB	1	1	12	22.5	33.8	33.8	485,150
SB	1	1	12	17.5	20.8	20.8	549,372
SB	1	1	12	12.5	4.2	4.2	613,593
SB	1	1	12	7.5	8.9	8.9	677,815
SB	1	1	12	2.5	1.0	1.0	742,037
SB	1	2	1	42.5	0.3	0.3	319,101
SB	1	2	1	37.5	33.5	33.5	383,465
SB	1	2	1	32.5	191.8	191.8	447,828
SB	1	2	1	27.5	96.3	96.3	512,192
SB	1	2	1	22.5	42.4	42.4	576,556
SB	1	2	1	17.5	91.5	91.5	640,919
SB	1	2	1	12.5	30.6	30.6	705,283
SB	1	2	1	7.5	19.3	19.3	769,647
SB	1	2	1	2.5	8.2	8.2	834,010
SB	1	2	2	57.5	4.3	4.3	116,025
SB	1	2	2	52.5	7.9	7.9	180,724
SB	1	2	2	47.5	25.7	25.7	245,423
SB	1	2	2	42.5	28.6	28.6	310,123
SB	1	2	2	37.5	47.4	47.4	374,822
SB	1	2	2	32.5	72.6	72.6	439,521
SB	1	2	2	27.5	68.8	68.8	504,220
SB	1	2	2	22.5	90.0	90.0	568,919
SB	1	2	2	17.5	44.0	44.0	633,618
SB	1	2	2	12.5	29.0	29.0	698,317
SB	1	2	2	7.5	13.9	13.9	763,016
SB	1	2	2	2.5	26.8	26.8	827,715
SB	1	2	2	-2.5	5.2	5.2	892,414
SB	1	2	3	67.5	1.7	1.7	2,791
SB	1	2	3	62.5	4.9	4.9	39,536
SB	1	2	3	57.5	2.8	2.8	104,187
SB	1	2	3	52.5	13.3	13.3	168,838
SB	1	2	3	47.5	34.6	34.6	233,489
SB	1	2	3	42.5	42.3	42.3	298,139
SB	1	2	3	37.5	95.4	95.4	362,790
SB	1	2	3	32.5	200.9	200.9	427,441
SB	1	2	3	27.5	60.8	60.8	492,092
SB	1	2	3	22.5	47.2	47.2	556,742
SB	1	2	3	17.5	10.0	10.0	621,393
SB	1	2	4	87.5	2.5	2.5	0

SB	1	2	4	82.5	7.1	7.1	0
SB	1	2	4	77.5	7.2	7.2	0
SB	1	2	4	72.5	16.3	16.3	0
SB	1	2	4	67.5	32.8	32.8	1,134
SB	1	2	4	62.5	23.3	23.3	31,292
SB	1	2	4	57.5	27.0	27.0	95,799
SB	1	2	4	52.5	33.4	33.4	160,306
SB	1	2	4	47.5	60.6	60.6	224,812
SB	1	2	4	42.5	137.9	137.9	289,319
SB	1	2	4	37.5	94.1	94.1	353,826
SB	1	2	4	32.5	45.0	45.0	418,332
SB	1	2	4	27.5	10.0	10.0	482,839
SB	1	2	5	87.5	0.3	0.3	0
SB	1	2	5	82.5	5.5	5.5	0
SB	1	2	5	77.5	25.4	25.4	0
SB	1	2	5	72.5	39.3	39.3	0
SB	1	2	5	67.5	69.5	69.5	84,079
SB	1	2	5	62.5	74.1	74.1	147,974
SB	1	2	5	57.5	90.0	90.0	211,870
SB	1	2	5	52.5	89.1	89.1	275,765
SB	1	2	5	47.5	77.8	77.8	339,661
SB	1	2	5	42.5	36.1	36.1	403,556
SB	1	2	5	37.5	6.6	6.6	467,451
SB	1	2	6	92.5	13.1	13.1	0
SB	1	2	6	87.5	12.9	12.9	0
SB	1	2	6	82.5	34.4	34.4	0
SB	1	2	6	77.5	48.6	48.6	0
SB	1	2	6	72.5	84.9	84.9	0
SB	1	2	6	67.5	98.9	98.9	75,424
SB	1	2	6	62.5	81.5	81.5	138,909
SB	1	2	6	57.5	93.9	93.9	202,394
SB	1	2	6	52.5	25.0	25.0	265,880
SB	1	2	6	47.5	4.0	4.0	329,365
SB	1	2	7	92.5	2.6	2.6	0
SB	1	2	7	87.5	24.7	24.7	0
SB	1	2	7	82.5	50.5	50.5	0
SB	1	2	7	77.5	83.8	83.8	0
SB	1	2	7	72.5	171.3	171.3	0
SB	1	2	7	67.5	111.3	111.3	73,846
SB	1	2	7	62.5	55.4	55.4	136,977
SB	1	2	7	57.5	12.0	12.0	200,107
SB	1	2	7	52.5	2.0	2.0	263,238
SB	1	2	8	92.5	4.5	4.5	0
SB	1	2	8	87.5	17.6	17.6	0

SB	1	2	8	82.5	33.4	33.4	0
SB	1	2	8	77.5	92.3	92.3	0
SB	1	2	8	72.5	166.0	166.0	0
SB	1	2	8	67.5	131.8	131.8	80,822
SB	1	2	8	62.5	57.2	57.2	143,693
SB	1	2	8	57.5	9.0	9.0	206,564
SB	1	2	8	52.5	2.0	2.0	269,435
SB	1	2	9	92.5	6.4	6.4	0
SB	1	2	9	87.5	6.6	6.6	0
SB	1	2	9	82.5	9.5	9.5	0
SB	1	2	9	77.5	35.5	35.5	0
SB	1	2	9	72.5	86.5	86.5	0
SB	1	2	9	67.5	65.5	65.5	95,109
SB	1	2	9	62.5	112.2	112.2	158,504
SB	1	2	9	57.5	84.5	84.5	221,900
SB	1	2	9	52.5	48.8	48.8	285,296
SB	1	2	9	47.5	33.6	33.6	348,692
SB	1	2	9	42.5	8.0	8.0	412,087
SB	1	2	10	82.5	1.0	1.0	0
SB	1	2	10	77.5	3.8	3.8	0
SB	1	2	10	72.5	11.1	11.1	0
SB	1	2	10	67.5	33.3	33.3	4,094
SB	1	2	10	62.5	66.0	66.0	46,102
SB	1	2	10	57.5	89.2	89.2	109,859
SB	1	2	10	52.5	126.1	126.1	173,617
SB	1	2	10	47.5	83.0	83.0	237,374
SB	1	2	10	42.5	58.0	58.0	301,131
SB	1	2	10	37.5	39.3	39.3	364,889
SB	1	2	10	32.5	3.0	3.0	428,646
SB	1	2	11	62.5	1.0	1.0	63,929
SB	1	2	11	57.5	18.0	18.0	128,198
SB	1	2	11	52.5	68.3	68.3	192,467
SB	1	2	11	47.5	66.1	66.1	256,736
SB	1	2	11	42.5	112.9	112.9	321,005
SB	1	2	11	37.5	64.4	64.4	385,274
SB	1	2	11	32.5	72.0	72.0	449,543
SB	1	2	11	27.5	68.8	68.8	513,812
SB	1	2	11	22.5	18.9	18.9	578,081
SB	1	2	11	17.5	4.7	4.7	642,350
SB	1	2	11	12.5	2.0	2.0	706,619
SB	1	2	12	57.5	4.3	4.3	131,938
SB	1	2	12	52.5	2.7	2.7	196,159
SB	1	2	12	47.5	14.9	14.9	260,381
SB	1	2	12	42.5	48.7	48.7	324,603

SB	1	2	12	37.5	91.8	91.8	388,825
SB	1	2	12	32.5	108.8	108.8	453,047
SB	1	2	12	27.5	77.1	77.1	517,268
SB	1	2	12	22.5	64.2	64.2	581,490
SB	1	2	12	17.5	44.3	44.3	645,712
SB	1	2	12	12.5	29.8	29.8	709,934
SB	1	2	12	7.5	14.1	14.1	774,156
SB	1	2	12	2.5	13.0	13.0	838,378

APPENDIX B

APPENDIX B

Computer Program Listing

```

C*****
C THIS PROGRAM SOLVES 1D, UNSTEADY HEAT EQUATION BY EMPLOYING
C IMPLICIT CRANK-NICOLSON SCHEME FOR A COMPOSITE MEDIUM
C THE OUTPUT WILL BE IN CN.OUT
C*****
C DESCRIPTION OF INPUT PARAMETERS
C
C TSLAB      SLAB THICKNESS.
C NSLAB      NO. OF CVS IN SLAB.
C DLS        POSITION OF LINE SOURCE W.R.T SLAB.
C NLS        NO. OF CVS IN REGION BETWEEN SLAB AND LINE SOURCE.
C DIN        DISTANCE FROM LINE SOURCE TO INSULATION.
C NIN        NO. OF CVS IN DIN.
C TIN        INSULATION THICKNESS.
C NTIN       NO. OF CVS IN INSULATION.
C DGRGD      POSTION OF TGRD BELOW INSULATION.
C NGRD       NO OF CVS IN DGRD.
C TGRD       GROUND TEMPERATURE.
C TINF       T INFINITY.
C HCON       CONVECTIVE HEAT TRANSFER COEFFICIENT.
C KCONC      K FOR CONCRETE.
C KSAND      K FOR SAND.
C KEART      K FOR EARTH.
C KINSL      K FOR INSULATION.
C RHOCC      RHO*C FOR CONCRETE.
C RHOCS      RHO*C FOR SAND.
C RHOCE      RHO*C FOR EARTH.
C RHOCI      RHO*C FOR INSULATION.
C NTOT       TOTAL NO. OF GRID POINTS
C
C DT         TIME STEP.
C DX         GRID SIZE.
C MTIME      THE MAXIMUM TIME.
C NSTEP      THE NUMBER OF TIME STEPS AFTER WHIC PRINTOUT OCCURS.
C
C T          THE SOLUTION VARIABLE AT THE NTH TIME STEP.
C TOL        THE SOLUTION VARIABLE AT THE N-1TH TIME STEP.
C
C*****
C
      DIMENSION T(3000),TOL(3000)
      DIMENSION A(3000),B(3000),C(3000),R(3000),SOLN(3000)
      REAL

```

```
TSLAB,TIN,TINF,TGRD,HCON,KCONC,KSAND,MTIME,TIME,PI,TINF1,
+ KEARTH,KINSL,RHOCC,RHOCS,RHOCE,RHOCL,RNIN,KEQ1,KEQ2,KEQ3,L
INTEGER NSLAB,NLS,NIN,NTIN,NGRD
```

C

```
PRINT*, 'ENTER SLAB THICKNESS, TSLAB='
READ(*,*)TSLAB
PRINT*, 'ENTER NO. OF CVS IN SLAB, NSLAB='
READ(*,*)NSLAB
PRINT*, 'ENTER LINE SOURCE POSTION, DLS='
READ(*,*)DLS
PRINT*, 'ENTER NO. OF CVS IN DLS, NLS='
READ(*,*)NLS
PRINT*, 'ENTER DIN='
READ(*,*)DIN
PRINT*, 'ENTER NO. OF CVS IN DIN, NINR='
READ(*,*)RNIN
PRINT*, 'ENTER INSULATION THICKNESS, TIN='
READ(*,*)TIN
PRINT*, 'ENTER NO OF CVS IN TIN, NTIN='
READ(*,*)NTIN
PRINT*, 'ENTER DGRD='
READ(*,*)DGRD
PRINT*, 'ENTER NGRD='
READ(*,*)NGRD
PRINT*, 'DT='
READ(*,*)DT
PRINT*, 'ENTER MAXIMUM NO. OF TIME STEPS, MTIME='
READ(*,*)MTIME
PRINT*, 'PRINTOUT STEP, NSTEP='
READ(*,*)NSTEP
PRINT*, 'ENTER HEAT GENERATION TERM='
READ(*,*)GH
PRINT*, 'TIME HEAT SOURCE ON?'
READ(*,*)TIME1
PRINT*, 'TIME HEAT SOURCE OFF?'
READ(*,*)TIME2
PRINT*, 'INITIAL CONDITIONS=?'
READ(*,*)TINT
```

C

```
OPEN(10,STATUS='OLD',FILE='CN.DAT')
READ(10,5)TINF,TGRD,HCON,KCONC,KSAND,KEARTH,KINSL,RHOCC,RHOCS,
+ RHOCE,RHOCL
5  FORMAT(7(1X,F9.4)/4(1X,F9.4))
```

C

```
NIN=INT(.5+RNIN)
TSLAB=TSLAB/(12.)
DLS=DLS/(12.)
TIN=TIN/(12.)
DIN=DIN/(12.)
DGRD=DGRD/(12.)
```

C

```

DX1=TSLAB/(NSLAB+.5)
DX3=DIN/RNIN
DX2=(DLS-.5*DX3)/NLS
DX4=TIN/NTIN
DX5=DGRD/NGRD

C
ALFAC=KCONC/RHOCC
ALFAS=KSAND/RHOCS
ALFAE=KEARTH/RHOCE
ALFAI=KINSL/RHOCI

C
KEQ1=KCONC*KSAND*(DX1+DX2)/(KCONC*DX1+KSAND*DX2)
KEQ2=KSAND*KINSL*(DX3+DX4)/(KSAND*DX3+KINSL*DX4)
KEQ3=KINSL*KEARTH*(DX4+DX5)/(KINSL*DX4+KEARTH*DX5)

C
ALFAQ1=KEQ1/RHOCC
ALFAQ2=KEQ1/RHOCS
ALFAQ3=KEQ2/RHOCS
ALFAQ4=KEQ2/RHOCI
ALFAQ5=KEQ3/RHOCI
ALFAQ6=KEQ3/RHOCE

C
FOC=ALFAC*DT/(2.*DX1**2)
FOS1=ALFAS*DT/(2.*DX2**2)
FOS2=ALFAS*DT/(2.*DX3**2)
FOI=ALFAI*DT/(2.*DX4**2)
FOE=ALFAE*DT/(2.*DX5**2)

C
FOEQ =2.*ALFAS*DT/(DX2+DX3)**2
FOEQ1=2.*ALFAQ1*DT/(DX1+DX2)**2
FOEQ2=2.*ALFAQ2*DT/(DX1+DX2)**2
FOEQ3=2.*ALFAQ3*DT/(DX4+DX3)**2
FOEQ4=2.*ALFAQ4*DT/(DX4+DX3)**2
FOEQ5=2.*ALFAQ5*DT/(DX5+DX4)**2
FOEQ6=2.*ALFAQ6*DT/(DX5+DX4)**2

C
BIOT=.5*HCON*DX1/KCONC
NTOT=NSLAB+NLS+NIN+NTIN+NGRD

C
C OPEN THE OUTPUT FILE THEN WRITE THE BASIC INPUT DATA
C
OPEN(20,STATUS='OLD', FILE='CN.OUT')
OPEN(50,STATUS='OLD', FILE='TEMP.OUT')
WRITE(20,100)
WRITE(20,101)TSLAB,NSLAB,DLS,NLS,DIN,NIN,TIN,NTIN,DGRD,NGRD
WRITE(20,102)KCONC,RHOCC,KSAND,RHOCS,KEARTH,RHOCE,
+ KINSL,RHOCI,TINF,TGRD,HCON,DT,NTOT,GH,TIME1,TIME2

C
C WRITE CALCULATED PARAMETERS ONTO OUTPUT FILE
C
WRITE(20,200)DX1,DX2,DX3,DX4,DX5,ALFAC,ALFAS,ALFAI,ALFAE,

```

```

+ KEQ1,KEQ2,KEQ3,ALFAQ1,ALFAQ2,ALFAQ3,ALFAQ4,ALFAQ5,ALFAQ6,
+ FOC,FOS1,FOS2,FOI,FOE,FOEQ,FOEQ1,FOEQ2,FOEQ3,FOEQ4,FOEQ5,
+ FOEQ6,G,BIOT
  ISTEP1=0
  ISTEP2=0
  ISTEP3=0
  TIME=0.
C
C SET THE INITIAL CONDITION
C
      DO 90 I=1, NTOT+1
      T(I)=TINT
      TOL(I)=TINT
90 CONTINUE
C
C SOLVE FOR T ON INTERIOR POINTS AT (N+1)TH TIME STEP
C INCREMENT THE ITERATION COUNTERS AND CHECK THE MAXIMUM LIMIT
C OF ITERATIONS
C
      20 ISTEP1=ISTEP1+1
      ISTEP2=ISTEP2+1
      ISTEP3=ISTEP3+1
      TIME=TIME+DT
      G=0.
      IF(ISTEP1.GT.MTIME)GO TO 40
      IF(ISTEP3.GE.(TIME1/DT))THEN
      IF(ISTEP3.LE.(TIME2/DT))THEN
      G=GH*DT/(RHOCS*DX3)
      ENDIF
      ENDIF
C
C FORM THE TRIDIAGONAL SYSTEM OF EQUATIONS
C
      CALL FMTDIG(NSLAB,NLS,NIN,NTIN,NGRD,NTOT,G,BIOT,TGRD,
+ FOC,FOS1,FOS2,FOI,FOE,FOEQ,FOEQ1,FOEQ2,FOEQ3,FOEQ4,FOEQ5,
+ FOEQ6,TINF,A,B,C,R,T,TOL,RHOCC,DX1,DT)
C
C INVERT THE TRIDIAGONAL SYSTEM OF EQUATIONS
C
      CALL TDIG(A,B,C,R,SOLN,QI,QO,HCON,TINF,NTOT,NGRD,KINSL,DX4)
C
C SAVE THE OLD SOLUTION
C
      DO 25 I=1,NTOT+1
      T(I)=SOLN(I)
      TOL(I)=T(I)
25 CONTINUE
C
C WRITE THE TEMPERATURE FIELD ON OUTPUT FILE
C

```

```

IF(ISTEP2.EQ.NSTEP)THEN
  WRITE(50,99)TIME,T(1),T(NSLAB+NLS+2)
C WRITE THE HEAT FLUX ON OUTPUT FILE QT.OUT
C
  OPEN(30,STATUS='OLD',FILE='QI.OUT
  OPEN(40,STATUS='OLD',FILE='QO.OUT')
  WRITE(30,77)(TIME/24),QI
  WRITE(40,77)TIME,QO
77 FORMAT(1X,F9.3,5X,F20.6)
  ISTEP2=0
  GO TO 20
  ENDIF
  GO TO 20
C
88 FORMAT(/,1X,'AT T = ',F7.3,1X,'TEMPERATURE FIELD IS:')
99 FORMAT(1X,3(F8.4,2X))
C
100 FORMAT(20X,'*****'/
+ 32X,'OUTPUT FOR CRANKNC'/20X,
+ '*****'//2X,
+ '**BASIC INPUT DATA FOR CRANKNC:')/
C
101 FORMAT(1X,'SLAB THICKNESS',10X,F9.4,12X,'NSLAB'5X,I4/
+ 1X,'LINE SOURCE POSITION',4X,F9.4,12X,'NLS',7X,I4/
+ 1X,'INSULATION POSITION',5X,F9.4,12X,'NIN',7X,I4/
+ 1X,'INSULATION THICKNESS',4X,F9.4,12X,'NTIN',6X,I4/
+ 1X,'POSITION OF WATER TABLE',1X,F9.4,12X,'NGRD',6X,I4)
C
102 FORMAT(/1X,'K CONCRETE',4X,F8.4,12X,'RHOC CONCRETE',4X,F8.4/
+ 1X,'K SAND',8X,F8.4,12X,'RHOC SAND',8X,F8.4/
+ 1X,'K EARTH',7X,F8.4,12X,'RHOC EARTH',7X,F8.4/
+ 1X,'K INSULATION',2X,F8.4,12X,'RHOC INSULATION',2X,F8.4//
+ 1X,'T INFINITY =',2X,F6.2,3X,'T GROUND =',2X,F6.2,3X,
+ 'h CONVECTION =',2X,F6.2,3X/1X,'DT =',1X,F6.2,5X,'NTOT',I5,
+ 3X,'HEAT SOURCE =',1X,F6.2,2X,'TIME1 =',F4.1,2X,'TIME2 =',F4.1)
C
200 FORMAT(/1X,'DX1=',F8.4,3X,'DX2=',F8.4,3X,'DX3=',F8.4,
+ 3X,'DX4=',F8.4,3X,'DX5=',F8.4//1X,'ALFAC=',F8.4,3X,
+ 'ALFAS=',F8.4,3X,'ALFAI=',F8.4,3X,'ALFAE=',F8.4//1X,
+ 'KEQ1=',F8.4,3X,'KEQ2=',F8.4,3X,'KEQ3=',F8.4,3X,'ALFAQ1=',
+ F8.4//1X,'ALFAQ2=',F8.4,3X,'ALFAQ3=',F8.4,3X,'ALFAQ4=',F8.4,3X,
+ 'ALFAQ5=',F8.4//1X,'ALFAQ6=',F8.4,3X,'FOC=',F8.4,3X,'FOS1=',
+ F8.4,3X,'FOS2=',F8.4//1X,'FOI=',F8.4,3X,'FOE=',F8.4,3X,'FOEQ=',
+ F8.4,3X,'FOEQ1=',F8.4,3X,'FOEQ2=',F8.4//1X,'FOEQ3=',F8.4,3X,
+ 'FOEQ4=',F8.4,3X,'FOEQ5=',F8.4,3X,'FOEQ6=',F8.4//1X,'G=',F8.4,3X,
+ 'BIOT=',F8.4//)
C
40 STOP
END
C

```

```

C*****
      SUBROUTINE FMTDIG(NSLAB,NLS,NIN,NTIN,NGRD,NTOT,G,BIOT,
+ TGRD,FOC,FOS1,FOS2,FOI,FOE,FOEQ,FOEQ1,FOEQ2,FOEQ3,FOEQ4,
+ FOEQ5,FOEQ6,TINF,A,B,C,R,T,TOL,RHOCC,DX1,DT)
C
C THIS SUBROUTINE FORMS THE TRIDIAGONAL MATRIX FOR THE
C CRANK-NICOLSON METHOD. THE GENERIC FORM OF THE EQUATIONIS:
C
C       $A*T(I-1) + B*T(I) + C*T(I+1) = R$ 
C
C      DIMENSION T(3000),TOL(3000),A(3000),B(3000),C(3000),R(3000)
C      C1=3.E-09
C
C FIRST BOUNDARY CONDITION AT X=0.
C
      B(1)=1.+2.*FOC+4.*FOC*BIOT+2.*C1*DT*(TINF**3.)/(RHOCC*DX1)
      C(1)=-2.*FOC
      R1=2.*FOC*TOL(2)+(1.-2.*FOC-4.*FOC*BIOT)*TOL(1)
      R2=8.*FOC*BIOT*TINF
      R3=C1*DT*(2.*(TINF**4)-3.*(TINF**2)*(TOL(1)-TINF)**2)/(RHOCC*DX1)
      R(1)=R1+R2+R3
C
C INTERIOR NODES FOR FIRST LAYER
C
      IF(NSLAB.EQ.1)THEN
        A(2)=-FOC*2.
        B(2)=1.+FOEQ1+2.*FOC
        C(2)=-FOEQ1
        R(2)=FOEQ1*TOL(3)+2.*FOC*TOL(1)+(1-FOEQ1-FOC*2.)*TOL(2)
      ENDIF
C
      IF(NSLAB.GE.2)THEN
        A(2)=-FOC*2.
        B(2)=1.+3.*FOC
        C(2)=-FOC
        R(2)=FOC*(TOL(3)+TOL(1)*2.)+(1-3.*FOC)*TOL(2)
        DO 10 I=2, NSLAB
          A(I)=-FOC
          B(I)=1.+2.*FOC
          C(I)=-FOC
          R(I)=FOC*(TOL(I+1)+TOL(I-1))+(1-2.*FOC)*TOL(I)
10    CONTINUE
        A(NSLAB+1)=-FOC
        B(NSLAB+1)=1.+FOC+FOEQ1
        C(NSLAB+1)=-FOEQ1
        R(NSLAB+1)=FOEQ1*TOL(NSLAB+2)+FOC*TOL(NSLAB)+
+ (1.-FOC-FOEQ1)*TOL(NSLAB+1)
      ENDIF
C

```

```

                P=NSLAB+2
C
C INTERIOR NODES FOR SECOND LAYER
C
                IF(NLS.EQ.1)THEN
                    A(P)=-FOEQ2
                    B(P)=1.+FOEQ+FOEQ2
                    C(P)=-FOEQ
                R(P)=FOEQ*TOL(P+1)+FOEQ2*TOL(P-1)+(1.-FOEQ-FOEQ2)*TOL(P)
                ENDIF
C
                IF(NLS.GE.2)THEN
                    A(P)=-FOEQ2
                    B(P)=1.+FOS1+FOEQ2
                    C(P)=-FOS1
                    R(P)=FOS1*TOL(P+1)+FOEQ2*TOL(P-1)+(1.-FOS1-FOEQ2)*TOL(P)
                    P=NSLAB+NLS
                    DO 20 I=NSLAB+3, P
                        A(I)=-FOS1
                        B(I)=1.+2.*FOS1
                        C(I)=-FOS1
                        R(I)=FOS1*(TOL(I+1)+TOL(I-1))+(1.-2.*FOS1)*TOL(I)
20                CONTINUE
                    A(P+1)=-FOS1
                    B(P+1)=1.+FOS1+FOEQ
                    C(P+1)=-FOEQ
                    R(P+1)=FOEQ*TOL(P+2)+FOS1*TOL(P)+(1.-FOEQ-FOS1)*TOL(P+1)
                ENDIF
C
                P=NSLAB+NLS+1
C
C INTERIOR NODES FOR THIRD LAYER
C
                IF(NIN.EQ.1)THEN
                    A(P+1)=-FOEQ
                    B(P+1)=1.+FOEQ3+FOEQ
                    C(P+1)=-FOEQ3
                    R(P+1)=FOEQ3*TOL(P+2)+FOEQ*TOL(P)+(1.-FOEQ-FOEQ3)*TOL(P+1)+G
                ENDIF
C
                IF(NIN.GE.2)THEN
                    A(P+1)=-FOEQ
                    B(P+1)=1.+FOEQ+FOS2
                    C(P+1)=-FOS2
                    R(P+1)=FOS2*TOL(P+2)+FOEQ*TOL(P)+(1.-FOS2-FOEQ)*TOL(P+1)+G
                    DO 30 I=P+2, P+NIN-1
                        A(I)=-FOS2
                        B(I)=1.+2.*FOS2
                        C(I)=-FOS2
                        R(I)=FOS2*(TOL(I+1)+TOL(I-1))+(1.-2.*FOS2)*TOL(I)
30                CONTINUE

```

```

P=P+NIN
A(P)=-FOS2
B(P)=1.+FOS2+FOEQ3
C(P)=-FOEQ3
R(P)=FOEQ3*TOL(P+1)+FOS2*TOL(P-1)+(1.-FOS2-FOEQ3)*TOL(P)
ENDIF
C
P=NSLAB+NLS+NIN+1
C
C INTERIOR NODES FOR FOURTH LAYER
C
IF(NTIN.EQ.1)THEN
A(P+1)=-FOEQ4
B(P+1)=1.+FOEQ4+FOEQ5
C(P+1)=-FOEQ5
R(P+1)=FOEQ5*TOL(P+2)+FOEQ4*TOL(P)+(1.-FOEQ4-FOEQ5)*TOL(P+1)
ENDIF
C
IF(NTIN.GE.2)THEN
A(P+1)=-FOEQ4
B(P+1)=1.+FOEQ4+FOI
C(P+1)=-FOI
R(P+1)=FOI*TOL(P+2)+FOEQ4*TOL(P)+(1.-FOI-FOEQ4)*TOL(P+1)
DO 40 I=P+2, P+NTIN-1
A(I)=-FOI
B(I)=1.+2.*FOI
C(I)=-FOI
R(I)=FOI*(TOL(I+1)+TOL(I-1))+(1.-2.*FOI)*TOL(I)
40 CONTINUE
P=P+NTIN
A(P)=-FOI
B(P)=1.+FOI+FOEQ5
C(P)=-FOEQ5
R(P)=FOEQ5*TOL(P+1)+FOI*TOL(P-1)+(1.-FOEQ5-FOI)*TOL(P)
ENDIF
P=NTOT-NGRD+1
C
C INTERIOR NODES FOR FIFTH LAYER
A(P+1)=-FOEQ6
B(P+1)=1.+FOEQ6+FOE
C(P+1)=-FOE
R(P+1)=FOE*TOL(P+2)+FOEQ6*TOL(P)+(1.-FOE-FOEQ6)*TOL(P+1)
C
DO 50 I=P+2, NTOT
A(I)=-FOE
B(I)=1.+2.*FOE
C(I)=-FOE
R(I)=FOE*(TOL(I+1)+TOL(I-1))+(1.-2.*FOE)*TOL(I)
50 CONTINUE
C

```


C BOUNDARY NODE AT X=L.

C

```

      A(NTOT+1)=-FOE
      B(NTOT+1)=1.+3.*FOE
      C(NTOT+1)=-FOE*2.
      R(NTOT+1)=FOE*(TOL(NTOT)+4.*TGRD)+(1.-3.*FOE)*TOL(NTOT+1)

```

C

```

      RETURN
      END

```

C

C*****

```

      SUBROUTINE TDIG(A,B,C,R,SOLN,QI,QO,HCON,TINF,NTOT,NGRD,
+ KINSL,DX4)
      REAL KINSL

```

C

C THIS SUBROUTINE USES GAUSS-ELIMINATION THEN BACK SUBSTITUTION
C TO GIVE THE SOLUTION OF THE SYSTEM OF EQUATIONS

C

```

      DIMENSION A(3000),B(3000),C(3000),BN(3000),R(3000),SOLN(3000)
      DO 10 I=1,NTOT+1
         BN(I)=B(I)
10  CONTINUE
      DO 20 I=2,NTOT+1
         D=A(I)/BN(I-1)
         BN(I)=BN(I)-C(I-1)*D
         R(I)=R(I)-R(I-1)*D
20  CONTINUE
      SOLN(NTOT+1)=R(NTOT+1)/BN(NTOT+1)
      N=NTOT+1
      DO 30 I=1,NTOT
         J=N-I
         SOLN(J)=(R(J)-C(J)*SOLN(J+1))/BN(J)
30  CONTINUE
      N=NTOT-NGRD
      QI=(SOLN(1)-TINF)*HCON+.15e-08*(SOLN(1)**4-TINF**4)
      QO=KINSL*(SOLN(N)-SOLN(N+1))/DX4
      RETURN
      END

```

MICHIGAN STATE UNIV. LIBRARIES



31293008987509